JOURNAL OF THE AERONAUTICAL SCIENCES

THE JOHN CRERAR LIBRARY AUG 21 1947

VOLUME 14 AUGUST, 1947 NUMBER 8

A Survey of the Calculated Efficiencies of Jet Power Plants ..... JOSEPH H. KEENAN AND JOSEPH KAYE 437

A Method for Calculating Airfoil Sections from Specifications on the Pressure Distributions ..... GLENN H. PEEBLES 451

Pure Bending in the Plastic Range ..... HARRY A. WILLIAMS 457

The Problem of Escape from the Earth by Rocket ..... FRANK J. MALINA AND MARTIN SUMMERFIELD 471

Numerical Procedures for Calculation of Stress Distribution in Sheet-Stringer-Frame Combinations ..... MARVIN STERN 481

A Tabulation Method for the Calculation of the Critical Speed of Wing Divergence ..... WALTER P. TARGOFF 487

Letters to the Editor 450, 456, 469

Published by the

INSTITUTE OF THE AERONAUTICAL SCIENCES, INC.

JOURNAL OF THE AERONAUTICAL SCIENCES

Editor: HUGH L. DRYDEN, *Associate Director, National Bureau of Standards*

Associate Editor: ROBERT R. DEXTER *Associate Editor:* BERNEICE H. JARCK

The Institute of the Aeronautical Sciences publishes monthly the JOURNAL OF THE AERONAUTICAL SCIENCES and the AERONAUTICAL ENGINEERING REVIEW.

The JOURNAL OF THE AERONAUTICAL SCIENCES prints papers of scientific and technical interest to Institute members and subscribers. In general, it provides an opportunity for specialists to publish articles disclosing new knowledge and new applications in the field of the aeronautical sciences. The JOURNAL restricts itself to the aeronautical aspects of advances in science and engineering, and papers printed have either been submitted directly to the JOURNAL or have been previously presented at a meeting of the Institute.

The AERONAUTICAL ENGINEERING REVIEW keeps members and subscribers informed regarding the contents of new books and current periodicals in the field of aeronautics. It reviews new developments in the aircraft industry and reports on progress from house organs and catalogs published by aircraft and engine manufacturers and other companies engaged in aeronautical activities. It publishes papers on applied engineering and aircraft production. News of Institute activities is published in the REVIEW.

Statements and opinions expressed in the JOURNAL are to be understood as individual expressions of the authors and not those of the Institute.

SUBSCRIPTION RATES

Journal of the Aeronautical Sciences
Published Monthly

United States and Possessions		Foreign Countries Including Canada (American Currency Rates)	
1 Year	$7.00	1 Year	$9.00
Single Copies	0.70	Single Copies	1.00

Aeronautical Engineering Review
Published Monthly

United States and Possessions		Foreign Countries Including Canada (American Currency Rates)	
1 Year	$3.00	1 Year	$3.50
Single Copies	0.30	Single Copies	0.35

Notices of change of address should be sent to the Institute at least 30 days prior to actual change of address.

Manuscripts for publication, proofs, and all correspondence should be addressed to the Editorial Office of the JOURNAL.

Correspondence regarding subscriptions may be addressed to Publication Office, 20th and Northampton Sts., Easton, Pa., or to the Editorial Office of the JOURNAL OF THE AERONAUTICAL SCIENCES, 2 East 64th Street, New York 21, New York.

Copyright, 1947, by the Institute of the Aeronautical Sciences, Inc.

Entered as Second Class Matter at the Post Office, Easton, Pa., May 1, 1937. Acceptance for mailing at a special rate of Postage provided for in the Act of August 24, 1912. Authorized April 29, 1937.

INSTITUTE of the AERONAUTICAL SCIENCES

President

P. R. BASSETT

Vice-Presidents

WELLWOOD E. BEALL
REX B. BEISEL
LUIS DE FLOREZ
JOHN K. NORTHROP

Director

S. PAUL JOHNSTON

Executive Vice-President

BENNETT H. HORCHLER

Past-Presidents

J. C. HUNSAKER
CHARLES L. LAWRANCE
DONALD W. DOUGLAS
GLENN L. MARTIN
CLARK B. MILLIKAN
T. P. WRIGHT
GEORGE W. LEWIS
JAMES H. DOOLITTLE
FRANK W. CALDWELL
HALL L. HIBBARD
HUGH L. DRYDEN
R. H. FLEET
CHARLES H. COLVIN
ARTHUR E. RAYMOND

Secretary

ROBERT R. DEXTER

Treasurer

BURDETTE S. WRIGHT

Controller

JOSEPH J. MAITAN

Counsel

ALLAN D. EMIL

COUNCIL

E. E. ALDRIN
LAWRENCE D. BELL
GEORGE W. BRADY
W. A. M. BURDEN
VICTOR E. CARBONARA
CARL DE GANAHL
JAMES H. DOOLITTLE
WILLIAM K. EBEL
SHERMAN M. FAIRCHILD
C. C. FURNAS
J. A. HERLIHY
WILLSON H. HUNTER
JEROME LEDERER
JOHN C. LESLIE
A. ELLIOTT MERRILL
EARL D. OSBORN
EARL A. SPERRY, JR.
JOHN C. SQUIRES
M. F. STOUGHTON
ERNEST G. STOUT
C. FAYETTE TAYLOR

ADVISORY COMMITTEE

Chairman: CHARLES H. COLVIN

WALTER BEECH
FRANK W. CALDWELL
RALPH S. DAMON
KENNETH S. M. DAVIDSON
R. H. FLEET
R. PAUL HARRINGTON
R. M. HAZEN
HALL L. HIBBARD
J. C. HUNSAKER
TH. VON KÁRMÁN
THOMAS A. KNOWLES
I. M. LADDON
GROVER LOENING
GLENN L. MARTIN
CLARK B. MILLIKAN
THOMAS A. MORGAN
R. C. MUIR
ARTHUR E. RAYMOND
F. W. REICHELDERFER
L. B. RICHARDSON
RUSSELL G. ROBINSON
LAURANCE S. ROCKEFELLER
T. CLAUDE RYAN
EDWARD P. WARNER

HONORARY MEMBERS

JOHN C. ADAMS
GRIFFITH BREWER
JOHN N. BROWN
W. A. M. BURDEN
E. U. CONDON
L. C. CRAIGIE
IRA C. EAKER
HARRY F. GUGGENHEIM
HENRY G. HOUGHTON
GEORGE C. KENNEY
CURTIS E. LE MAY
GEORGE B. PEGRAM
E. M. POWERS
J. LAURANCE PRITCHARD
ARTHUR W. RADFORD
F. W. REICHELDERFER
H. B. SALLADA
CARL SPAATZ
L. C. STEVENS
NATHAN F. TWINING

HONORARY FELLOWS

H. H. ARNOLD
FRANK W. CALDWELL
SIR GEOFFREY DE HAVILLAND
DONALD W. DOUGLAS
HUGH L. DRYDEN
W. F. DURAND
SIR RICHARD FAIREY
SIR ROY FEDDEN
J. C. HUNSAKER
SIR MELVILL JONES
GEORGE W. LEWIS
GLENN L. MARTIN
GEORGE J. MEAD
SIR FREDERICK HANDLEY PAGE
D. R. PYE
IGOR I. SIKORSKY
SIR GEOFFREY TAYLOR
TH. VON KÁRMÁN
EDWARD P. WARNER
ORVILLE WRIGHT
T. P. WRIGHT

BENEFACTORS

E. E. ALDRIN
HART O. BERG (Deceased)
W. A. M. BURDEN
E. L. CORD
DONALD W. DOUGLAS
SHERMAN M. FAIRCHILD
SIR RICHARD FAIREY
R. H. FLEET
FLORENCE GUGGENHEIM (Deceased)
C. D. HANSCOM
JOHN P. V. HEINMULLER
ALEXANDER KLEMIN
PAUL KOLLSMAN
BELLA C. LANDAUER
WILLIAM LANDAUER
GROVER LOENING
EDMUND C. LYNCH (Deceased)
F. W. MAGIN
GLENN L. MARTIN
GEORGE J. MEAD
S. A. REED (Deceased)
LAURANCE S. ROCKEFELLER
EDWARD P. WARNER

AMERICAN FELLOWS

JOHN D. AKERMAN
E. E. ALDRIN
HARRY G. ARMSTRONG
KARL ARNSTEIN
J. L. ATWOOD
PAUL S. BAKER
RALPH S. BARNABY
P. R. BASSETT
WELLWOOD E. BEALL
REX B. BEISEL
G. M. BELLANCA
DON R. BERLIN
HENRY A. BERLINER
WILLIAM BOLLAY
B. C. BOULTON
GEORGE W. BRADY
LYMAN J. BRIGGS
W. G. BROMBACHER
WILLIAM G. BROWN
CHARLES P. BURGESS
KENNETH CAMPBELL
CHARLES H. CHATFIELD
ALLAN CHILTON
V. E. CLARK
FRANKLIN R. COLLBOHM
CHARLES H. COLVIN
KARL T. COMPTON
EMERSON W. CONLON
JOHN W. CROWLEY, JR.
RALPH S. DAMON
LUIS DE FLOREZ
SMITH J. DE FRANCE
J. P. DEN HARTOG
WALTER S. DIEHL
JAMES H. DOOLITTLE
C. S. DRAPER
IVAN H. DRIGGS
WILLIAM K. EBEL
C. L. EGTVEDT
FREDERIC FLADER
CHARLES FROESCH
JACK FRYE
GARLAND FULTON
LESTER D. GARDNER
RICHARD C. GAZLEY
MICHAEL E. GLUHAREFF
MELVIN N. GOUGH
LEROY R. GRUMMAN
HAROLD R. HARRIS
R. M. HAZEN
ALBERT F. HEGENBERGER
EDWARD H. HEINEMANN
S. D. HERON
HALL L. HIBBARD
L. S. HOBBS
PAUL E. HOVGAARD
WILLIAM HOVGAARD
ROBERT INSLEY
EASTMAN N. JACOBS
CLARENCE L. JOHNSON
S. PAUL JOHNSTON
ALEXANDER KARTVELI
PAUL H. KEMMER
J. H. KINDELBERGER
OTTO E. KIRCHNER
ARTHUR L. KLEIN
ALEXANDER KLEMIN
W. B. KLEMPERER
PAUL KOLLSMAN
OTTO C. KOPPEN
B. V. KORVIN-KROUKOVSKY
S. M. KRAUS
I. M. LADDON
E. S. LAND
CHARLES L. LAWRANCE
JEROME LEDERER
JOHN G. LEE
JOHN C. LESLIE
CHARLES A. LINDBERGH
WILLIAM LITTLEWOOD
GROVER LOENING
ALBERT E. LOMBARD
W. RANDOLPH LOVELACE, II
EUGENE E. LUNDQUIST
R. D. MACCART
JOHN R. MARKHAM
ERLE MARTIN
WM. H. MCAVOY
C. J. MCCARTHY
CLARK B. MILLIKAN
ROBERT J. MINSHALL
JOSEPH S. NEWELL
ALFRED S. NILES
JOHN K. NORTHROP
ARTHUR NUTT
SHATSWELL OBER
ROBERT R. OSBORN
W. BAILEY OSWALD
GEORGE A. PAGE, JR.
F. W. PAWLOWSKI
F. W. PENNOYER, JR.
A. A. PRIESTER
ARTHUR E. RAYMOND
F. W. REICHELDERFER
ELLIOTT G. REID
H. J. E. REID
H. C. RICHARDSON
RUSSELL G. ROBINSON
LEONARD E. ROOT
C. E. ROSENDAHL
ADDISON M. ROTHROCK
WILLIAM T. SCHWENDLER
FRANCIS R. SHANLEY
JAMES M. SHOEMAKER
MAC SHORT
IGOR ALEXIS SIKORSKY
ABE SILVERSTEIN
SELDEN B. SPANGLER
ELMER A. SPERRY, JR.
JOHN STACK
WILLIAM B. STOUT
HARRY A. SUTTON
C. FAYETTE TAYLOR
EDWARD S. TAYLOR
PHILIP B. TAYLOR
TH. THEODORSEN
T. E. TILLINGHAST
S. TIMOSHENKO
L. B. TUCKERMAN
RALPH H. UPSON
J. PARKER VAN ZANDT
J. G. VINCENT
RICHARD VON MISES
FRANK L. WATTENDORF
P. V. H. WEEMS
FRED E. WEICK
R. D. WEYERBACHER
JOHN B. WHEATLEY
ANDREW V. WILLGOOS
DONALD H. WOOD
ROBERT J. WOODS
JOHN E. YOUNGER
ALBERT F. ZAHM
STEPHEN J. ZAND

An Appreciation
To Corporate Members of the Institute of the Aeronautical Sciences

Listed below are the leading aeronautical and industrial companies that make possible the publication of the *Journal of the Aeronautical Sciences*.

They enable the Institute to publish scientific and technical papers in the *Journal* and to devote its pages exclusively to editorial material.

Dues from individual members which would normally be used to publish this scientific and engineering monthly are thus released for additional services to the profession and industry.

The *Aeronautical Engineering Review* and the *Aeronautical Engineering Catalog*, together with the *Journal*, provide a comprehensive technical information service for the benefit of the aircraft and related industries.

Academy of Aeronautics, Inc.
Casey Jones School of Aeronautics
Aero Insurance Underwriters
Aerojet Engineering Corporation
Aeronca Aircraft Corporation
Aeroproducts Division, General Motors Corporation
Aeroquip Corporation
Agawam Aircraft Products, Inc.
Airborne Instruments Laboratory, Inc.
Airchox Company Division, Joyce Aviation, Inc.
Aircraft Radio Corporation
AiResearch Manufacturing Company
AiResearch Manufacturing Company of Arizona, Inc.
Allis-Chalmers Manufacturing Company
Allison Division, General Motors Corporation
Aluminum Company of America
American Airlines System
American Overseas Airlines, Inc.
American Bosch Corporation
American Phenolic Corporation
Associated Aviation Underwriters
Associated Foundries & Manufacturers, Inc.
Atlas Supply Company
Baker Steel & Tube Company
Beech Aircraft Corporation
Bell Aircraft Corporation
Bendix Aviation Corporation
Bendix Products Division
Bendix Radio Corporation
Eclipse-Pioneer Division
Export Division
Friez Instrument Division
Pacific Division
Scintilla Magneto Company
The BG Corporation
Boeing Aircraft Company
Breeze Corporations, Inc.
Essex Tool & Die Company
Federal Laboratories, Inc.
Cal-Aero Technical Institute, A Division of Grand Central Airport Company
Carrier Corporation
Cessna Aircraft Company
Chandler-Evans Division, Niles-Bement-Pond Company
Chase National Bank of the City of New York
The Cleveland Graphite Bronze Company
The Cleveland Pneumatic Tool Company
Automotive-Aircraft Division
Clifford Manufacturing Company
Consolidated Vultee Aircraft Corporation
Nashville Division
Stinson Aircraft Division
Continental Motors Corporation
Cox and Stevens Aircraft Corporation
Curtiss-Wright Corporation
Airplane Division
Development Division
Propeller Division
Wright Aeronautical Corporation
Doak Aircraft Company, Inc.
Douglas Aircraft Company, Inc.
El Segundo Plant
Long Beach Plant
The Dow Chemical Company
Dzus Fastener Company, Inc.
Eastern Air Lines, Inc.
Eaton Manufacturing Company
Thomas A. Edison, Incorporated, Instrument Division
Edo Aircraft Corporation

Electrol Incorporated
Engineering and Research Corporation
Ethyl Corporation
Fairchild Camera & Instrument Corporation
  Fairchild Aerial Surveys, Inc.
Fairchild Engine and Airplane Corporation
  Duramold Division
  Fairchild Aircraft Division
  Ranger Aircraft Engines Division
Federal Telephone and Radio Corporation
Firestone Aircraft Company
General Aviation Equipment Company, Inc
General Electric Company
The B. F. Goodrich Company
The Goodyear Tire & Rubber Company
Grumman Aircraft Engineering Corporation
W. & L. E. Gurley
The International Nickel Company
Irving Air Chute Company, Inc.
Jack & Heintz Precision Industries, Inc.
Johns-Manville Sales Corporation
Kaiser Fleetwings, Inc.
Walter Kidde & Company, Inc.
Kollsman Instrument Division, Square D Company
Lavelle Aircraft Corporation
Lear Incorporated
Link Aviation Devices, Inc.
The Liquidometer Corporation
Lockheed Aircraft Corporation
Longines-Wittnauer Watch Company, Inc.
The Glenn L. Martin Company
Warren McArthur Corporation
Menasco Manufacturing Company
Micromatic Hone Corporation
Minneapolis-Honeywell Regulator Company
Moore Drop Forging Company
National City Bank of New York
National Credit Office, Inc.
North American Aviation, Inc.
  North American Aviation, Inc., of Texas
Northrop Aircraft, Inc.
Northwest Airlines, Inc.
Owens-Corning Fiberglas Corporation
Pan American World Airways System
The Parker Appliance Company
Pesco Products Company Division, Borg-Warner Corporation
Phillips Petroleum Company
Pioneer Parachute Company, Inc.
Piper Aircraft Corporation
Pure Oil Co.
Radioplane Company
Republic Aviation Corporation
A. V. Roe Canada Limited
John A. Roebling's Sons Company
Rohr Aircraft Corporation
The Ryan Aeronautical Company
Scott Aviation Corporation
Shell Oil Company, Inc.
Simmonds Aerocessories, Inc.
Skydyne, Inc.
Socony-Vacuum Oil Company
Solar Aircraft Company
Sperry Gyroscope Company, Inc.
Square D Company
Standard Oil Company of California
Standard Oil Company (Indiana)
Standard Oil Company of New Jersey
The Texas Company
Thompson Products, Inc.
Tinnerman Products, Inc.
Trans World Airline
Union Carbide and Carbon Corporation
  Bakelite Corporation
  Haynes Stellite Company
  Linde Air Products Company
  National Carbon Company
United Aircraft Corporation
  Chance Vought Aircraft Division
  Hamilton Standard Propellers Division
  Pratt & Whitney Aircraft Division
  Pratt & Whitney Aircraft Corporation of Missouri
  Sikorsky Aircraft Division
United Air Lines, Inc.
United States Aviation Underwriters, Inc.
United States Rubber Company
  Dominion Rubber Company, Ltd.
Vickers, Inc.
The Waco Aircraft Company
Warner Aircraft Corporation
The Weatherhead Company
Western Air Lines, Inc.
Westinghouse Electric Corporation
Weston Electrical Instrument Corporation
Willys-Overland Motors, Inc., Aircraft Research and Development Division
Wyman-Gordon Company
Young Radiator Company

EDITORIAL COMMITTEE

HUGH L. DRYDEN, *Chairman*

Aerodynamics

Francis Clauser
Howard Emmons
R. Paul Harrington
R. T. Jones
W. B. Klemperer
Otto C. Koppen
John G. Lee
H. P. Liepmann
H. F. Ludloff
John R. Markham
Clark B. Millikan
Shatswell Ober
W. Bailey Oswald
Allen E. Puckett
Elliott G. Reid
H. J. E. Reid
Russell Robinson
L. E. Root
G. B. Schubauer
W. R. Sears
John Stack
Th. von Kármán
Richard von Mises

Air Transport

A. W. Dallas
Charles Froesch
J. A. Herlihy
Otto E. Kirchner
John C. Leslie

Aircraft Design

W. E. Beall
Rex B. Beisel
W. K. Ebel
Hall L. Hibbard
C. L. Johnson
I. M. Laddon
C. J. McCarthy
Fred E. Weick
Robert J. Woods

Physiologic Problems

H. G. Armstrong
Louis H. Bauer
Eugene Du Bois
W. Randolph Lovelace II
Ross A. McFarland
A. D. Tuttle

Aircraft Propulsion

George W. Brady
Frank W. Caldwell
L. S. Hobbs
E. E. Johnson
Joseph Keenan
R. P. Kroon
Arthur Nutt
Hans Reissner
Abe Silverstein
C. Fayette Taylor
E. S. Taylor
P. Taylor

Structures and Materials

W. B. Bleakney
E. W. Conlon
J. P. Den Hartog
L. H. Donnell
E. C. Hartmann
N. J. Hoff
H. L. Langhaar
E. E. Lundquist
C. F. Nagel, Jr.
J. S. Newell
Alfred S. Niles
W. Ramberg
E. Reissner
F. R. Shanley
H. W. Sibert
C. R. Strang
S. Timoshenko
H. S. Tsien
Chi-Teh Wang

Meteorology

C. F. Brooks
D. M. Little
E. J. Minser
F. W. Reichelderfer
H. C. Willett

Fuels and Oils

A. L. Beall
J. H. Doolittle
Graham Edgar
R. T. Goodwin
S. D. Heron
A. M. Rothrock

Instruments

Allan G. Binnie
W. G. Brombacher
J. Callahan
Charles H. Colvin
C. S. Draper
O. E. Esval
David W. Moore
W. A. Reichel
C. F. Savage
O. Hugo Schuck
R. Sylvander

Rotating Wing Aircraft

Robert Coleman
M. L. Deutsch
G. Horvay
Alexander Klemin
Ralph McClarren
R. H. Prewitt
Igor I. Sikorsky
Robert A. Wolf

Vibration and Flutter

Lee Arnold
M. A. Biot
William Bollay
J. P. Den Hartog
Manfred Rauscher

Flight Testing

William K. Ebel
R. R. Gilruth
Melvin N. Gough
Robert Stanley
E. A. Stout

I.A.S. REPRESENTATIVES TO OTHER ORGANIZATIONS

Aircraft Industries Association of America, Inc.—CHARLES MARCUS

American Association for the Advancement of Science—J. C. HUNSAKER

American Society of Mechanical Engineers—CHARLES H. COLVIN

American Standards Association—P. R. BASSETT

Engineering Society of Detroit—DONALD C. HUNT, GEORGE TWENEY

Greater New York Safety Council—WILLIAM LITTLEWOOD

Daniel Guggenheim Medal Board of Award—CHARLES H. COLVIN, GROVER LOENING, LESTER D. GARDNER

Institute of Radio Engineers—L. M. HULL

Manufacturers Aircraft Association—ARTHUR E. RAYMOND

National Aeronautic Association—WILLIAM R. ENYART

National Fire Protection Association—E. E. ALDRIN

National Research Council Engineering Division—HUGH L. DRYDEN

National Safety Council—JEROME LEDERER

New York Museum of Science and Industry—LESTER D. GARDNER

Society of Automotive Engineers—STEPHEN J. ZAND

JOURNAL OF THE AERONAUTICAL SCIENCES

VOLUME 14 AUGUST, 1947 NUMBER 8

A Survey of the Calculated Efficiencies of Jet Power Plants

JOSEPH H. KEENAN* AND JOSEPH KAYE†

Massachusetts Institute of Technology

ABSTRACT

The development of the gas turbine and of jet propulsion has indicated that aircraft power plants of the future will consist of various combinations of certain elements. These elements are propeller, diffuser, compressor, combustor, turbine, propulsive nozzle, and reciprocating engine. In order to bring the subject of aircraft power plants into somewhat better focus, the combinations of these elements which appear to be important have been studied for the effect of certain major variables, namely, pressure ratio, speed, and—to a lesser extent—maximum temperature and diffuser efficiency. An attempt is made to compare the efficiencies of moving power plants with stationary ones so as to give the whole subject some degree of coherence.

The principal reference lines for correlating the efficiencies of moving and stationary power plants are, aside from the axes of coordinates, the line of constant pressure ratio for compression to the temperature at turbine inlet, the line of constant efficiency for Carnot efficiency corresponding to atmospheric and turbine-inlet temperatures, and the curve for the simple gas turbine with reversible compressor and turbine—the last being also the curve of maximum efficiency for the moving turbopropeller with reversible propeller, diffuser, compressor, turbine, and exhaust nozzle, and being approximately the curve for the reversible ram-jet with infinitesimal fuel-air ratio.

The calculated efficiencies of ram-jet, turbojet, turbopropeller, and compound engine are compared between speeds of zero and 3,000 m.p.h.

METHOD

THE LABOR OF COMPUTATION was kept within reasonable bounds by the introduction of simplifying assumptions. These were selected so as not to sacrifice to any important degree the precision of the resulting data or the validity of the comparisons over the range of variables of greatest interest. Some of these assumptions cannot under all circumstances be defended. To show the effect of speed, for example, the efficiency is calculated at speeds for which the performance of certain elements is quite unknown. Nevertheless, the results of the calculations are shown and an effort is made to point out their limitations. Even where the curves do not show the performance of practicable systems they may serve to indicate the effects of certain variables.

The principal simplification consists of the substitution of a heating process for the combustion process. This substitution results in equal mass rates of flow in all elements, whereas in the real gas turbine the flow in the compressor is less than that in the turbine. It results also in the computation of the performance in terms of the efficiency—namely, work produced divided by heat supplied—instead of the specific fuel consumption—namely, fuel supplied divided by work produced. Although no simple general relation exists between the efficiency of the heat engine and the specific fuel consumption of the combustion gas turbine, the following equation is a good approximation in most instances:

$$s = 2{,}545/h^*\eta$$

where s denotes the specific fuel consumption in lbs. per hp.-hr.; h^*, the decrease in enthalpy per pound of fuel between a state consisting of liquid fuel and air and another at the same temperature consisting of gaseous products of complete combustion; and η, the efficiency of the power plant in which a heat transfer, which results in the same turbine-inlet temperature, is substituted for the combustion process.

The mass flow and the state of chemical aggregation of the fluid is the same in all processes when a heat transfer is substituted for combustion. This consideration makes it possible to view the entire process as part of a cycle that requires for its completion the restoration of the initial velocity and temperature, the restoration of the initial pressure being implied in the description of the power plant.

Presented at the Aircraft Propulsion Session, Fifteenth Annual Meeting, I.A.S., New York, January 28–30, 1947.

* Professor of Mechanical Engineering.

† Assistant Professor of Mechanical Engineering.

For a stationary power plant with negligible exhaust velocity or for a moving power plant with negligible exhaust velocity relative to a stationary observer, this final process of restoring the initial state consists only of a heat rejection from the working fluid. The efficiency of the power plant then becomes identical with the efficiency of the corresponding cycle. The efficiency of the cycle, in turn, is governed, as in all heat-engine cycles, by the temperatures at which heat is received and rejected and the degrees of irreversibility in the various processes.

For moving power plants with finite exhaust velocities relative to a stationary observer it is doubtful whether the discussion of cycles is fruitful. The interpretation of the cycle efficiency in terms of the power-plant efficiency must involve the kinetic energy of the exhaust relative to a stationary observer. Usually this additional complication destroys the utility of the method.

Assumptions

The following assumptions were made in all calculations:

(1) The fluid is air having properties as given by reference 1.

(2) The temperature of the air entering the power plant is −48°F. This is the value of atmospheric temperature at an altitude of 30,000 ft. as given by the altitude table of the N.A.C.A. in reference 2.

(3) The air entering a moving power plant is diffused reversibly and adiabatically, unless otherwise stated, to zero velocity.

(4) Upon leaving the turbine the air expands reversibly and adiabatically, unless otherwise stated, in a nozzle that ejects the stream backwards in the line of motion of the power plant.

(5) No changes in pressure occur between elements of the power plant or in any heater or regenerator.

Notations

The following notations are used in combination to describe the various power plants:

- B = combustor or the heater that is substituted for it
- C = compressor
- E = reciprocating engine, including geared supercharger that may be required to make the intake and exhaust pressures for E identical
- I = intercooler between stages of compression
- J = exhaust propulsive nozzle in combination with intake diffuser
- P = propeller operating in free stream
- T = turbine
- X = regenerator that exchanges heat between turbine exhaust and combustor intake

Subscripts

- r = reversibility of P, C, T, X, and J
- i = irreversibility in P, C, E, T, and X and, where so indicated, in J

The Stationary Power Plant

Reversible Cycles

The efficiency of reversible stationary power plants may be discussed, as explained previously, in terms of the corresponding heat-engine cycles. The efficiency of any reversible cycle η_r is given by

$$\eta_r = (\bar{T}_1 - \bar{T}_2)/\bar{T}_1 \qquad (1)$$

where $\bar{T}_1$ and $\bar{T}_2$ denote, respectively, mean temperatures of heat reception and rejection, weighted according to the changes in entropy. Any alteration in a cycle which increases $\bar{T}_1$ without increasing $\bar{T}_2$ or which decreases $\bar{T}_2$ without decreasing $\bar{T}_1$ will increase the efficiency of the cycle. Alterations of the opposite kinds will decrease the efficiency of the cycle.

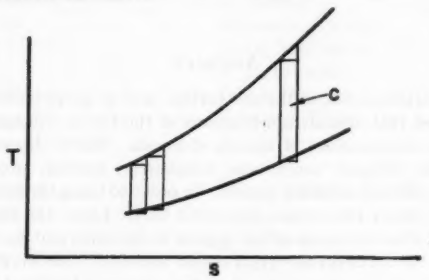

Fig. 1.

A cycle corresponding to the simple reversible system $(CBT)_r$ is shown on the temperature-entropy diagram of Fig. 1. This cycle may be subdivided into an infinite number of Carnot cycles as indicated. The efficiency of the cycle as a whole will lie between the efficiency of the best of these Carnot cycles and that of the worst. If air were to have a constant specific heat, and therefore a constant exponent in the expression relating the pressure and volume for isentropic change—namely,

$$pv^k = \text{constant}$$

then the efficiency of all these Carnot cycles would be identical, because the temperature ratio for each would be

$$r^{(k-1)/k}$$

where r denotes the pressure ratio. In this event the efficiency of the cycle would be fixed by the pressure ratio r and would be independent of the temperature at turbine inlet T_c.

The specific heat of air, however, is not constant. It increases with increase in temperature, so that k decreases and the temperature ratio decreases in consequence. Thus the Carnot cycles on the right in Fig. 1 are less efficient than those on the left. As the temperature at turbine inlet is increased for a fixed pressure ratio the efficiency of the cycle gradually decreases.

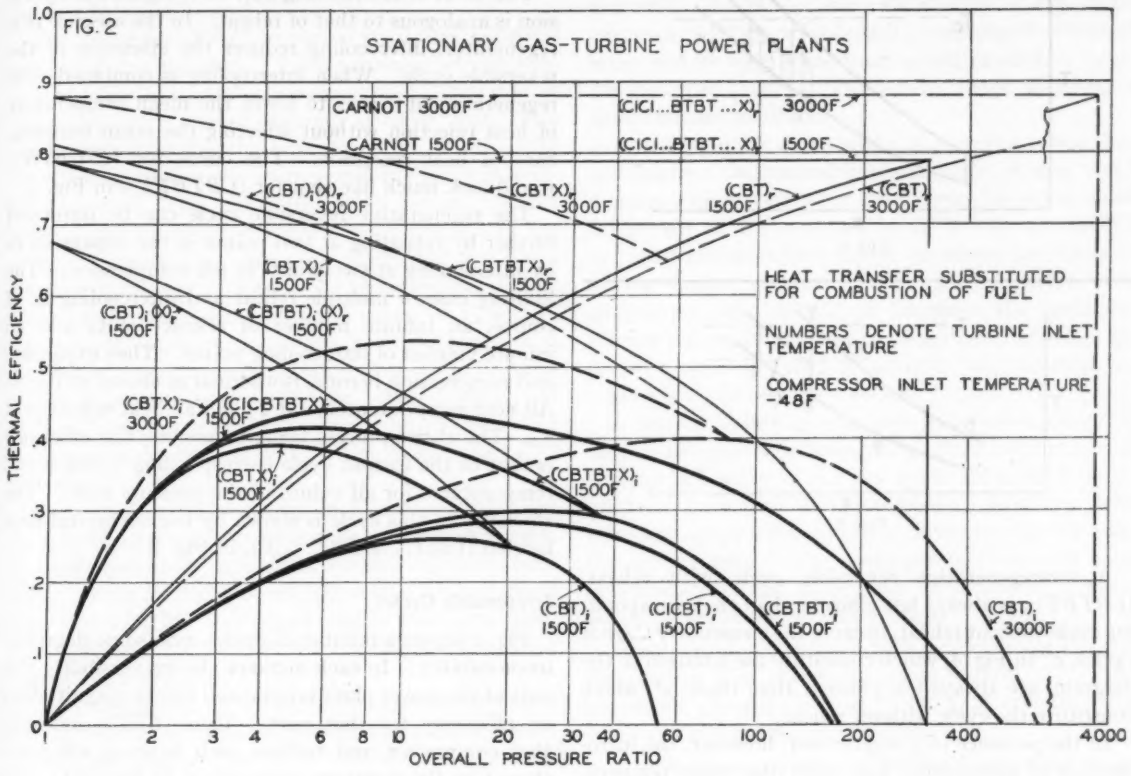

This characteristic is shown by the curves labeled $(CBT)_r$, in Fig. 2, in which the curve for a turbine-inlet temperature of 3,000°F. lies a little below that for 1,500° F.

The pressure ratio may be increased for a given turbine-inlet temperature until the temperature at compressor outlet is only infinitesimally less than that at turbine inlet, as shown by cycle 12341 of Fig. 3. Then the heat input along 23 occurs at temperature T_c and the heat rejection along 41 occurs at temperature T_a. The efficiency of the cycle is the Carnot efficiency corresponding to these two temperatures. This condition is shown at the right-hand extremity of each of the curves labeled $(CBT)_r$ in Fig. 2. Through these extreme points a curve (not shown in Fig. 2) could be drawn which would lie slightly above the curves for $(CBT)_r$ and would be joined by them at their extremities, which would represent Carnot efficiencies corresponding to the temperatures at compressor inlet and outlet at each pressure ratio.

When a reversible regenerator is added to $(CBT)_r$ to form $(CBTX)_r$ the cycle becomes 15781 in Fig. 3 with the regenerator heating the compressed air from 5 to 6 and cooling the exhaust from the turbine from 8 to 9. Heat input from the source occurs between 6 and 7, and heat rejection to the sink between 9 and 1. The mean temperature of heat input now lies between the temperatures at 6 and 7 instead of between those at 5 and 7, as in $(CBT)_r$, and the mean temperature of heat rejection lies between the temperatures at 9 and 1 instead of between those at 8 and 1. The efficiency, according to Eq. (1) is therefore improved.

It will be evident from Fig. 3 that as the pressure ratio for $(CBTX)_r$ decreases toward 1, the mean temperatures of heat reception and rejection approach, respectively, T_c and T_a, and the efficiency approaches the Carnot efficiency for those temperatures. This is shown by the left-hand extremities of the curves labeled $(CBTX)_r$ in Fig. 2. The right-hand extremity of a curve for $(CBTX)_r$ is the intersection with the curve for $(CBT)_r$. At this intersection the temperature at the turbine exhaust is the same as that at the compressor exit, states 5 and 6 in Fig. 3 are identical, and no regeneration is possible.

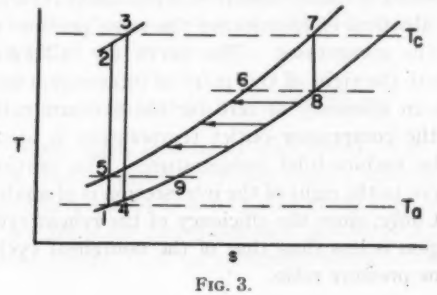

FIG. 3.

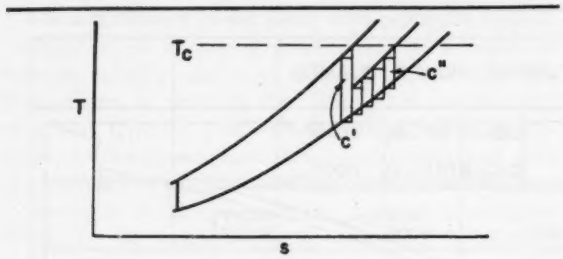

FIG. 4.

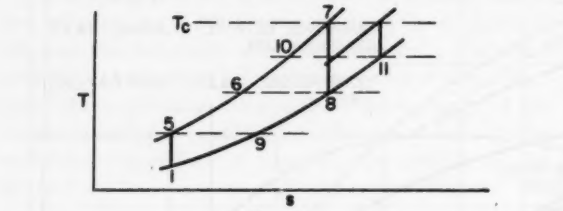

FIG. 5.

A nonregenerative reversible cycle with reheat, $(CBTBT)_r$, is always less efficient than the corresponding cycle without reheat, because the elementary Carnot cycles, c'' in Fig. 4, which constitute the addition to the diagram, are always less efficient than those, c', which constitute the cycle without reheat.

In the presence of a regenerator, however, the introduction of reheat does not affect the mean temperature of heat rejection. It serves only to raise the mean temperature of heat reception. In Fig. 5 heat rejection occurs between 9 and 1 with and without reheat, whereas heat reception occurs between the temperatures at 6 and 7 without reheat and between those at 10 and 7 with reheat.

For each pressure ratio across the compressor there is a best ratio of reheat pressure to turbine exhaust pressure. The curve labeled $(CBTBTX)_r$ in Fig. 2 shows the efficiency for this best condition. For a pressure ratio across the compressor of 1 all heat input occurs at T_c and all heat rejection at T_a with and without reheat. Therefore, the curves for $(CBTX)_r$ and $(CBTBTX)_r$ join at their left-hand extremities at the Carnot efficiency for the maximum and minimum temperatures. In the middle of Fig. 2 the curve for $(CBTBTX)_r$ crosses the curve for $(CBT)_r$ but does not, as for $(CBTX)_r$, end there. The intersection represents two different systems, namely $(CBT)_r$ and $(CBTBTX)_r$, having identical efficiencies for the same pressure ratio across the compressor. The curve for $(CBTBTX)_r$ extends to the right of this point of intersection until it reaches an efficiency of zero for the pressure ratio at which the compressor outlet temperature is identical with the turbine-inlet temperature. The portion of this curve to the right of the intersection is of analytical interest only, since the efficiency of the reheat cycle in this region is less than that of the nonreheat cycle for the same pressure ratio.

The effect of intercooling between stages of compression is analogous to that of reheat. In the absence of a regenerator, intercooling reduces the efficiency of the reversible cycle. When intercooling is combined with regeneration it serves to lower the mean temperature of heat rejection without affecting the mean temperature of heat reception. The curve for $(CICBTX)_r$ would look much like that for $(CBTBTX)_r$ in Fig. 2.

The regenerative reversible cycle can be improved further by reheating at two points in the expansion or by intercooling at two points in the compression. The limiting case of multiple reheat and intercooling is, of course, an infinite number of reheat points and an infinite number of intercooling points. Then expansion and compression become isothermal as shown in Fig. 6. All heat reception occurs at T_c and all heat rejection at T_a. The entire process being reversible, the efficiency is that of the Carnot cycle corresponding to these two temperatures for all values of the pressure ratio. The efficiency of this cycle is shown by the horizontal lines labeled $(CICI \ldots BTBT \ldots X)_r$ in Fig. 2.

Irreversible Cycles

Fig. 2 shows a number of cycles with some degree of irreversibility. In each instance the irreversibility of a part of the power plant is indicated by the magnitude of an efficiency for that part. Thus $(CBT)_i$ indicates that compressor and turbine each have an efficiency (based on the isentropic process) of 80 per cent. The heater B is considered to be the same as in $(CBT)_r$ except insofar as the temperature change of the air passing through it is affected by compressor efficiency. The symbol $(CBT)_i(X)_r$ indicates that a reversible regenerator, one with zero temperature differences across the heat-transfer surface, has been added to $(CBT)_i$. The symbol $(CBTX)_i$ indicates that the regenerator has an efficiency of 80 per cent, that is, 80 per cent as much heat is exchanged in the regenerator as in a reversible regenerator.

From the curves for 1,500°F. in Fig. 2 it may be observed that for given temperatures T_a and T_c at compressor and turbine inlets, respectively, the curves for all cycles, reversible and irreversible, lie within a rectangle formed by the axes of coordinates, the ordinate for the Carnot efficiency for T_a and T_c, and the

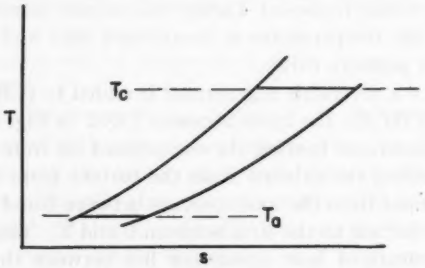

FIG. 6.

abscissa for the pressure ratio across an isentropic extending between T_a and T_c.

The curve for $(CBT)_t$ occupies the lower left-hand portion of this rectangle. For a turbine-inlet temperature of 1,500°F. it reaches a maximum of 26 per cent as compared with a Carnot efficiency of 79 per cent. This comparison indicates the high degree of sensitivity of the efficiency of the cycle to irreversibility in the individual processes. This sensitivity arises because the net work in the reversible cycle is a small fraction of the turbine work or the compressor work, and any small decrease in the one or increase in the other has a large effect on the net work. For fixed values of T_a and T_c the ratio of net work to turbine work decreases with increase in pressure ratio, and the sensitivity to irreversibility increases correspondingly. For 1,500°F. at turbine inlet and a pressure ratio of 53 the net work vanishes for compressor and turbine efficiencies of 80 per cent.

A rise in T_c without change in T_a serves to increase the ratio of net work to turbine work or compressor work, and correspondingly to reduce the sensitivity to irreversibility. Thus for 3,000°F. at turbine inlet the maximum efficiency for $(CBT)_t$ is 45 per cent of the Carnot efficiency, whereas for 1,500°F. it is only 33 per cent of the Carnot efficiency.

The introduction of a reversible regenerator into a system with irreversible compressor and turbine results in the curve labeled $(CBT)_t(X)_r$. This curve shows the greatest efficiency at a pressure ratio of 1, as does the curve for $(CBTX)_r$. The right-hand limit of the curve for $(CBT)_t(X)_r$ is the point of intersection with the curve for $(CBT)_t$. This intersection occurs at the pressure ratio for which the temperature at compressor outlet is the same as that at turbine outlet and the regenerator vanishes.

When a regenerator of 80 per cent efficiency is substituted for the reversible regenerator the efficiency is shown by the curve labeled $(CBTX)_t$. For a pressure ratio of 1 the efficiency is now zero because an infinitesimal work output per pound of fluid is obtained at the expense of a finite heat input. The irreversible regenerator vanishes, however, at the same pressure ratio as the reversible one, so that the curves for $(CBT)_t(X)_r$ and $(CBTX)_r$ intersect each other and the curve for $(CBT)_t$ at the same point.

Comparing the curves for $(CBT)_t$ and $(CBTX)_t$ both for 1,500°F. at turbine inlet, one observes that the effect of the introduction of the regenerator is an increase in the maximum efficiency and a decrease in the pressure ratio at maximum efficiency. Thus at 1,500°F. the maximum efficiency increases from 26 per cent to 38 per cent, and the pressure ratio for maximum efficiency decreases from 12 to 4.5.

It should be noted that irreversibility in the regenerator is limited in this discussion to incomplete heat exchange and does not include frictional effects in the regenerator. The frictional effects can be kept small only at the expense of added weight and size of the regenerator. If friction were allowed for in Fig. 2, the curve for $(CBTX)_t$ would reach a somewhat lower maximum and its right-hand limit would lie slightly below the curve for $(CBT)_t$. The general shape of the curve would remain unaltered.

Although in the absence of a regenerator reheat does not improve the reversible power plant, it may result in a small improvement in the irreversible power plant. A comparison of the curves for $(CBTBT)_t$ and $(CBT)_t$ in Fig. 2 indicates that reheat improves the efficiency at the higher pressure ratios. For a turbine-inlet temperature of 1,500°F. it increases the maximum efficiency from 26 per cent to 30 per cent, although the pressure ratio required to achieve the maximum increases from 12 to 25.

A similar result is obtained with intercooling, although the gain in efficiency is slightly less for a heat-transfer efficiency of 80 per cent. It should be remarked, however, that intercooling involves heat-transfer surface whereas reheat involves only an additional combustor in the actual gas turbine. For gains in efficiency of the same order of magnitude, reheat would be preferable to intercooling.

When reheat is combined with a regenerator the performance is that shown by curve $(CBTBTX)_t$. The maximum efficiency is now 42 per cent and the pressure ratio at this efficiency is about 6.

Regeneration, reheat, and intercooling constitute an entirely practicable combination for central-station or marine power plants. Curve $(CICBTBTX)_t$ in Fig. 2 shows that this combination may attain an efficiency of 44 per cent at a pressure ratio of 8. If pressure losses are allowed for in regenerator and intercooler, the maximum efficiency will be lowered somewhat. On the other hand, this effect could be cancelled by an improvement in the efficiencies of compressor and turbine above the assumed value of 80 per cent.

This latter system is now in process of development for marine propulsion in which it will doubtless play an important role. The efficiency of the marine power plant, however, will be appreciably less than the value of 44 per cent indicated in Fig. 2. In the marine plant the temperature at compressor inlet will average about 50°F., whereas for Fig. 2 it is −48°F. In the marine plant the present value of turbine-inlet temperature appears to be about 1,200°F., whereas for Fig. 2 it is 1,500°F. The maximum efficiency for the marine plant will be less than 35 per cent until the turbine-inlet temperature can be increased.

The Aircraft Power Plant

A power plant moving at high speed, as in aircraft, differs from a stationary power plant primarily in that a propulsive thrust or a drag may result from reception of a stream of air and rejection of a stream of products of combustion. The force corresponding to this thrust

or drag may be added algebraically to the thrust of the propeller, or, if a thrust, it may be used to supplant the propeller entirely.

Each of the power plants subsequently discussed is assumed to have at inlet a reversible diffuser (unless otherwise stated) which compresses the air stream to higher pressure and zero velocity before it enters the compressor or the combustor, as the case may be, and at outlet a reversible nozzle (unless otherwise stated) which exhausts the stream of products backwards in the line of motion of the airplane. Nozzles can be made so nearly reversible that the assumption of reversibility introduces, as a rule, no serious error. Diffusers will doubtless be somewhat lower in efficiency, but less is known about them.

The assumption of reversibility for the diffuser may be partially justified on two counts: first, it simplifies the calculations, and, second, it introduces no serious error except at extremely high speeds of flight. Where extremely high speeds of flight are discussed the effect of diffuser efficiencies less than 1 will be demonstrated.

In the letter code employed here for describing the power plants no separate symbol for the diffuser has been included. The symbol J may be taken to indicate the presence of a nozzle and diffuser in all systems.

The symbol P refers to a propeller which receives the excess of turbine power over compressor power. For a reversible propeller this entire excess becomes propulsive power—that is, the product of the speed of the airplane and its drag. An irreversible propeller $(P)_i$, unless otherwise stated, is assumed to convert 80 per cent of the excess into propulsive power—that is, the propeller efficiency is 80 per cent.

The remaining symbols have the same significance as in the stationary power plant.

The introduction of motion of the power plant greatly complicates the problem of power-plant performance. Two new independent variables appear, namely, the speed of the power plant and the velocity of the exhaust jet.

In order to show the effect of speed of the power plant a comprehensive set of curves is shown for each of the speeds 400 and 800 m.p.h. and a few curves are shown for 1,200 m.p.h. It is true that at speeds of 800 and 1,200 m.p.h. the assumed performance of certain elements of the power plant, such as the diffuser and the propeller, does not correspond to reality. Nevertheless, the values computed for these speeds illustrate certain effects of change of speed.

In each of these sets of curves the abscissa is the ratio of the pressure in the first heating chamber B to the pressure of the undisturbed atmosphere. This is not, as in the stationary power plant, the ratio of the pressures on either side of the compressor, because the pressure at compressor inlet is greater than the pressure of the undisturbed atmosphere by the amount of the pressure rise in the diffuser.

The ordinate is the highest efficiency that the system can attain at the given pressure ratio. The highest efficiency is limited, of course, by prescribed conditions as to speed, temperature at turbine inlet, efficiency of the elements, etc.

The term efficiency as applied here to moving power plants *is defined as the work of propulsion divided by the heat supplied in the element or elements B.* The work of propulsion is defined in turn as the product of the propulsive thrust and the distance through which the power plant moves.

The determination of the highest efficiency is often a complex process. For example, in a reheat system such as $(PCBTBTJ)_i$ there is for each jet speed a highest efficiency corresponding to a certain value of the pressure drop in the turbine before reheat. Of the series of such highest values corresponding to a series of jet speeds the greatest value was found and plotted.

In nonregenerative systems it may be shown that the jet velocity for maximum efficiency, the conditions before the last stage of turbine expansion being fixed, is given by

$$V_j = S/\eta_p\eta_t'$$

where V_j denotes the jet velocity for maximum efficiency, S the speed of the airplane, η_p the efficiency of the propeller, and η_t' the efficiency of that part of the turbine displaced by the exhaust nozzle. For low pressure ratios the efficiency of the turbine η_t may be substituted for η_t', but for high pressure ratios η_t' may be appreciably less than η_t because of reheat effect.

In regenerative systems the exhaust nozzle does not directly displace a part of the turbine, in that regeneration occurs between the turbine and the nozzle. The jet velocity for maximum efficiency is then not so simply expressed.

Reversible Jet Propulsion Systems

The performance of the simple turbojet $(CBTJ)_r$ with all elements reversible is shown in Fig. 7 for speeds of 400, 800, and 1,200 m.p.h. and for temperatures at turbine inlet of 1,500° and 3,000°F. In this system the compressor work must be identical with the turbine work because in the absence of a propeller all turbine work must be absorbed by the compressor.

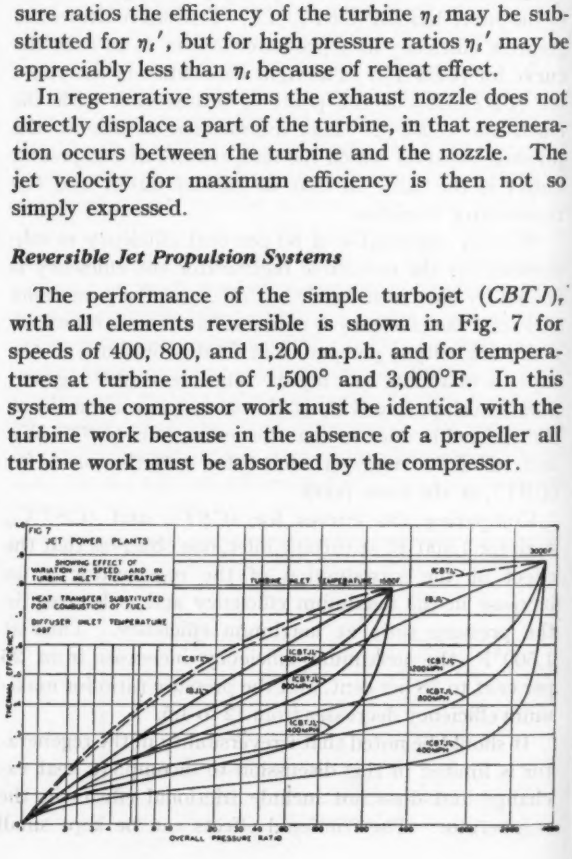

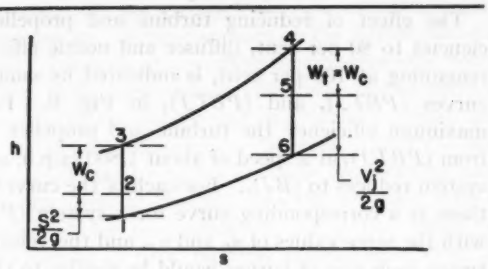

FIG. 8.

The processes of $(CBTJ)_r$ are shown in the enthalpy-entropy diagram of Fig. 8. The process 12 occurs in the diffuser, 23 in the compressor, 34 in the heater, 45 in the turbine, and 56 in the nozzle. The corresponding cycle for $(CBT)_r$ is 13461 with processes 13 and 46 in the compressor and turbine, respectively. The efficiency of $(CBT)_r$ was shown in Fig. 2 and is indicated again by the dash curves of Fig. 7. The efficiency of $(CBTJ)_r$ is the product of that for $(CBT)_r$ and a propulsive efficiency ϵ given by the expression

$$\epsilon = 2S/(V_j + S)$$

For a given pressure ratio and turbine-inlet temperature the efficiency of $(CBTJ)_r$ increases with the speed of the airplane, as shown by Fig. 7; the increase being entirely accounted for by the increase in ϵ. The value of ϵ has an upper limit, which is generally less than 1, corresponding to the speed for which

$$h_3 - h_1 = S^2/2g$$

so that the compressor is no longer required, as may be seen from Fig. 8. For this condition the turbine is not needed and the system reduces to $(BJ)_r$ or a reversible ram-jet.

The efficiency of $(BJ)_r$ for fixed temperature at combustor outlet is shown by the curves so labeled in Fig. 7. Along these curves the speed is a single function of the pressure ratio. Thus, for a pressure ratio of 5.4 the speed is 1,200 m.p.h., the speed for which the pressure ratio across the diffuser is 5.4. At this speed and pressure ratio $(BJ)_r$ and $(CBTJ)_r$ are identical and the corresponding curves intersect. The intersection is the left-hand limit of the curve for $(CBTJ)_r$.

The right-hand limit of the curve for $(CBTJ)_r$ is found at the pressure ratio for which the compressor outlet temperature has reached the prescribed turbine-inlet temperature. For this condition the heat input per pound of air is infinitesimal, V_j exceeds S by only an infinitesimal amount, and ϵ is 1. The efficiency is then the Carnot efficiency corresponding to the temperatures at diffuser inlet and turbine inlet.

For a fixed turbine-inlet temperature the various curves for $(CBTJ)_r$ at different speeds converge on the same right-hand limit as shown by Fig. 7. The curves for $(BJ)_r$ and $(CBT)_r$ have the same limit. The speed for $(BJ)_r$ at this limit may be extremely high—3,040 m.p.h. for a combustor exit temperature of 1,500°F.

An increase in turbine-inlet temperature results in an increase in the maximum efficiency (the Carnot efficiency) attainable by a reversible jet propulsion system, but the pressure ratio required to attain the maximum efficiency increases considerably, as shown in Fig. 7. For fixed airplane speed and pressure ratio the efficiency decreases with increase in turbine-inlet temperature. Almost all this decrease in efficiency may be accounted for by a decrease in ϵ which follows from the increase in nozzle jet velocity V_j.

Somewhat similar conclusions may be reached concerning the irreversible turbojet $(CBTJ)_i$. An increase in turbine-inlet temperature will result in an improvement in efficiency only if it is accompanied by a considerable increase in pressure ratio. For fixed airplane speed and for a pressure ratio below that of maximum efficiency, an increase in turbine-inlet temperature will cause a decrease in efficiency.

Ram-Jet Systems

In Fig. 9 curves are shown to represent the performance of ram-jet systems—that is, systems without a compressor. Since the pressure ratio for any ram-jet system is fixed by the speed of the airplane, the speed varies along each of these curves. A scale of speed is shown along the horizontal axis.

The curve labeled $(BJ)_r$ in Fig. 9 is identical with the similarly labeled curve in Fig. 7 for 1,500°F. at combustor outlet (turbine inlet). This represents the simple ram-jet system with reversible diffusion and expansion. Its efficiency is zero at zero speed and is the Carnot efficiency when the temperature at diffuser outlet is only infinitesimally less than that at combustor outlet.

The light dash curve labeled $(BJ)_r^0$ gives the maximum efficiency of a simple ram-jet with reversible diffusion and expansion. It differs from $(BJ)_r$ in that the temperature at combustor outlet is only infinitesimally greater than that at diffuser outlet. The value of ϵ is therefore unity, whereas for $(BJ)_r$ the value of ϵ is

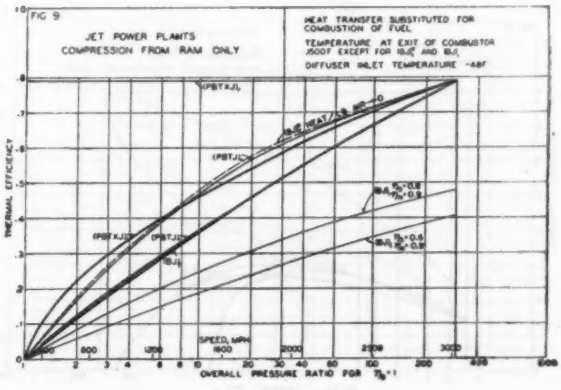

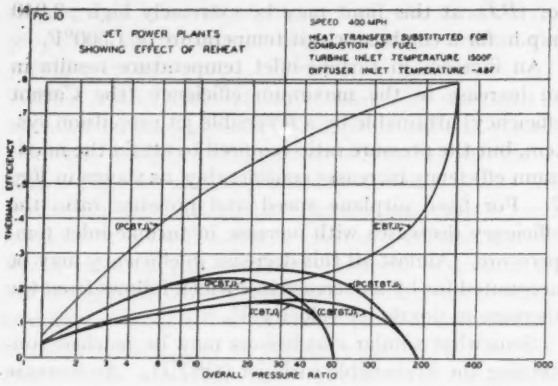

less than unity except at the right-hand extremity where $(BJ)_r$ and $(BJ)_r^0$ are identical. The ordinates of the curve for $(BJ)_r^0$ represent the Carnot efficiencies corresponding to the temperature and the stagnation temperature at diffuser inlet.

The two curves labeled $(BJ)_t$ in Fig. 9 represent ram-jets with irreversible diffusers and nozzles, the efficiencies of these elements being indicated in the figure. Each point on either of these curves gives the maximum efficiency for the ram-jet system in question. To get this maximum efficiency the temperature at combustor outlet must have the appropriate value and this value increases with decrease in diffuser efficiency. The ordinates of these curves are plotted against the speed scale on the abscissa axis—the pressure-ratio scale does not apply.

A ram-jet system may include a turbine and a propeller that receives the turbine work, but it cannot include either of these elements separately. The maximum efficiency of such a system is given by the curve labeled $(BJ)_r^0$, in Fig. 9 and it is attained, as in system $(BJ)_r^0$, when the heat input per pound of air is infinitesimal. Such systems must be infinite in size for finite thrust. For finite heat input per pound of air, system $(PBTJ)_r$ gives better efficiencies than $(BJ)_r$. The two curves so labeled in Fig. 9 are both for a temperature of 1,500°F. at combustor outlet. The distribution of pressure drop between turbine and nozzle is selected to give maximum efficiency.

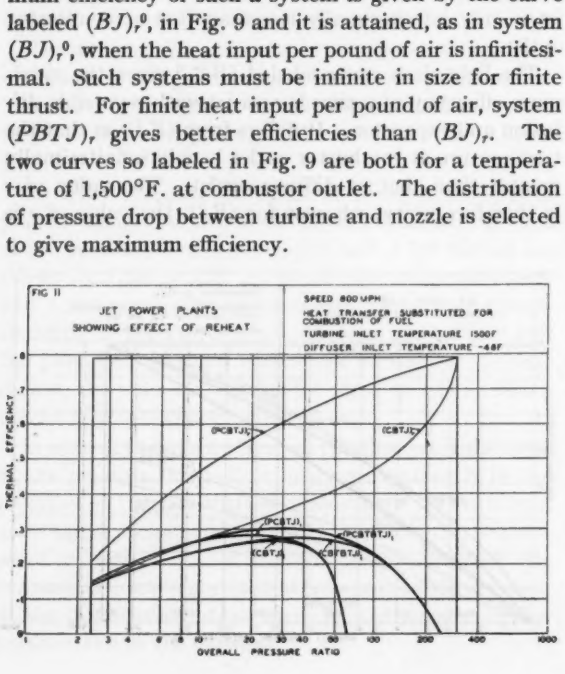

The effect of reducing turbine and propeller efficiencies to 80 per cent, diffuser and nozzle efficiencies remaining at 100 per cent, is indicated by comparing curves $(PBTJ)_r$ and $(PBTJ)_t$ in Fig. 9. For the maximum efficiency the turbine and propeller vanish from $(PBTJ)_t$ at a speed of about 1,800 m.p.h. and the system reduces to $(BJ)_r$. For each of the curves $(BJ)_t$ there is a corresponding curve for a system $(PBTJ)_t$, with the same values of η_D and η_N, and the relation between each pair of curves would be similar to that between curves $(PBTJ)_t$ and $(BJ)_r$ which are shown.

A regenerator may be added to a ram-jet system only in combination with a turbine and a propeller. In the reversible system, $(PBTXJ)_r$, Fig. 9, the maximum efficiency then becomes the Carnot efficiency at all speeds, but the propulsive work per pound of air becomes infinitesimal. When irreversibility is introduced into propeller, turbine, and regenerator (but not into diffuser and nozzle) by the usual efficiency of 80 per cent, the performance is given by the curve labeled $(PBTXJ)_t$. It should be noted that all curves for propeller efficiencies of 80 per cent or more are of only analytical interest at speeds above 600 m.p.h.

Nonregenerative Gas-Turbine Power Plants

Figs. 10 and 11 show the efficiency of certain nonregenerative gas-turbine power plants moving with speeds of 400 and 800 m.p.h., respectively. The turbine-inlet temperature is 1,500°F. As in Fig. 2 for the stationary power plant, the entire set of curves lies within a rectangular frame bounded by the axes of coordinates (efficiency zero and pressure ratio unity), the ordinate for Carnot efficiency corresponding to temperatures at diffuser inlet and turbine inlet, and the pressure ratio corresponding to isentropic compression between these two temperatures.

Diagonally across this framed area lies the lightweight curve, labeled $(CBT)_r$ in Figs. 2 and 7, which represents the efficiency of the simple reversible gas-turbine cycle. This same curve now represents the efficiency of system $(PCBTJ)_r$ at its best, that is, a reversible gas turbine driving a reversible propeller and exhausting through a nozzle the velocity in which exceeds the airplane speed by only an infinitesimal amount.

For the conditions just described the position of the curve for $(PCBTJ)_r$ is independent of the speed of the airplane. For any value of the pressure ratio it is applicable to any speed from zero up to that for which the compressor vanishes because the entire pressure rise occurs across the diffuser. Thus, this same curve represents the performance of the limiting system $(PBTJ)_r$, the speed of which is a function of the pressure ratio only.

The efficiency of the reversible turbojet $(CBTJ)_r$ is also shown by a lightweight line in Fig. 10. The two lightweight lines on this figure constitute a pair of lines from Fig. 7 appropriate to the conditions of Fig. 10.

The curve for the turbojet $(CBTJ)_t$ with irreversible compressor and turbine appears as the lowest curve in Fig. 10. It begins at the left at the pressure ratio corresponding to the pressures on either side of the diffuser. At this point the compressor and turbine vanish and with them the distinction between $(CBTJ)_r$ and $(CBTJ)_t$. Thus the curves for these two systems have a common limit at the left. As the pressure ratio is increased above this minimum value the curve for $(CBTJ)_t$ rises at first, but less rapidly than that for $(CBTJ)_r$. It reaches a maximum efficiency and then falls to zero efficiency at the pressure ratio for which the velocity of the jet is no greater than the speed of the airplane, the potential excess having been dissipated by irreversibility in compressor and turbine.

When a propeller is added to the turbojet *CBTJ* to make system *PCBTJ*, the power delivered by the turbine is no longer fixed by the power requirement of the compressor but is merely limited to values greater than that. The greater the power delivered by the turbine for a fixed pressure ratio, the less will be the jet velocity V_j. Thus the upper limit for turbine power is that corresponding to a jet velocity of zero. The distribution of pressure drop between turbine and jet for the curves of Figs. 10 and 11 is determined by selecting for the jet velocity the value corresponding to maximum efficiency, as given by the relation

$$V_j = S/\eta_p\eta_t'$$

which was explained above.

The curve for $(PCBTJ)_t$ in Fig. 10 begins at the pressure ratio of diffusion at an efficiency lower than that for the corresponding reversible system $(PCBTJ)_r$. The ratio of the two is somewhat less than the propeller efficiency. As the pressure ratio increases the efficiency of system $(PCBTJ)_t$ increases to a maximum, being always greater than for $(CBTJ)_t$. As the pressure ratio increases beyond the value for maximum efficiency the amount of shaft work available to the propeller decreases. When the propeller work becomes zero the curves for $(CBTJ)_t$ and $(PCBTJ)_t$ meet at a point of tangency and the latter ends at this point.

The gain in efficiency resulting from the addition of a propeller to a jet propulsion system is evident from a comparison of the curves for $(CBTJ)_t$ and $(PCBTJ)_t$ in Figs. 10 and 11. It will also be seen from a comparison of Figs. 10 and 11 that the gain resulting from the addition of a propeller is less at higher speeds. In practice this effect of increase in speed from 400 to 800 m.p.h. will be even greater because of the decrease in propeller efficiency. In both Figs. 10 and 11 the propeller efficiency is assumed to be 80 per cent.

The effect of reheat in a moving power plant is shown in Figs. 10 and 11. As in the stationary power plant, the reversible nonregenerative systems cannot be improved by reheat, but some improvement can be shown for irreversible systems, particularly if the pressure ratio is increased when reheat is introduced. At 400

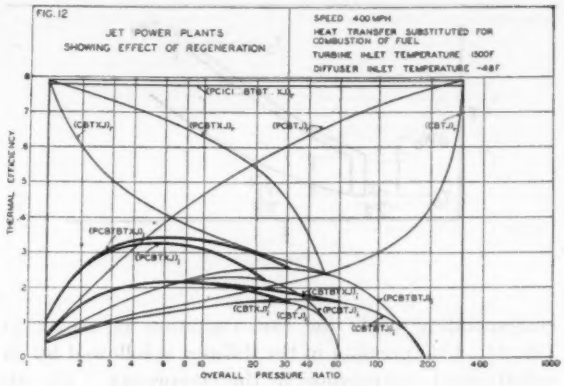

m.p.h. the maximum efficiencies for propeller systems with and without reheat are 25.5 and 23 per cent, respectively—a gain of 10 per cent. The corresponding pressure ratios are 25 and 14, respectively. The gains from reheat in the turbojet are smaller.

In the reheat calculations the efficiency of the portion of the turbine before reheat and that after reheat were each taken to be 80 per cent, whereas in the absence of reheat the efficiency of the whole turbine was taken to be 80 per cent. These assumptions favor the reheat system in that a turbine without reheat having two parts in series, each of 80 per cent efficiency, would have an efficiency greater than 80 per cent.

Regenerative Gas-Turbine Power Plants

Figs. 12 and 13 show the efficiency of certain regenerative gas-turbine power plants moving with speeds of 400 and 800 m.p.h., respectively. The turbine-inlet temperature is 1,500°F. The curves of Fig. 12 lie within the same frame as those of Fig. 10 and the curves of Fig. 10 are reproduced in Fig. 12 with lightweight lines.

The curves for certain reversible regenerative power plants are also shown by lightweight lines in Fig. 12. The curve for the regenerative turbojet $(CBTXJ)_r$ has its left-hand limit at the Carnot efficiency corresponding to T_a and T_c and at the pressure ratio corresponding to the pressures at either end of the diffuser. The

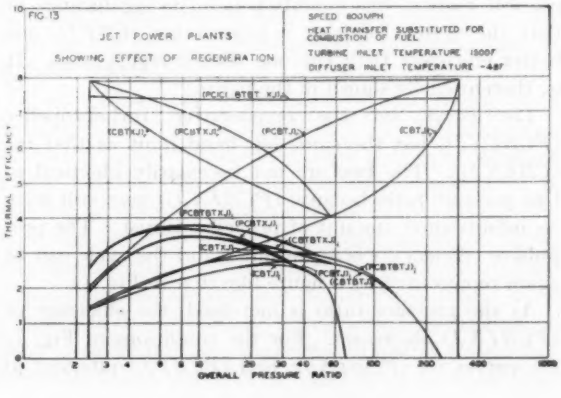

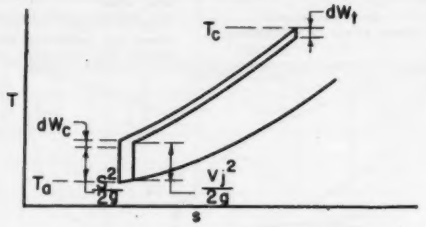

FIG. 14.

corresponding cycle for this condition is shown in Fig. 14. Compression in the diffuser is followed by an infinitesimal compression in the compressor. The air from the compressor is heated in the regenerator to within an infinitesimal interval of the temperature T_c, the final interval being added in the heater B. The work of compression is provided by expansion in the turbine through an interval of pressure smaller than that in the compressor. The exhaust from the turbine enters the regenerator and leaves it at the temperature of the compressor outlet and at a pressure slightly greater than that of the diffuser outlet. Thus the jet velocity V_j will exceed by an infinitesimal amount the airplane speed S because both pressure and temperature are infinitesimally greater at nozzle inlet than at diffuser outlet. These processes may be treated as parts of a reversible cycle since the propulsive efficiency

$$\epsilon = 2S/(V_j + S)$$

is unity. Since all heat input occurs at T_c and all heat rejection at T_a the efficiency of the cycle is the Carnot efficiency corresponding to these two temperatures.

The right-hand limit of the curve for $(CBTXJ)_r$ is the point of intersection with the curve for $(CBTJ)_r$. At this point the temperature at turbine exhaust is identical with that at compressor outlet, the regenerator vanishes, and systems $(CBTJ)_r$ and $(CBTXJ)_r$ become identical.

The curve for $(CBTXJ)_r$ could be extended to the right of this point of intersection, but beyond the intersection the turbine exhaust temperature is less than the compressor outlet temperature and the direction of heat flow in the regenerator is reversed. Despite its possible reality, this condition is of no significance in that the system without a regenerator $(CBTJ)_r$ has better efficiency than the one with a regenerator. It is, therefore, not shown in the figure.

The curve for the regenerative turbopropeller $(PCBTXJ)_r$ has the same left-hand limit as that for $(CBTXJ)_r$. The two are not necessarily identical at this pressure ratio because $(PCBTXJ)_r$ may still have an infinitesimal amount of propeller thrust. The propulsive efficiency ϵ is again unity and the cycle can be again represented by a figure like that in Fig. 14.

As the pressure ratio is increased, the efficiency of $(PCBTXJ)_r$ decreases. For the conditions of Fig. 12 the curves for $(PCBTXJ)_r$ and $(PCBTJ)_r$ intersect at a pressure ratio of about 18. Unlike the intersection of the curves for the jet propulsion systems with no propeller, this intersection does not correspond to the disappearance of the regenerator. It represents two systems, a regenerative one and a nonregenerative one, of equal efficiency.

The curve for $(PCBTXJ)_r$ extends to the right of this point of intersection in two branches. The lower branch corresponds to normal regenerative action in which the exhaust from the turbine is used to heat the air from the compressor. The upper branch corresponds to reversed regenerative action in which the heat flows in the opposite direction. This is not shown in Figs. 12 and 13. The lower branch ends upon intersecting the curve for $(CBTJ)_r$. At the pressure ratio corresponding to this intersection the best normal regenerative system has vanishingly small regenerative and propeller effects.

These branches of the curve for $(PCBTXJ)_r$ are of little significance because better efficiencies may be obtained at any pressure ratio by eliminating the regenerator, as indicated by the relative position of the curve for $(PCBTJ)_r$ in Fig. 12. The essential distinction between the curves for $(PCBTXJ)_r$ and that for $(PCBTJ)_r$ is that in the former the temperature at the inlet to the propulsive nozzle is so restrained that it is always equal to the temperature at compressor outlet.

Curves for the reversible reheat systems $(CBTBTXJ)_r$ and $(PCBTBTXJ)_r$ are omitted from Figs. 12 and 13 in the interest of simplicity. The positions of these lines relative to their nonreheat counterparts would be approximately as for systems $(CBTBTX)_r$ and $(CBTX)_r$ in Fig. 2. That is, the curves for reheat and nonreheat would have a common left-hand limit and would diverge to the right—the reheat curve lying above the other.

As in the stationary power plant, the regenerative reversible cycle can be improved further by reheating at two points in the expansion or by intercooling at two points in the compression. The limiting case of multiple reheat and intercooling is an infinite number of reheat points and an infinite number of intercooling points. The expansion and compression become isothermal as shown in Fig. 15.

The processes in the diffuser and in the nozzle, however, remain isentropic. If these were to coincide, then the efficiency of the hypothetical cycle would be

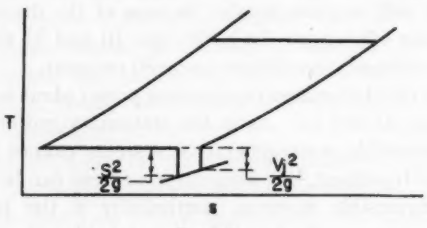

FIG. 15.

the Carnot efficiency corresponding to the temperatures in compressor and turbine. If the pressure at turbine exhaust is made less than that at compressor inlet, then some heat rejection would occur in the hypothetical cycle at temperatures below the compressor temperature. This effect in itself is beneficial but it reduces the efficiency of jet propulsion ϵ and results in fact in a net drag from diffuser and nozzle. The nearly horizontal curve labeled $(PCICI \ldots BTBT \ldots XJ)_t$ in Fig. 12 shows for each value of the pressure ratio the greatest efficiency for a system of this sort. The turbine exhaust pressure for greatest efficiency is always slightly less than the compressor inlet pressure and the nozzle thrust is always slightly less than the diffuser drag. Consideration of Fig. 15 makes it evident that, as the pressure ratio increases, the efficiency will approach from higher values the Carnot efficiency corresponding to compressor temperature and turbine temperature.

The heavy lines of Fig. 12 show the efficiency of practicable regenerative systems. The left-hand limit of each curve is at the diffuser pressure ratio. The right-hand limit is the intersection with the corresponding nonregenerative curve. The regenerative curves actually extend beyond these points of intersection. For the jet propulsion systems the extension corresponds to reversed operation of the regenerator. For the systems with propeller the extension consists of two branches as for the corresponding reversible system. As in the reversible system, however, these extensions of the curves are of no practical significance, because for the same pressure ratio the curves for a nonregenerative system show higher efficiency.

As in the stationary power plant, the effect of the regenerator is to increase the maximum value of the efficiency and to lower the pressure ratio at which the maximum occurs. The maximum efficiencies for systems $(PCBTXJ)_t$ and $(PCBTBTXJ)_t$ are 33 and 35 per cent, respectively, at 400 m.p.h. The corresponding pressure ratios are 5.5 and 6.5.

A comparison of Fig. 12 for 400 m.p.h. with Fig. 13 for 800 m.p.h. shows that an increase in speed reduces the range of values of the maximum efficiency for the various irreversible systems. That is, the higher the speed, the better the simple turbojet $(CBTJ)_t$ as compared with the more complex systems.

If an intercooler is introduced into these regenerative systems to make, for example, systems $(PCICBTXJ)_t$ and $(PCICBTBTXJ)_t$, the curves will lie slightly higher at higher pressure ratios than those for the same system without the intercooler. Both intercoolers and regenerators, however, are massive elements that increase considerably the weight of the power plant. It appears that the intercooler is somewhat worse in this respect, for equal improvements in efficiency, than the regenerator. To date it has not been proved that the weight of a regenerator can be justified by the improvement in efficiency that it brings. Further development of lightweight heat exchangers for high-temperature service may make the regenerator a practicable device. Intercoolers of the conventional type will become practicable, if at all, at a later date.

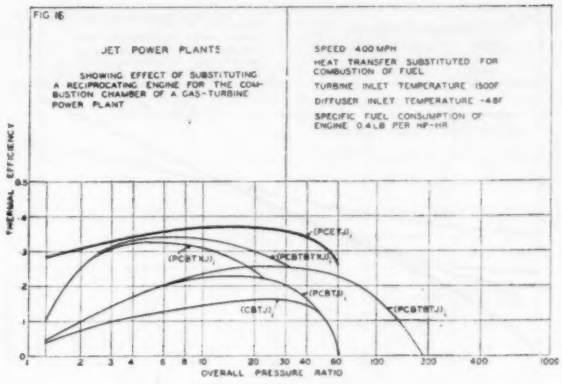

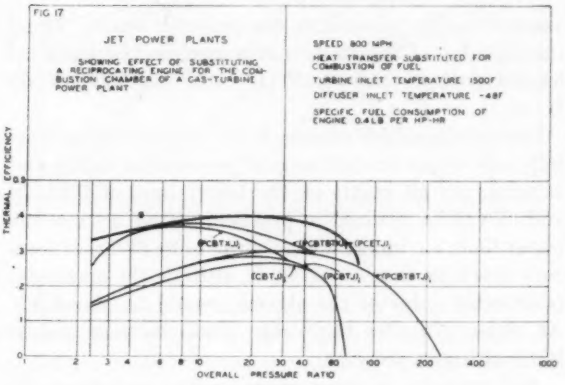

Substitution of Reciprocating Engine for Combustor

The heavy lines of Figs. 16 and 17, $(PCETJ)_t$, show the performance of a moving power plant when a reciprocating engine E is substituted for the usual combustor B. For these curves the reciprocating engine is assumed to have equal pressures at intake and exhaust. If the intake-manifold pressure is greater than the exhaust-manifold pressure, then the engine E must include a geared supercharger that provides the necessary difference in pressure between the outlet of compressor C and the intake manifold. The abscissa scale is the ratio of the pressure at compressor outlet to that at diffuser inlet.

The specific fuel consumption of the engine E is assumed to be 0.4 lb. per hp.-hr. In all systems not involving E it was assumed that heat was supplied rather than fuel, so that the rise in temperature in B was not accompanied by an increase in the mass rate of flow. In order to make the calculations involving E correspond with those involving B, it was assumed that in place of each pound of fuel 19,450 B.t.u. of heat were supplied to E. Of this amount 20 per cent was assumed to be transferred to the atmosphere in cooling the engine. Simultaneously, 2544/0.4 or 6,360 B.t.u. of work were

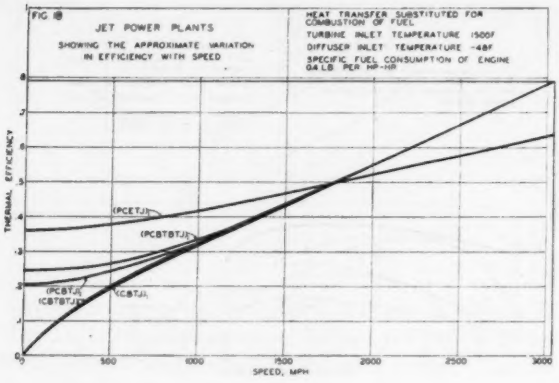

assumed to be delivered to the propeller shaft. Thus, the enthalpy of the air stream is increased between inlet and outlet of E by 19,450 (1 − 0.2) − 6,360 or 9,200 B.t.u.

Since the available engines E can be operated successfully only over a limited range of pressures at intake and exhaust, not all points on the heavy lines of Figs. 16 and 17 can be realized in practice. If we assume the upper limit for intake and exhaust to be 50 in. of mercury absolute, then at 30,000 ft. altitude the maximum practicable value of the abscissa would be about 5.5. At higher altitudes this value would increase and at lower altitudes decrease.

For purposes of comparison, curves are shown by lightweight lines for some systems with the simple combustor B. Of these only one, *CBTJ*, has been reduced to practice. The efficiency of *PCETJ* is two or more times the best efficiency of *CBTJ* at a speed of 400 m.p.h., as shown by Fig. 16. As the speed is increased *CBTJ* improves more rapidly than *PCETJ*, so that at 800 m.p.h., as shown by Fig. 17, the difference is less than 40 per cent.

The gas-turbine power plant now in process of development is system *PCBTJ*. At 400 m.p.h. this may attain an efficiency of 23 per cent as compared with about 33 per cent for *PCETJ*. The reheat system *PCBTBTJ* may prove to be the next step in the program of development. This is also shown in Figs. 16 and 17.

Two curves are shown for regenerative gas-turbine systems. These attain efficiencies approximating those of *PCETJ*. It should be remembered, however, that a regenerator is a heavy piece of equipment that can be justified only for flights of relatively long duration, if at all. The engine E is also heavy, but it differs from the regenerator X in that it delivers additional work.

At present, regenerative systems are probably not practicable for aircraft propulsion. They will become practicable when the thickness of heat-transfer surfaces can be reduced to not more than a few thousandths of an inch.

It has sometimes been stated that a power plant comprising a gas turbine and a reciprocating engine will be at best a compromise system that might be employed during the transition from the reciprocating to the rotating power plant. To demonstrate this point reference is sometimes made to the combination reciprocating and turbine engines which appeared for a time in steam power plants during a transition stage of their development. The analogy, however, is imperfect in that the steam turbine was suited to higher maximum temperatures than the reciprocating steam engine, whereas the gas turbine is limited to much lower maximum temperatures than the reciprocating internal-combustion engine. The substitution of E for B raises the temperature at the beginning of the expansion of the gases by thousands of degrees. This increase in temperatures is the principal reason for the high efficiency of system *PCETJ*.

Variation of Efficiency with Speed

For the more practicable of the power-plant systems discussed above the variation of the calculated efficiency with speed is shown in Fig. 18. For each of these systems the efficiencies of diffuser and nozzle are each 100 per cent, and the efficiencies of propeller, compressor, and turbine are each held constant at 80 per cent. The pressure ratio is varied with speed along the curves of Fig. 18 so as to give the maximum efficiency at each speed.

It may be seen from Fig. 18 that even if the propeller efficiency could be maintained at the high value of 80 per cent, a propeller could not be justified at speeds in excess of 1,000 m.p.h. because of the high efficiency of jet propulsion at those speeds. For this reason the curves for all the systems without the element E converge at the higher speeds. At a speed slightly in excess of 3,000 m.p.h. the temperature at diffuser exit is 1,500°F. Since this is the value that was fixed by assumption at the outlet of the combustor, the amount of heat added (or fuel burned) can be only infinitesimal. The efficiency then is the Carnot efficiency corresponding to 1,500°F. and the temperature at diffuser inlet.

The line for *PCETJ* is much flatter than the corresponding lines for the systems without the element E. The high efficiency of work production in E requires for maximum overall efficiency that a large fraction of the propulsion work should be provided by the propeller. Because the propeller efficiency is assumed constant, the change in efficiency with speed results only from the change in the efficiency of the jet portion of the propulsive work.

At speeds above 1,800 m.p.h. the efficiency of jet propulsion is so much better than that of the *PE* combination that system *PCETJ* has lower efficiency than the systems without the element E.

The assumptions upon which the curves of Fig. 18 are based are defective in several respects. The diffuser efficiency is assumed to be 100 per cent. This value is probably a satisfactory approximation at low speeds for

systems other than ram-jets, but it is doubtless greatly in error for all systems at high speeds. The propeller efficiency is assumed to be 80 per cent, which is a satisfactory approximation for certain intermediate speeds but not for extremely low or extremely high speeds.

In order to obtain curves with some practical validity over a wide range of speeds, the efficiencies of diffuser and propeller were each taken to be functions of speed expressed as Mach Number. The selected variation in diffuser efficiency is shown in Fig. 19 by the heavy line. For comparison the light line shows the variation in diffuser efficiency corresponding to a transverse shock at intake velocity in combination with a reversible subsonic diffuser. It seems probable that the values given by the light line can be exceeded in practice at Mach Numbers greater than 2. The selected variation in propeller efficiency is shown in Fig. 20. This is intended to represent the envelope of the efficiency curves for a series of propellers with practicable disc loadings. At low speeds, because the thrust is finite at zero speed, the efficiency approaches zero along with the speed. At higher speeds, because of compressibility effects, the efficiency falls as the speed approaches that of sound.

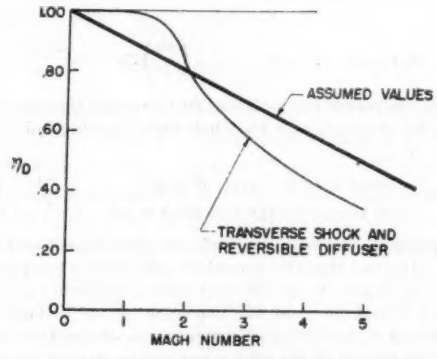

FIG. 19. Diffuser efficiencies.

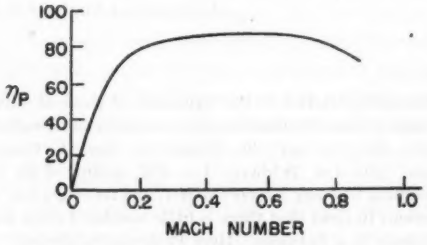

FIG. 20. Propeller efficiencies for Fig. 21.

Values from Figs. 19 and 20 and a constant nozzle efficiency of 90 per cent were used in computing the performance of several practicable systems. The results are shown in Fig. 21 plotted against a speed scale which is warped so as to spread out the low-velocity range at the expense of the high-velocity range.

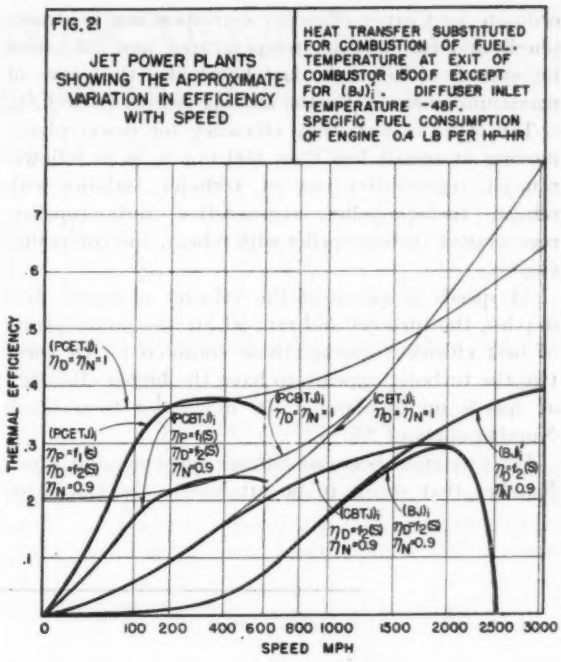
FIG. 21
JET POWER PLANTS SHOWING THE APPROXIMATE VARIATION IN EFFICIENCY WITH SPEED
HEAT TRANSFER SUBSTITUTED FOR COMBUSTION OF FUEL. TEMPERATURE AT EXIT OF COMBUSTOR 1500F EXCEPT FOR $(BJ)_i$. DIFFUSER INLET TEMPERATURE -48F. SPECIFIC FUEL CONSUMPTION OF ENGINE 0.4 LB PER HP-HR
THERMAL EFFICIENCY
.7
.6
.5
.4
.3
.2
.1
$(PCETJ)_i$ $\eta_D=\eta_N=1$
$(PCETJ)_i$ $\eta_P=f_1(S)$ $\eta_D=f_2(S)$ $\eta_N=0.9$
$(PCBTJ)_i$ $\eta_P=f_1(S)$ $\eta_D=f_2(S)$ $\eta_N=0.9$
$(PCBTJ)_i$ $\eta_D=\eta_N=1$
$(CBTJ)_i$ $\eta_D=\eta_N=1$
$(CBTJ)_i$ $\eta_D=f_2(S)$ $\eta_N=0.9$
$(BJ)_i$ $\eta_D=f_2(S)$ $\eta_N=0.9$
$(BJ)_i$ $\eta_D=f_2(S)$ $\eta_N=0.9$
0 100 200 400 600 800 1000 1500 2000 2500 3000
SPEED MPH

Two curves are shown in Fig. 21 for the ram-jet, the lower one being for a fixed temperature of 1,500°F. at combustor outlet, the upper one being for the temperature corresponding to maximum efficiency. Since the curve for $(CBTJ)_i$ is for a fixed temperature of 1,500°F. at turbine inlet, this curve and the lower ram-jet curve meet in a point of tangency when the optimum pressure drop across the turbine in the turbojet is zero.

The curves of Fig. 21 show that as the speed increases from zero the propeller systems gain efficiency much more rapidly than the pure jet systems. The efficiencies of the propeller systems reach their maxima at speeds between 400 and 500 m.p.h. and decline with further increase in speed.

The high efficiency—namely, 37 per cent—attained by the compound system $(PCETJ)_i$ at subsonic speeds is not attained by any alternative system shown except for the ram-jet at speeds in excess of 2,500 m.p.h. At intermediate speeds the turbojet gives highest efficiency between 700 and 1,800 m.p.h. At about 1,800 m.p.h. turbojet and ram-jet have equal efficiency at a calculated value of 29 per cent.

Conclusions

A comprehensive representation of the efficiency of moving power plants is of necessity more complex than a correspondingly comprehensive representation of the efficiency of stationary power plants.

The principal reference lines for correlating the efficiencies of moving and stationary power plants are, aside from the axes of coordinates, the abscissa for compression to the temperature at turbine inlet, the

ordinate for Carnot efficiency corresponding to atmospheric and turbine-inlet temperatures, and the curve for system $(CBT)_r$—the last being also the curve of maximum efficiency for the moving system $(PCBTJ)_r$.

The order of increasing efficiency for power plants moving at speeds less than 600 m.p.h. is as follows: ram-jet, regenerative ram-jet, turbojet, turbojet with reheat, turbopropeller, regenerative turbopropeller, regenerative turbopropeller with reheat, and compound engine.

At speeds in excess of the velocity of sound (680 m.p.h.), the turbojet and ram-jet are the power plants of best efficiency among those considered. Of these two the turbojet appears to have the higher efficiency at speeds up to about 1,700 m.p.h., or to a Mach Number of about 2.5.

For a relation between diffuser efficiency and Mach Number that seems to be attainable, the calculated efficiency of the ram-jet increases with speed to Mach Numbers greater than 4.5.

Acknowledgments

The study presented here was made for the United Aircraft Corporation, which has kindly granted permission to publish. John G. Lee, Assistant Director of Research for the United Aircraft Corporation, proposed the topic and aided the work by providing not only collateral data but guidance and encouragement as well.

References

[1] Keenan, Joseph H., and Kaye, Joseph, *Thermodynamic Properties of Air;* John Wiley & Sons, Inc., New York, 1945.

[2] Diehl, Walter S., N.A.C.A. Report No. 218, 1925.

Letters to the Editor

Dear Sir:

In a recent Letter to the Editor in the JOURNAL OF THE AERONAUTICAL SCIENCES, April, 1947, by Prof. David T. Williams, a discussion of the propulsive efficiency of rockets was made. Because of the assumption that the useful work was equal to the thrust times velocity, the relation for propulsive efficiency was obtained as:

$$\eta_p = 2(V/C)$$

That analysis neglects the kinetic energy that is being continually lost because of the decrease of rocket mass caused by fuel consumption. Considering a rocket accelerating in a field-free vacuum, the kinetic energy is $\frac{1}{2}mV^2$, and the time rate of change of the rocket energy is

$$mV(dV/dt) - \tfrac{1}{2}V^2(dm/dt)$$

(if dm/dt is the rate of fuel consumption). The kinetic energy per second of the jet relative to the rocket is

$$\tfrac{1}{2}C^2(dm/dt)$$

Then

$$\eta_p = \frac{\text{rate of useful work}}{\text{rate of work input}} = \frac{mV(dV/dt) - \frac{1}{2}V^2(dm/dt)}{\frac{1}{2}(dm/dt)C^2}$$

when

$$\frac{dV}{dt} = \frac{\text{thrust}}{\text{instantaneous mass}} = \frac{C(dm/dt)}{m_0 - t(dm/dt)}$$

The propulsive efficiency is then

$$\eta_p = 2(V/C) - (V/C)^2$$

This efficiency reaches a maximum of 100 per cent when $V = C$ and returns to zero when $V = 2C$. This relation is entirely different from Professor Williams' relation, which goes to infinity as V increases. This equation shows that the kinetic energy of the rocket is a maximum when $V = 2C$ (i.e., η_p is no longer positive).

Since $m = m_0/e^2$ for $V = 2C$ then the maximum kinetic energy of a rocket starting at rest in a field-free vacuum is

$$(\text{K.E.})_{max.} = \tfrac{1}{2}mV^2 = \tfrac{1}{2}\left(\frac{m_0}{e^2}\right)(2C)^2 = \frac{2m_0C^2}{e^2}$$

provided the rocket has sufficient fuel to reach this speed. The average jet efficiency over the whole flight starting from rest in a vacuum is

$$\eta_{p_{av.}} = \frac{\text{final kinetic energy of rocket}}{\text{total kinetic energy expended in jet}} = \frac{1}{e^{V/C} - 1}\left(\frac{V}{C}\right)^2$$

This average η_p reaches a maximum of about 65 per cent at $V/C = 1.6$. The fact that this propulsive efficiency is independent of the fuel or engine is no different from considering a propeller efficiency independent of the efficiency of the driving engine. The internal rocket motor efficiency simply determines the value of C. The overall rocket efficiency is the product of internal and propulsive efficiencies.

H. REESE IVEY
Aeronautical Engineer N.A.C.A.

Dear Sir:

The increasing interest in the dynamics of gases at supersonic speeds suggests the introduction of an appropriate English technical term in place of the frequently used German word "Schlieren" (plural of "Schliere," f.). The spelling of the German word is baffling to many a report writer, and its origin has become so mysterious to most that there is little wonder if some interpret it as a tribute to a fictitious "Herr Professor Schlieren's" supersonic genius.

A perfectly apt English word exists that conveys a nitid word picture to specialist and layman alike—namely, *striation* (*Webster's New International Dictionary*, Second Edition, page 2495, column 1). Hence, high-speed aerodynamic testing by means of the *striation method*, wherein areas of expansion and compression appear as (*optical*) *striations*.

MAURICE A. GARBELL
Consulting Engineer

A Method for Calculating Airfoil Sections from Specifications on the Pressure Distributions

GLENN H. PEEBLES*

Douglas Aircraft Company, Inc.

ABSTRACT

In 1938, W. Mangler solved a problem in the theory of conformal transformations, which may be loosely stated as follows: *The magnitude of the velocity on an airfoil section is given as a function of the profile arc length. Find the profile having this predetermined velocity distribution.* A thorough investigation of his solution shows that, by changing the approach and by devising accurate and speedy means of performing the naturally lengthy calculations, the notion of constructing an airfoil section to give a prescribed pressure distribution can be made to yield an excellent tool for airfoil design—within the limits, of course, set by the theory of incompressible inviscid flow. A profile design is begun by tentatively specifying the pressure distributions desired at selected angles of attack. These specifications, which usually conflict with each other, are reconciled so as to correspond to an existing but unknown profile. The coordinates of the section are then accurately and rapidly calculated.

INTRODUCTION

THE PROBLEM indicated by the title has been attacked for incompressible inviscid flow in a number of ways with varying degrees of success. The solution to be discussed here has been in almost daily use for 4 years and is believed to represent something in the way of an optimum in speed, accuracy, and flexibility. Its origin lies in a paper by Mangler,[1] who approached the problem by asking for a method of finding that profile which corresponds to a velocity distribution more or less arbitrarily specified with respect to arc length along the profile. This formulation, however, considers only the one pressure distribution at an unspecified angle of attack and unnecessarily limits the usefulness of the method. As will be shown subsequently, the notion of constructing a profile to yield a prescribed velocity distribution can be extended so that the velocity distributions at all angles of attack are brought under the control of the aerodynamicist. The designer begins by tentatively specifying the pressure distributions desired at selected angles of attack. These specifications, which usually conflict with each other, are reconciled so as to correspond to an existing but unknown profile. The coordinates of the profile are then accurately and directly calculated without the use of iteration or other time-consuming process. Only 5 to 10 hours are required to obtain the coordinates if suitable devices for simplifying and shortening the computations are employed.

THEORY OF SOLUTION

The method is based on the usual notion of transforming a circle into a profile. Suppose $z = x + iy$ and $\zeta = \xi + i\eta$ are, respectively, the complex variables in the planes of the circle and the profile (Fig. 1), and let

$$\Omega = \Phi + i\Psi = f(z)$$

be the complex potential function representing a flow about the circle. Then, if $\zeta = g(z)$ represents a transformation of the circle into a profile, the function

$$\Omega = f[g^{-1}(\zeta)] = F(\zeta)$$

gives a corresponding flow about the profile. But

$$d\zeta/dz = (d\Omega/dz)/(d\Omega/d\zeta)$$

where $d\Omega/dz$ and $d\Omega/d\zeta$ are the complex velocities in the two planes and may be written in the form

$$d\Omega/dz = V_K e^{-i\nu_K}, \qquad d\Omega/d\zeta = V_P e^{-i\nu_P}$$

with V_K and V_P representing the magnitudes and ν_K and ν_P the directions of the velocities in the circle and profile planes. Hence, we can express the transformation in terms of the velocities by the relation

$$d\zeta/dz = (V_K/V_P)e^{i(\nu_P - \nu_K)} = (V_K/V_P)e^{i\tau}$$

Now the flow about a circle is known for a variety of cases. Suppose V_K is given on the circle as a function of the central angle φ and suppose, for the moment,

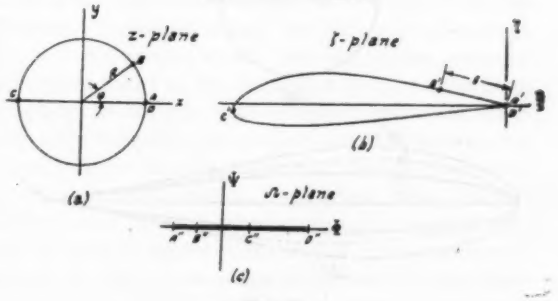

FIG. 1.

Presented at the Aerodynamics Session, Fifteenth Annual Meeting, I.A.S., New York, January 29–31, 1947.

* Design Research Engineer, Santa Monica Division.

that V_P, the desired velocity on the profile, is also known as a function of φ so that $\log (V_K/V_P)$ is determined. Since $\log (V_K/V_P)$ and τ are harmonic conjugate functions and since $\log (d\zeta/dz)$ is by nature regular outside the circle, $\tau(\varphi)$ is calculable on the circle by the Poisson integral formula

$$\tau(\varphi) = \frac{1}{2\pi}\int_0^{\pi} [L(\varphi+\theta) - L(\varphi-\theta)] \cot\frac{\theta}{2}\, d\theta$$

where $L(\varphi)$ represents $\log (V_K/V_P)$ on the circle. The mapping of the circle into the profile comes readily out of the relation

$$\zeta = \xi + i\eta = \int_{Re^{i\varphi_0}}^{Re^{i\varphi}} \frac{d\zeta}{dz}\, dz = iR\int_{\varphi_0}^{\varphi} \frac{V_K}{V_P}\, e^{i(\tau+\varphi)}\, d\varphi$$

These principles, which are elementary and well known in the theory of conformal transformations, show that our problem, at least in the first stage, reduces to making good our assumption that V_P is known as a function of φ. Mangler, starting with V_P specified as a function of s, the length along the arc, correlates s to φ by use of the fact that corresponding points in the z- and ζ-planes map into the same point in the Ω-plane (Fig. 1). This principle applied to points on the profile leads to the relation

$$\Phi = \int^{s} V_P ds = \int^{\varphi} V_K R d\varphi$$

which implicitly defines s as a function of φ. Correlation in this manner, however, is a long process and confines our attention to only one velocity distribution. We shall discard Mangler's scheme without further consideration in favor of one simpler and more useful.

Instead, we shall use a rather obvious property of the class of transformations under consideration. Each member of the class may be written in the form

$$\zeta = A + B[z + \sum_{n=1}^{\infty} (C_n/z^n)]$$

The constants A and B may be varied without changing the shape of the profile, since A represents merely a translation and B represents a rotation and stretching. Suppose we map the circle into a succession of profiles, using the same plane for ζ, and in each case insist that the constants C_n put the trailing edge singularity at the same point on the circle, that A translates the trailing edge to the same point in the ζ-plane, and that B gives the same rotation and stretches the maximum chord to the same length. The profiles will then lie together in close proximity (Fig. 2). If a common chord line is now drawn, it will be found that the points that correspond to the same point on the circle project into roughly the same point on the chord Consequently, we have a means of obtaining an approximate correlation between the points on the chord and the circle and, with the aid of Bernoulli's equation, are able to transform a pressure distribution, specified in the usual manner along the chord into velocity on the profile as a function of φ. Using this V_P, we determine $L(\varphi)$, $\tau(\varphi)$, the coordinates of the profile, and, finally, the exact pressure distribution, which will not differ significantly from the one originally specified.

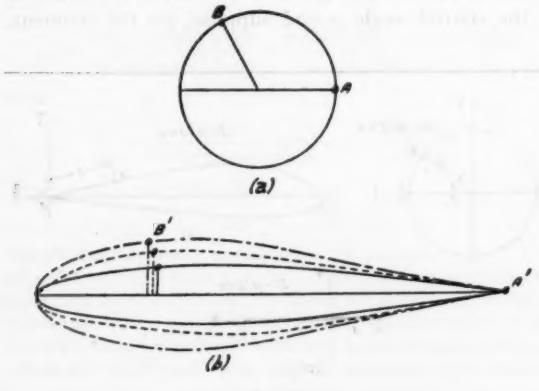

FIG. 2.

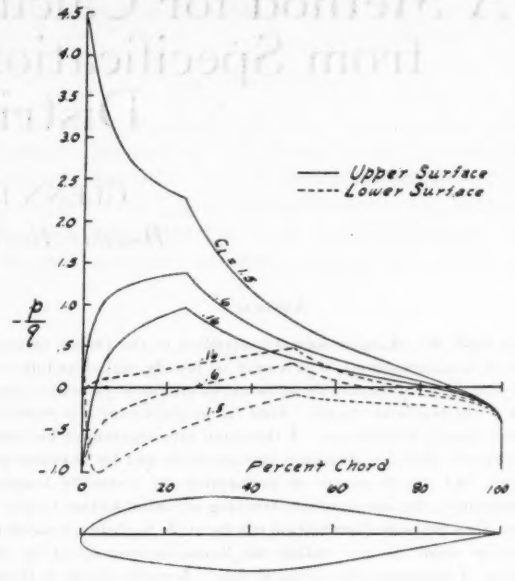

FIG. 3.

ADVANTAGES OF THE METHOD

We need not, however, limit ourselves to one pressure distribution, for, once $d\zeta/dz$ is fixed, the ratio of the velocity in the two planes at corresponding points is also fixed, as the velocity ratio form of $d\zeta/dz$ shows. This means that we can choose our velocity ratio with full knowledge of the effect on the pressure distributions for any type of flow about the profile for which the corresponding flow about the circle is known. We can, for instance, contemplate, more or less simultaneously, flows combining streaming, circulation, sinks, and sources, although we are, of course, chiefly interested in

streaming motions with the circulation adjusted to satisfy the Kutta-Joukowsky condition.

To emphasize this aspect, consider the set of pressure distributions shown in Fig. 3 for a particular profile. In this instance V_K/V_P, and consequently the transformation, was determined by the following considerations: On the top surface from the trailing edge forward to about 25 per cent of the chord, V_K/V_P was so drawn that, at the high lift condition represented by the pressure distribution at a theoretical lift coefficient of 1.5, the pressure recovery gradients are gentle enough to avoid turbulent separation. From 25 per cent forward to about 5 per cent, V_K/V_P was drawn to give a steeply rising gradient to $-p/q$ at a lift coefficient of 0.6, with the hope that laminar flow would be less easily lost through surface irregularities. For the most forward portion of the section, V_K/V_P was again fixed by insisting that the gradients at the nose be gentle enough to avoid laminar separation at high lift. It will also be noted that at the high lift $-p/q$ is not allowed to rise above 4.5. Thus, good maximum lift and laminar flow characteristics designed the top surface. The bottom surface was shaped by much the same considerations, extent of laminar flow at a lift coefficient of 0.16 largely controlling the behavior of V_K/V_P. As the pressure distributions show, the section is not for a high-speed airfoil. If it were, then of course, at some lift coefficient, say 0.3 or 0.4, V_K/V_P would have been shaped from perhaps 3 to 50 per cent to put a low flat level on $-p/q$ on the top surface. Without elaborating on such matters further, it can be seen how it is possible to "tailor" an airfoil section, within the limits set by the assumption of incompressible inviscid flow and by the skill of the designer, to a particular set of requirements.

Limitations on V_K/V_P

One is not so free, however, to arrange the pressure distributions to his taste as might be inferred from the discussion so far. To discover the nature of the restrictions, let us temporarily abandon the velocity form of $d\zeta/dz$ and consider Laurent's expansion about the origin at the center of the circle. Since the velocity ratio must remain finite at infinity, the transformation, as implied earlier, must have the form

$$d\zeta/dz = A_0 + (A_1/z) + (A_2/z^2) + \dots$$

If the velocities in the two planes are to be equal in magnitude and have the same direction at infinity, it is necessary that $A_0 = 1$. This is not a condition that must be met; in fact the requirement that the imaginary part of A_0 be zero is an automatic consequence of Poisson's formula. But when we come to calculating $-p/q$, we must know the real part of A_0 in order to find the ratio V_P/V_∞, and it so happens that in many instances it is convenient to the point of necessity to have $A_0 = 1$.

Much more important is the necessity of getting a closed profile. It will be recalled that we are to obtain the profile coordinates by integrating $d\zeta/dz$ around the circle. When we have completed the circle, ζ must have returned to its initial value. To meet this requirement we must have, according to the theory of residues, $A_1 = 0$.

The condition that $A_0 = 1$ and $A_1 = 0$ must be reduced to relations dependent on V_K/V_P and not on τ, for nothing is known about the direction of the velocities. Now, the expansion for $\log (d\zeta/dz)$, developed from the series for $d\zeta/dz$, is

$$\log \frac{V_K}{V_P} + i\tau = \log A_0 + \frac{A_1}{A_0}\frac{1}{z} + \left(\frac{A_2}{A_0} + \frac{1}{2}\frac{A_1^2}{A_0^2}\right)\frac{1}{z^2} + \dots$$

which becomes on the unit circle

$$L(\varphi) + i\tau(\varphi) = \log A_0 + \frac{A_1}{A_0}(\cos\varphi - i\sin\varphi) + \left(\frac{A_2}{A_0} + \frac{1}{2}\frac{A_1^2}{A_0^2}\right)(\cos 2\varphi - i\sin 2\varphi) + \dots$$

Clearly, the relations $A_0 = 1$ and $A_1 = 0$ require, since the Laurent series on the circle amounts to a Fourier series expansion of the two functions $L(\varphi)$ and $\tau(\varphi)$, that the three integrals

$$\int_0^{2\pi} L(\varphi)\begin{Bmatrix} 1 \\ \sin\varphi \\ \cos\varphi \end{Bmatrix} d\varphi$$

all vanish. Within the limits imposed by these integrals we are free to draw $L(\varphi)$ so as to obtain whatever set of pressure distributions pleases our fancy; that is to say, if the three integrals are satisfied, a closed profile corresponding to $L(\varphi)$ exists, and its pressure distributions are approximately those specified. There is one exception to a literal interpretation of this statement: The pressures can be set so as to cause the profile to intersect itself, but one must depart far from the usual pressure distributions to bring it about.

Further Details and Theory

The nature of the method is such that the shape of the profile necessarily plays a subordinate role, inasmuch as the coordinates appear at the end of the calculations. It cannot be said that this is an advantage, but, if it comes to a choice between known pressures and known shape at the beginning of the calculations, knowledge of the pressures is usually the more favorable, since requirements on pressure distributions are generally more important and troublesome than those on shape. Furthermore, comparison with profiles having known pressure distributions gives a good estimate of what to expect in the way of profile geometry. Failures in meeting estimates in the case of simple geometrical requirements such as a given thickness, a given nose radius, or straight lines forward of the

trailing edge are easily corrected by one or two changes on the pressures.

The trailing-edge angle, however, is one geometrical characteristic of the profile which is selected at the beginning. The trailing-edge angle corresponds to a finite discontinuity in $\tau(\varphi)$ and a negative infinity in $L(\varphi)$. Discontinuities present difficulties in the numerical processes that must be used, so that it is necessary to handle both $L(\varphi)$ and $\tau(\varphi)$ as the sum of two functions, one given analytically and containing the discontinuity and the other given graphically and free from discontinuities. The most convenient form for the analytical part is taken from the complex function

$$\log\left(1 - \frac{1}{z}\right) + \frac{1}{z} = \frac{1}{2}\frac{1}{z^2} - \frac{1}{3}\frac{1}{z^3} + \ldots$$

which separates on the unit circle into

$$\log\left(2\sin\frac{\varphi}{2}\right) + \cos\varphi + i\left(\frac{\pi}{2} - \frac{\varphi}{2} - \sin\varphi\right)$$

The imaginary part regarded as a function of period 2π has a discontinuity of jump π at 0, 2π, etc. Remembering that τ gives the difference between the direction of the velocities in the two planes, we see that a jump of π in $\tau(\varphi)$ at $\varphi = 0$ means an abrupt increase of amount π in the direction of the velocity on the profile over that on the circle, which in turn infers a trailing-edge angle equal to zero. Similarly, the function

$$[1 - (\delta/\pi)]\{\log[1 - (1/z)] + (1/z)\}$$

gives a trailing-edge angle δ.

Since the trailing-edge discontinuity is set by our function to correspond to $\varphi = 0$ on the unit circle, we must have, in order to satisfy the Kutta-Joukowsky condition, a stagnation point at $\varphi = 0$ for all angles of attack. This implies that the velocity on the circle is given by the formula

$$V_K = -2V_\infty[\sin(\varphi - \alpha) + \sin\alpha]$$

where the quantity $-2V_\infty \sin(\varphi - \alpha)$ corresponds to a streaming motion with velocity V_∞ in the direction α to the x-axis and $-2V_\infty \sin\alpha$ to a circulatory motion of strength $\Gamma = 4\pi R V_\infty \sin\alpha$, R being the radius of the circle. Since the magnitude and direction of the velocity at infinity are unchanged by our transformation, α is the absolute angle of attack, and the corresponding section lift coefficient is

$$c_l = \frac{\rho V_\infty \Gamma}{\frac{1}{2}\rho V_\infty{}^2 c} = 8\pi\frac{R}{c}\sin\alpha$$

where c is the chord of the profile.

To obtain the graphical part of $L(\varphi)$ from an assumed pressure distribution for a specified angle of attack, we calculate first

$$\log V_K{}^* = \log V_K - \left(1 - \frac{\delta}{\pi}\right)\left[\log\left(2\sin\frac{\varphi}{2}\right) + \cos\varphi\right]$$

and then the function

$$\log V_K{}^*/V_P = L^*(\varphi)$$

$L^*(\varphi)$ is the desired graphical part, for

$$L^*(\varphi) + \left(1 - \frac{\delta}{\pi}\right)\left[\log\left(2\sin\frac{\varphi}{2}\right) + \cos\varphi\right] = L(\varphi)$$

and, if $L^*(\varphi)$ is continuous, $L(\varphi)$ has the right order of infinite discontinuity. $\tau(\varphi)$, of course, is the sum of the conjugate of $L^*(\varphi)$ and the function $(\pi/2) - (\varphi/2) - \sin\varphi$. Closure conditions may be applied directly to $L^*(\varphi)$ instead of $L(\varphi)$, since the trailing-edge function also satisfies them.

The function

$$[1 - (\delta/\pi)]\{\log[1 - (1/z)] + (1/z)\}$$

is of some interest in itself. It satisfies the closure conditions and so may be considered as $\log(d\zeta/dz)$ of a transformation which maps the circle into a closed profile of some sort. Figs. 4a and 4b show the profiles corresponding to $\delta = 0$ and $\delta = \pi/10$, instances of usual trailing-edge angles. Figs. 4c and 4d are included to trace the development of the profile to the limiting case of $\delta = 2\pi$. The angles of Figs. 4c and 4d are obviously unsuitable for trailing-edge angles, although such large angles are occasionally required for unusual interior angles such as the two shown in Fig. 5.

The limiting case, $\delta = 2\pi$, is specially useful, since it leads to an extension of our method. Suppose t is the complex variable in the plane of the trailing-edge pro-

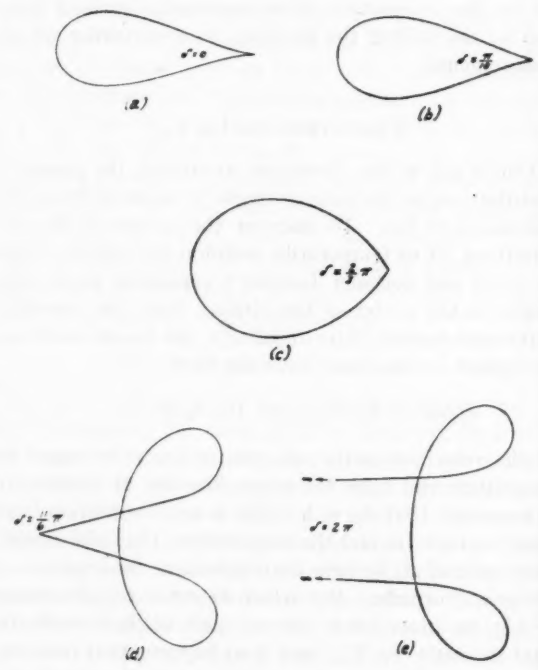

FIG. 4.

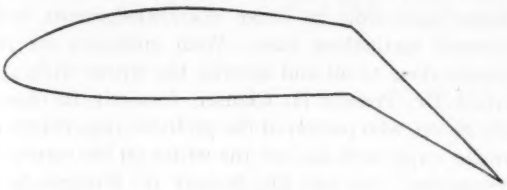

FIG. 5.

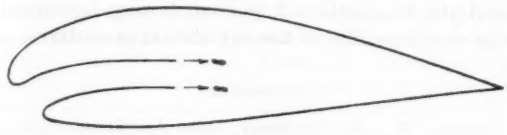

FIG. 6.

file. Then we can write, as in the case of the transformation from the circle,

$$d\zeta/dt = (d\Omega/dt)/(d\Omega/d\zeta)$$

where ζ is still in the plane of the airfoil profile. It is clear that $d\zeta/dt$ is the ratio of the complex velocities in the t- and ζ-planes and that the real part of log $(d\zeta/dt)$ on the two profiles, when referred back to the circle plane, is $L^*(\varphi)$. It follows that we may take the point of view that the profile in the t-plane is mapped into the profile in the ζ-plane by a transformation for which $L^*(\varphi)$ plays almost the same role as $L(\varphi)$ in the transformation from the circle and that the circle plane is introduced only as a convenience in the calculations. From this point of view the thought suggests itself that the profile in the t-plane, in the case of $\delta = 2\pi$, can be mapped into a profile in the ζ-plane such as shown in Fig. 6, and so, by placing a sink at the proper point in the circle plane, the design of leading edge air intakes can be studied. This interesting notion calls for considerable discussion, which will not be attempted here.

CALCULATION PROCEDURES

Since the function $L^*(\varphi)$ must be handled graphically, we shall need to use numerical integration to calculate the seven integral relations:

$$\int_0^{2\pi} L^*(\varphi)d\varphi = 0 \tag{1}$$

$$\int_0^{2\pi} L^*(\varphi) \sin \varphi d\varphi = 0 \tag{2}$$

$$\int_0^{2\pi} L^*(\varphi) \cos \varphi d\varphi = 0 \tag{3}$$

$$\int_0^{2\pi} L^*(\varphi) \sin 2\varphi d\varphi = {}^1/_4(c/R)^2 c_{m_0} \tag{4}$$

$$\int_0^{\pi} [L^*(\varphi + \theta) - L^*(\varphi - \theta)] \cot (\theta/2) d\theta = \tau^*(\varphi) \tag{5}$$

$$\int_0^{\varphi} e^{L(\varphi)} \sin (\tau + \varphi) d\varphi = -\xi(\varphi) \tag{6}$$

$$\int_0^{\varphi} e^{L(\varphi)} \cos (\tau + \varphi) d\varphi = \eta(\varphi) \tag{7}$$

In this list appears one integral not mentioned so far—namely, the fourth, which gives the moment coefficient at zero lift. It is readily established by means of a theorem of Blasius.[2]

All the integrals with the possible exception of the first and fourth must be calculated accurately, chiefly because the amount by which the profile fails to close is extremely sensitive to any inaccuracies in their evaluation. More than that, speed, which is always desirable, becomes imperative, for one must be prepared to calculate the closure integrals—i.e., the first three, and possibly the fourth—many times before reaching a satisfactory compromise between the closure conditions and desirable pressure distribution characteristics. What one usually does is to start with a curve for $L^*(\varphi)$ which yields the pressure characteristics desired and which by estimation with the eye seems to be reasonably near to closure. The closure integrals are calculated and one begins the unhappy business of surrendering a bit here and a bit there of the aerodynamically good qualities until finally closure is reached, each change representing a new calculation to determine the effect on closure. When the best compromise between closure and ideal characteristics has been reached, $\tau^*(\varphi)$ must be calculated at a large enough number of points to define $\tau^*(\varphi)$ accurately, which may mean a hundred or more points, the number depending on the nature of $L^*(\varphi)$ and the accuracy required for the profile. Flexibility is also necessary. Over a period of time enough variations occur in the nature of $L^*(\varphi)$ and the conditions under which one wishes to calculate $\tau^*(\varphi)$ and the closure integrals to make an unnecessarily limited system of calculation a severe handicap.

The extreme need for accuracy, speed, and flexibility makes it essential to put a good deal of thought and preliminary preparation into the numerical and graphical procedures required. Indeed, one should not think to use the method unless willing to go to the limit along this line, for success depends at least as much on good calculation procedures as upon any other aspect of the problem. A complete and detailed description of a system, which is thought to give an optimum in speed and controlled accuracy, is available, but since it is impossible to present briefly any notions of much use, the subject will be passed over here.

A skilled computer using suitable calculating machines with the system just mentioned requires about 20 hours to obtain the coordinates of the profile from the final closed form of $L^*(\varphi)$. The accuracy is sufficient to give a closure to the profile in the neighborhood of one hundredth of an inch on 100-in. chord. This is rather good for an error that represents an accumulation from two closure integrals, the integrals defining the conjugate and the integrals for the coordinates. If one is satisfied with less accuracy, the time for the computations can be shortened considerably. The system is also adapted to the use of punched card machines for the longer and more routine calculations. If use is made of this possibility, the time to pass from

$L^*(\varphi)$ to the coordinates is reduced to about 5 to 10 hours, the 5 hours corresponding to a closure of say three hundredths of an inch on 100-in. chord and the 10 hours to perhaps three thousandths of an inch. No estimates can be made of the total time from the beginning, since obviously such an estimate depends on how long it takes the designer to make up his mind with regard to the compromises represented by the final form of $L^*(\varphi)$. Suffice it to say that it is a matter of minutes to compute the closure integrals and that two computers familiar with the method and set on a clear and definite schedule of profiles can and do turn out a profile per day.

Acknowledgment

The method presented may be said to be the property of a group in the sense that the members at one time or another have had some hand in its application, development, or extension. Under such circumstances there is no neat separation of roles and contributions, and it becomes impossible to make acknowledgments with customary meticulous care. With apologies for the injustices done to all and several, the writer wishes to mention Dr. Francis H. Clauser, formerly in charge of the group, who perceived the probable importance of Mangler's approach and set the writer on the course of investigation. He and Dr. Robert W. Krueger have given considerable thought to extending the method to leading-edge intakes and fuselage scoops, the latter variation not described above. Howard Wampler should also be mentioned as contributing significantly to the simplifications of the calculation procedures.

References

[1] Mangler, W., *Die Berechnung eines Tragfluegelprofiles mit vorgeschriebener Druckverteilung*, Jahrbuch der deutschen Luftfahrtforschung, Vol. I, pp. 46–53, 1938.

[2] Milne-Thomson, L. M., *Theoretical Hydrodynamics*, p. 162: Macmillan and Co., Limited, London, 1938.

Letter to the Editor

Dear Sir:

In the paper "Exact and Approximate Solutions of Two-Dimensional Oblique Shock Flow" by Edmund V. Laitone, JOURNAL OF THE AERONAUTICAL SCIENCES, January, 1947, some erroneous conclusions are drawn by the author. In Busemann's original contribution (reference 6 of the author's paper) two misprints, if not errors, are found in the values of C_3 and D. The correct value of C_3 can be shown to be

$$C_3 = \frac{1}{6(M_1^2-1)^{7/2}}\{(\gamma+1)M_1^8 + (2\gamma^2-7\gamma-5)M_1^6 + 10(\gamma+1)M_1^4 - 12M_1^2 + 8\} \quad (1)$$

instead of the value given by Busemann and by the author. Also, the correct value of D should be

$$D = C_3 - b_3 = \frac{(\gamma+1)M_1^4}{12(M_1^2-1)^{7/2}}\left[\frac{5-3\gamma}{4}\left(M_1^2 - \frac{6-2\gamma}{5-3\gamma}\right)^2 - \frac{\gamma^2-1}{5-3\gamma}\right] \quad (2)$$

instead of the value given by Busemann's paper where the last term in the bracket [i.e., $-(\gamma^2+1)/(5-3\gamma)$] is in error as to sign.

It is unfortunate that Laitone has used Busemann's incorrect value of C_3, presumably without check, and made the pressure coefficient correction with C_3. Apparently, the curves of the third order correction on the pressure coefficient in both Figs. 2 and 3 are slightly in error.

Besides, Laitone tries to find D as the difference between the quoted wrong value of C_3 and the value of b_3 which was derived correctly in his paper. With this fact, the conclusions regarding values of C_3, $C_3 - b_3$, and D in Fig. 11 are incorrect.

It may be desirable to add a little more detail on the derivation of the pressure coefficient P. From the differential equation* of Prandtl-Meyer expansion flow where V is a function of θ only, we have

$$dV/V = -d\theta/\sqrt{M^2-1} \quad (3)$$

where θ is considered negative in expansion flow. For isentropic compression or assuming no change in entropy, the flow is reversible and the equation must be also true. Introducing the Bernoulli's equation $V_d V + (dp/\rho) = 0$, we have

$$dp = (PV^2/\sqrt{M^2-1})d\theta \quad (4)$$

As usual, define

$$P(\theta_1+\theta_s) = [p(\theta_1+\theta_s) - p(\theta_1)]/(\rho_1 V_1^2/2)$$

Now from Eq. (4) we can derive

$$p(\theta_1+\theta_s) - p(\theta_1) = \int_{\theta_1}^{\theta_1+\theta_s}(PV^2/\sqrt{M^2-1})d\theta \quad (5)$$

if P, V, and M are explicit functions of θ. On the other hand, if θ_s is small and if all derivatives of θ exist and are continuous, we can find $p(\theta_1+\theta_s)$ approximately by means of a Taylor series expansion. Thus,

$$P(\theta_1+\theta_s) = (2/\rho_1 V_1^2)\int_{\theta_1}^{\theta_1+\theta_s}(\rho V^2/\sqrt{M^2-1})d\theta = P'(\theta_1)\theta_s + \frac{1}{2!}P''(\theta_1)\theta_s^2 + \frac{1}{3!}P'''(\theta_1)\theta_s^3 + \ldots$$

Comparing with Eq. (12) in the author's paper, we have

$$C_1 = P'(\theta_1) = 2/\sqrt{M_1^2-1}$$

$$C_2 = \frac{1}{2!}P''(\theta_1) = [\gamma M_1^4 + (M_1^2-1)^2]/2(M_1^2-1)^2$$

$$C_3 = \frac{1}{3!}P'''(\theta_1) = \frac{1}{6(M_1^2-1)^{7/2}}[(\gamma+1)M_1^8 + (2\gamma^2-7\gamma-5)M_1^6 + 10(\gamma+1)M_1^4 - 12M_1^2 + 8]$$

where C_3 is given as Eq. (1).

CHIEH-CHIEN CHANG
Research Engineer
The Glenn L. Martin Company

* Eq. (3) is the same as Eq. (13.8) in a paper by Liepmann and Puckett, *Introduction to Aerodynamics of Compressible Fluid*, John Wiley & Sons, Inc., New York, p. 212, 1947.

Pure Bending in the Plastic Range*

HARRY A. WILLIAMS†
Stanford University

ABSTRACT

This paper illustrates the possibilities of the graphical solution of Saint-Venant's method by using what is termed a plastic bending factor which is plotted against outer fiber stress. The ultimate resisting moment of a number of materials may be readily obtained from curves which are shown. It is concluded also that the ultimate resisting moments of beams are approximately proportional to the ultimate tensile strengths of the materials involved if the stress-strain curves are of the same general form. The investigation is restricted to pure bending.

INTRODUCTION

PURE BENDING in the plastic range has been discussed by a number of investigators. Attempts to assume that the stress-strain curve or the stress distribution curve is a simple parabola have resulted in approximate solutions because only a portion of the curve usually followed such a law. When a more exact equation of the curve has been introduced, mathematical complications have resulted. The recent introduction of an equivalent trapezoidal area under the stress-strain curve offers good possibilities for practical purposes although in its present form the method has certain limitations and results in small approximations in certain problems.

In searching for a method that was basically sound and involved no simplifying assumptions other than that stress-strain relationships in a beam are identical with those of simple tension and compression, it seemed that the theory of Saint-Venant, as presented by Timoshenko,[1] offered the best possibilities. Further investigation revealed that the expression for resisting moment could be modified so that the radius of curvature was eliminated and the integral divided by the square of the outer fiber strain could be plotted against outer fiber stress. The integral itself was then evaluated by a conventional method of graphical integration which can result in a degree of accuracy approaching that of more exact mathematical methods if desired. The method, as finally proposed, becomes a modification and expansion of existing theory and is not essentially a new approach.

In the presentation that follows, first the method is described and expressions are derived for several typical cross sections. Solutions for other cross sections are then presented briefly in the Appendix.

Received December 4, 1946.

* This paper is based on an investigation by the author while employed as Stress Analyst in the Engineering Department of Douglas Aircraft Company, Inc., Santa Monica, Calif., and is published with the company's permission and cooperation.

† Associate Professor of Civil Engineering.

SYMBOLS

e	=	strain
e_m	=	strain in outer fibers of a beam
e'	=	strain in a layer of fibers where width of cross section changes
f	=	stress
f_m	=	bending stress in outer fibers of a beam
f'	=	bending stress corresponding to strain, e'
F_{tp}	=	proportional limit stress in a tension test
F_{ty}	=	yield strength in a tension test
F_{tu}	=	ultimate strength in a tension test
J_f	=	plastic bending factor for circular cross section
J_{fu}	=	value of J_f for ultimate loading condition
K_f	=	plastic bending factor for cross sections composed of rectangles
K_{fu}	=	value of K_f for ultimate loading condition
M	=	bending moment
M_u	=	ultimate bending moment

PLASTIC BENDING OF A RECTANGULAR BEAM—TENSION AND COMPRESSION STRESS-STRAIN CURVES IDENTICAL

Several investigators have shown experimentally that cross sections remain plane during pure bending in the plastic range. With this as a basis, it follows from Fig. 1a that a layer of fibers originally of length mn has its length increased a distance ns by the action of the couples M in bending the beam. Thus, from similar triangles the strain is

$$e = ns/mn = y/r \qquad (1)$$

where y is the distance from the neutral axis to the layer of fibers in question and r is the radius of curvature of the bent beam. The strain distribution from top to bottom of the beam is as shown in Fig. 1c. If we assume that the relation between stress and strain in a

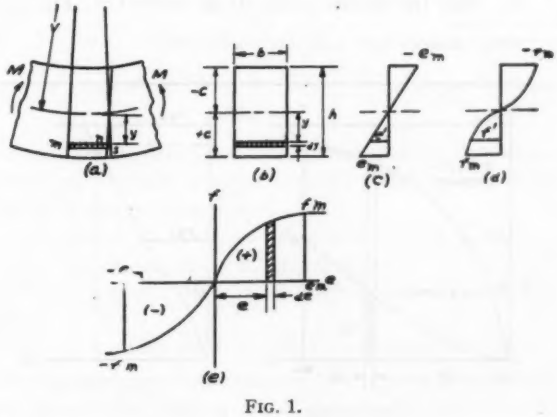

FIG. 1.

beam during bending is the same as in simple tension and compression, Fig. 1e, we can plot the stress distribution curve of Fig. 1d.

Since the tensile and compressive forces acting on the beam cross section must be equal, we can write the relationship

$$\int_0^{+c} f\,bdy = \int_0^{-c} f\,bdy \qquad (2)$$

From Eq. (1)

$$y = re, \qquad dy = rde$$

and Eq. (2) becomes

$$rb\int_0^{+e_m} f\,de = rb\int^{-e_m} f\,de \qquad (3)$$

This equation shows that the tension and compression areas under the stress-strain curves in Fig. 1e must be equal. Since we have assumed identical curves in this case, it follows that the neutral axis must be at the centroid of the cross section.

The moment of the force acting on the elementary area bdy is $y\,fb\,dy$. Hence

$$M = \int_{-c}^{+c} y\,fbdy = 2\,b\int_0^c f\,ydy$$
$$= 2br^2\int^{e_m} e\,de \qquad (4)$$

The derivation thus far follows Timoshenko's presentation.[1] However, the radius of curvature may now be eliminated and the moment expressed in terms of the strain in the outer fibers of the beam.*

From Eq. (1), when $y = c$, $e = e_m$, and $r = c/e_m$.

Substituting in Eq. (4):

$$M = 2bc^2\left(\int_0^{e_m} fede/{e_m}^2\right) = \frac{bh^2}{2}K_f = 3(I/c)K_f \qquad (5)$$

where

$$K_f = \left(\int^{e_m} fede/{e_m}^2\right)$$

The term, K_f, will be referred to as the plastic bending factor. It is equal to the moment of the area under one branch of the stress-strain curve divided by the square of the strain in the outer fibers of the beam. This factor can be evaluated as follows for any stress, f_m, in the outer fibers:

(1) Plot the tensile stress-strain curve OA (Fig. 2).

(2) Plot a second curve OB by multiplying values of strain, e, by corresponding values of stress, f.

(3) Determine the area under the curve OB. Sufficient accuracy is usually obtained by dividing the area into a few trapezoids and a triangle. In some cases the area is nearly triangular. Since the area of the shaded element as $fede$, evidently the area under the curve is equal to $\int_0^{e_m} fede$ in accordance with conventional methods of graphical integration.

(4) Divide the above area by ${e_m}^2$ and plot this value of K_f against f_m (point D in Fig. 3). If a complete curve is desired, the procedure is repeated for other selected values of f_m and e_m. Below the proportional limit $K_f = {}^1/_3 f_m$ and Eq. (5) reduces to the conventional flexure formula.

For some materials, the upper portion of the curve in Fig. 3 approaches a straight line, thus indicating that, for rectangular beams, the moment bears a straight-line relationship to outer fiber stress in this region.

The procedure outlined above is illustrated numerically in Fig. 4. All necessary computations and curves are shown in the figure. For example, when the stress in the outer fibers is $f_m = 25{,}600$ lbs. per sq.in., the corresponding strain, $e_m = 0.012$ and the area under the fe curve is 1.661 lbs. per sq.in. Then $K_f = 1.661 \div (0.012)^2 = 11{,}540$ lbs. per sq.in. and the point on the K_f vs. f_m curve is plotted as indicated. All curves should be plotted to large scales if any high degree of accuracy is desired for the values between the proportional limit and yield strength.

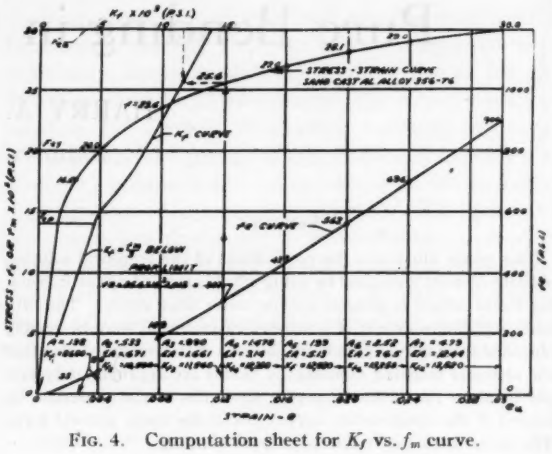

FIG. 4. Computation sheet for K_f vs. f_m curve.

* Other authors have used this modification.

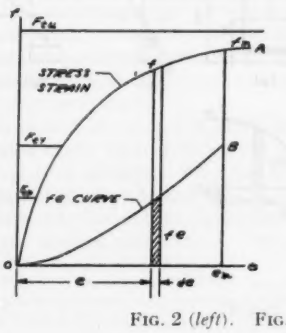

FIG. 2 (*left*).

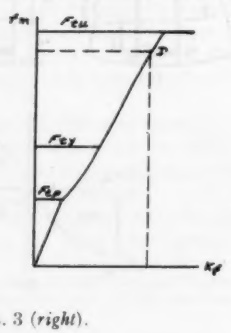

FIG. 3 (*right*).

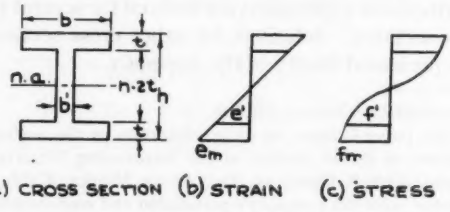

FIG. 5.

Plastic bending factor curves based on minimum specified values for four materials are shown in Figs. 10–13, inclusive. The tension and compression stress-strain curves for these materials are similar although not identical.

Plastic Bending of I-Beam or Channel-Neutral Axis Perpendicular to Web—Tension and Compression Stress-Strain Curves Identical

The bending moment expression for an I-beam or channel may be derived by the method outlined above. However, the same result may be obtained by considering the total moment as being the difference between the resisting moments of an outer and an inner rectangular beam. This approach is analogous to computing the moment of inertia of such a cross section by subtracting the moment of inertia of the inner rectangles from that of the outer rectangle.

In Fig. 5, the outer beam has a width b and a depth h. Its resisting moment from Eq. (5) is $3(I_0/c_0)K_f$. The inner beam has a width $b - b'$ and a depth $h - 2t$. Its resisting moment is $3(I_i/c_i)K_f'$.

Hence

$$M = 3\left(\frac{I_0}{c_0}K_f - \frac{I_i}{c_i}K_f'\right) = 3\left[\frac{bh^2}{6}K_f - \frac{(b-b')(h-2t)^2}{6}K_f'\right] = \frac{bh^2}{2}\left[K_f - \left(1-\frac{b'}{b}\right)\left(1-\frac{2t}{h}\right)^2 K_f'\right] \quad (6)$$

where

K_f = plastic bending factor corresponding to a stress f_m and a strain e_m in the outer fibers

K_f' = plastic bending factor corresponding to a stress f' and a strain e' at the inner surface of a flange (Figs. 5b and 5c.)

The solution of Eq. (6) requires the use of the stress-strain curve to evaluate the factor K_f'. If the outer fiber stress, f_m, is known, K_f and e_m can be determined from the K_f and stress-strain curves, respectively. The strain at the inner surface of a flange is $e' = [1 - (2t/h)]e_m$ (Fig. 5b). From the stress-strain curve f' is then determined and K_f' is the factor corresponding to this stress. It will be noted that f' is the outer fiber stress in the inner rectangular beam mentioned above.

Obviously, if the bending moment is known, the outer fiber stress can be determined from Eq. (6) only by trial. An approximate value can be readily determined as illustrated in the Appendix. However, margins of safety may be based on ratios of moments rather than on ratios of stresses.

Numerical illustrations will be found in the Appendix together with bending moment expressions for other beams of a rectangular type.

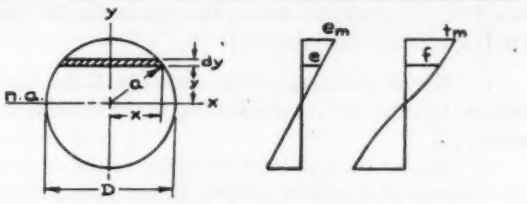

Fig. 6.

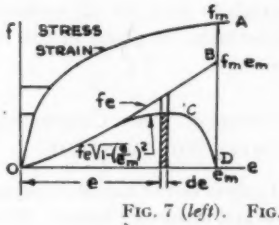

Fig. 7 (*left*).

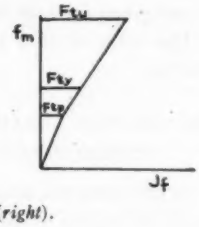

Fig. 8 (*right*).

Circular Beam—Tension and Compression Stress-Strain Curves Identical

An expression for the plastic bending moment of a beam of circular cross section can be solved in a manner similar to that for the rectangular beam but the plastic bending factor takes a different form.

It is assumed that tension and compression stress-strain curves are identical and that strain is linear as shown in Fig. 6b. Then, from the rectangular beam theory

$$e = y/r, \quad e_m = a/r, \quad y = re, \quad dy = r\,de$$

The moment of the force acting on the element in Fig. 6a is

$$y f 2x\,dy = 2f y\sqrt{a^2 - y^2}\,dy$$

Hence

$$M = 4\int_0^a f y\sqrt{a^2 - y^2}\,dy$$

or, from the above relationship, between y and e and between r and e_m

$$M = 4r^2\int_0^{e_m} f e\sqrt{a^2 - r^2e^2}\,de = 4a^3\frac{\int_0^{e_m} fe\sqrt{1-(e/e_m)^2}\,de}{e_m^2} = {}^1/_2D^3 J_f \quad (7)$$

where J_f is the plastic bending factor for a circular beam and is equal to the integral divided by the square of the strain in the extreme fibers.

The factor, J_f, is evaluated as follows (Fig. 7):

(1) Draw the stress-strain curve OA.

(2) Construct the *fe* curve OB as for the rectangular beam.

(3) Construct the curve OCD by multiplying values of *fe* by corresponding values of $\sqrt{1-(e/e_m)^2}$. It will be noted that the area of the shaded element is

$fe\sqrt{1-(e/e_m)^2}\,de$ and, hence, the area under the curve OCD is equal to the integral.

(4) Divide the area under curve OCD by e_m^2 to obtain the value of J_f corresponding to the extreme fiber stress, f_m.

(5) Repeat the procedure for other values of f_m and e_m. Values of J_f may be plotted against f_m as shown in Fig. 8. When f_m is below the proportional limit, it can be shown by direct integration that $J_f = (\pi/16)f_m$.

The procedure outlined above is numerically illustrated in Fig. 9 for three points on the curve. Values of J_f are given for four materials in Figs. 10–13, inclusive.

The solution of a tubular beam is given in the Appendix.

Rectangular Beam—Tension and Compression Stress-Strain Curves Not Identical

In this case, the neutral axis is not at the centroid and must be located by the method discussed below. After the neutral axis has been determined, the beam cross section can be considered as composed of two half-sections with different physical properties.

The neutral axis can be located as follows:

Let

c_1 = distance from neutral axis to outer tensile fibers

c_2 = distance to outer compressive fibers

e_{m1} and f_{m1} = maximum tensile strain and stress, respectively

e_{m2} and f_{m2} = maximum compressive strain and stress, respectively

Then Eq. (3) becomes

$$rb\int_0^{e_{m1}} fde = rb\int_0^{-e_{m2}} fde$$

and it is apparent that the area under the tension curve in Fig. 14d must equal the area under the compression curve.

If the stresses are well beyond the yield point, a high degree of accuracy is not essential and the areas can be balanced as follows:

(1) Draw the two stress-strain curves as shown in Fig. 15.

(2) The maximum tensile or compressive stress and strain will be known or can be estimated. Then, using the relationship,

$$e_{m1}/e_{m2} = c_1/c_2 = c_1/(h - c_1)$$

assume c_1 and make the construction indicated.

(3) Try various values of c_1 until the shaded areas are approximately equal. It will be noted that the neutral axis does not remain in the same position but shifts as the stresses vary with the applied moment.

To obtain the bending moment, we first construct $K_f - f_m$ curves for both tension and compression. From the development of Eq. (5), the resisting moment for the tension area of the cross section is $bc_1^2K_{ft}$ and for the compression area $bc_2^2K_{fc}$. Adding these values

$$M = b(c_1^2K_{ft} + c_2^2K_{fc}) \qquad (8)$$

The same general approach may be used for a shape such as an I-section, but, in locating the neutral axis, parts of the stress-strain curve must be expanded vertically before balancing areas.* The resisting moment of the tension and compression areas must be treated separately and added.

Approximate Correction Factor for Test Results

It is apparent from Eq. (5) that moment is directly proportional to the plastic bending factor when the beam is rectangular and the tension and compression stress-strain curves are identical. This relationship is only approximately true for other cross sections since the moment expressions are more complex, but it holds reasonably well as the ultimate loading condition is approached. It can be demonstrated further that, for two similar but not identical materials, the ultimate plastic bending factors are approximately proportional to ultimate tensile stresses so that ultimate bending moments are roughly proportional to ultimate stresses.

It will be noted that the K_f curves in Figs. 10–12, inclusive, are approximately straight lines beyond the yield point. This is true to a lesser extent for the 14-ST forging in Fig. 13. This results from the fact that the fe curve in each of these cases approximates a parabola of the form $y = ax^n$ and the area under the curve is equal to the base times the altitude divided by $n + 1$. Hence, the factor

$$K_f = \frac{\int_0^{e_m} fede}{e_m^2} = \frac{f_m e_m^2}{(n+1)e_m^2} = \frac{f_m}{n+1}$$

If the area under the stress-strain curve is rectangular, $n = 1$; if it is triangular $n = 2$. Hence, n will always lie between these values for conventional stress-strain curves.

Actually the variation in n is not large, particularly when the stress-strain curves are somewhat similar. For example, the values for the aluminum alloys 356-T6 and 195-T6 are 1.19 and 1.25, respectively. Even for quite different materials such as Dowmetal H and 14-ST forging, n equals 1.38 for the former and 1.11 for the latter.

The correction factor for a tested beam is determined as follows:

In Fig. 16, let

OA = the stress-strain curve based on certain minimum specified values. The yield and ultimate strengths are as indicated.

OB = the stress multiplied by the strain at any point on curve OA.

OA′ and OB′ = similar curves for a test beam coupon.

* See Timoshenko's analysis of a Tee-beam, reference 1, p. 366.

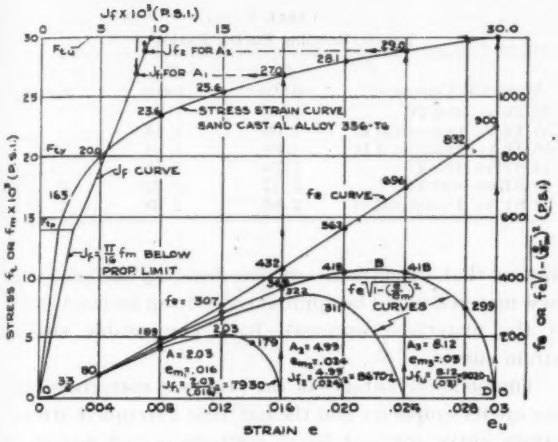

FIG. 9. Computation sheet for J_f vs. f_m curve showing method of obtaining three points on curve.

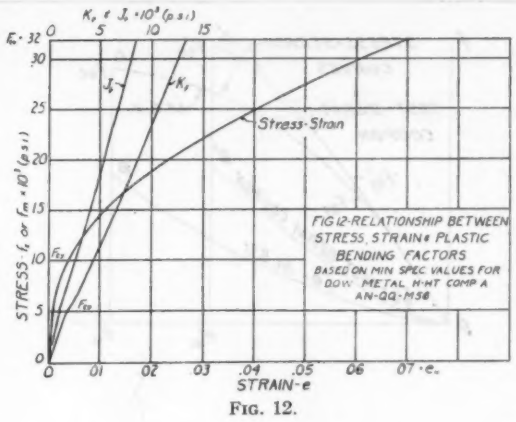
Stress-Strain
FIG 12-RELATIONSHIP BETWEEN STRESS, STRAIN & PLASTIC BENDING FACTORS
BASED ON MIN SPEC VALUES FOR DOW METAL H-HT COMP A AN-QQ-M58
STRAIN-e

FIG. 12.

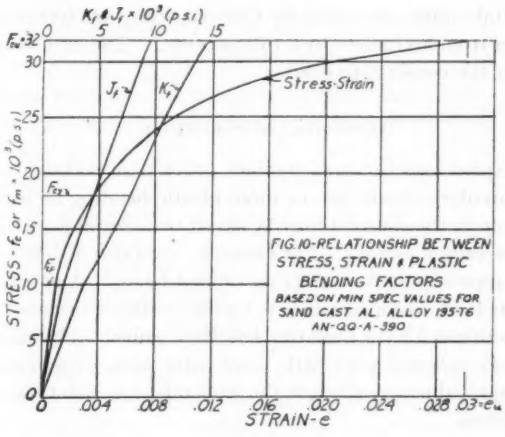
Stress-Strain
FIG.10-RELATIONSHIP BETWEEN STRESS, STRAIN & PLASTIC BENDING FACTORS
BASED ON MIN SPEC VALUES FOR SAND CAST AL ALLOY 195-T6 AN-QQ-A-390
STRAIN-e

FIG. 10.

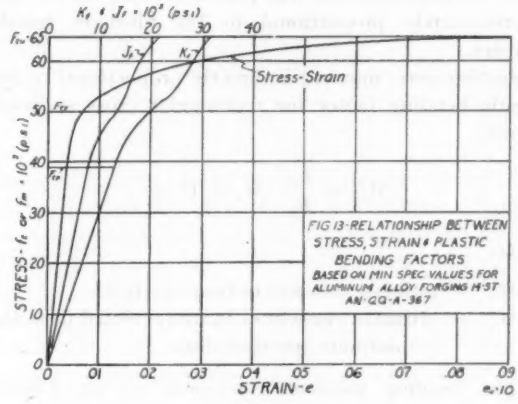
Stress-Strain
FIG 13-RELATIONSHIP BETWEEN STRESS, STRAIN & PLASTIC BENDING FACTORS
BASED ON MIN SPEC VALUES FOR ALUMINUM ALLOY FORGING H-ST AN-QQ-A-367
STRAIN-e

FIG. 13.

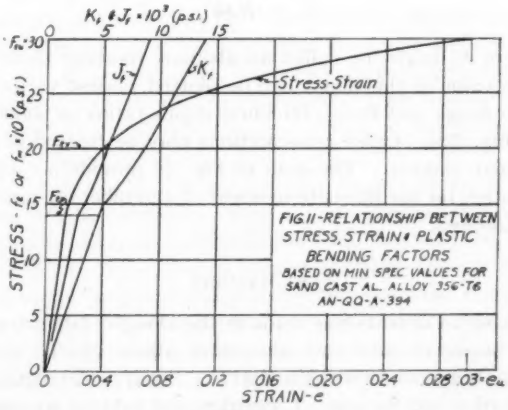
Stress-Strain
FIG.11-RELATIONSHIP BETWEEN STRESS, STRAIN & PLASTIC BENDING FACTORS
BASED ON MIN SPEC VALUES FOR SAND CAST AL. ALLOY 356-T6 AN-QQ-A-394
STRAIN-e

FIG. 11.

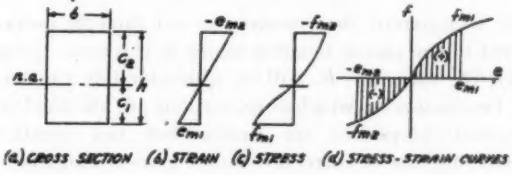

FIG. 14.

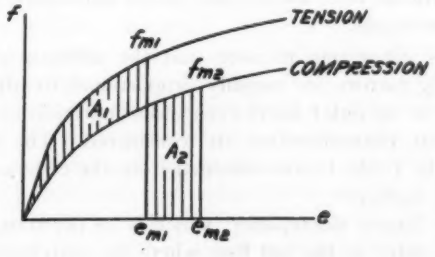

FIG. 15.

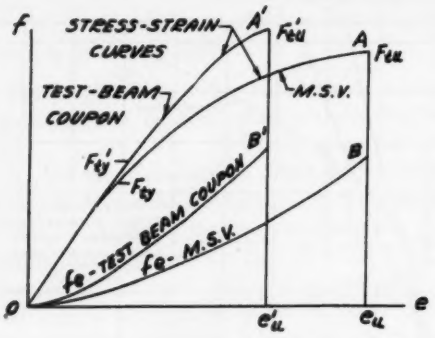

FIG. 16.

The value of n will be of the same order of magnitude for the two curves, OB and OB′. Hence, for the ultimate loading condition, the plastic bending factors are approximately proportional to the ultimate tensile stresses.

Furthermore, moment is directly proportional to the plastic bending factor for rectangular cross sections. Hence,

$$M_u' = \frac{F_{tu}'}{F_{tu}} M_u = C M_u$$

where

M_u' = ultimate moment of beam by test
M_u = ultimate moment of beam predicted from the minimum specified data

The bending moment expression for an I-beam [Eq. (6)] may be written

$$M = \frac{bh^2}{2} K_f \left[1 - \left(1 - \frac{b'}{b} \right) \left(1 - \frac{2t}{h} \right)^2 \frac{K_f'}{K_f} \right]$$

It is apparent that moment is not directly proportional to the plastic bending factor in this case. However, the ratio K_f'/K_f will be approximately the same for two beams for which cross sections are identical and physical properties are similar but not identical. Hence, the above correction factor gives reasonable results for this type of cross section.

The same method of correction can be used for circular and tubular beams since the J_f curves also approximate straight lines. Bending moment is directly proportional to J_f for circular beams and nearly so for tubular beams.

It is interesting to note that the ultimate plastic bending factors are roughly proportional to ultimate stress in the outer fibers even when materials of quite different characteristics are considered. The ratios given in Table 1 were obtained from the curves, Figs. 10–13, inclusive.

The largest discrepancy, which is 18 per cent, is in the J_f ratio, in the last line, where the materials compared have completely different properties. It would appear that the ultimate plastic bending factors for a new material might be approximated from known values if the materials concerned have comparable stress-strain curves.

TABLE 1
Plastic Bending Factor Ratios

Materials Compared	F_{tu} Ratio	K_{fu} Ratio	J_{fu} Ratio
195-T6 vs. 356-T6	1.06	1.09	1.05
195-T6 vs. Dowmetal H	1.00	1.13	1.13
356-T6 vs. Dowmetal H	0.94	1.04	1.07
14-ST vs. 195-T6	2.04	2.13	2.22
14-ST vs. 356-T6	2.17	2.32	2.32
14-ST vs. Dowmetal H	2.04	2.38	2.50

The main advantages of the proposed correction factor are its simplicity and the fact that a complete stress-strain curve for test beam coupons is not required. Admittedly, a correction factor that includes yield strength, as well as ultimate strength, should be more accurate than the one proposed. The factor suggested by Cozzone[3] meets this requirement. When the proposed correction factors are computed for the experimental values presented by Cozzone, they are found to differ from his factors by 3 to 5 per cent. The difference is on the conservative side.

APPROXIMATE SOLUTIONS

Expressions for cross sections other than rectangular or circular contain two or more plastic bending factors. A step in the solution may be saved by assuming a ratio between the factors. For example, the ratio $K_f'/K_f = 0.9$ approximately in the case of an I-beam. Any error in such an assumed value is further reduced because it is multiplied by a quantity less than unity. The ratio can be selected with little error after some experience. Rough values are given in the Appendix for each type of problem.

ULTIMATE MOMENT FACTORS

The expression for the ultimate moment of an I-beam may be written in the form

$$M_u = R_i b h^2$$

where R_i might be called an ultimate moment factor. The value of this factor can be plotted against various web-flange and flange thickness-depth ratios as shown in Fig. 22a. Other cross sections may be treated in a similar manner. The data in Fig. 22 provide a rapid solution for the ultimate moment of a number of standard shapes.

TEST RESULTS

A series of tests was made in the Douglas laboratory on beams of sand-cast aluminum alloys 195-T6 and 356-T6 and of Dowmetal H-HT. Square, rectangular (on edge and flatwise), I, circular, and tubular sections of each material were tested to failure in pure bending.

TABLE 2
Ratio of Actual Strength to Predicted Strength of Sand Cast Beams

Beam Shape	Material	F_{tu} M.S.V.* Lbs. per Sq.In.	F_{tu}' Average for Coupons Lbs. per Sq.In.	No. of Specimens Tested	Actual Ultimate Moments : Predicted Ultimate Moments Range	Average
Square	195 T-6	32,000	32,700	4	1.11–1.32	1.24
	356 T-6	30,000	28,600	4	0.97–1.08	1.00
	Dow H	32,000	19,000	3	1.13–1.52	1.38
Rectangle (on edge)	195 T-6	32,000	34,600	4	0.86–0.94	0.91
	356 T-6	30,000	25,300	5	1.01–1.33	1.19
	Dow H	32,000	23,500	3	1.32–1.38	1.35
Rectangle (flatwise)	195 T-6	32,000	34,900	3	0.92–1.17	1.03
	356 T-6	30,000	25,300	3	1.11–1.24	1.16
	Dow H	32,000	25,200	3	1.21–1.23	1.22
I-beam	195 T-6	32,000	39,000	3	1.09–1.12	1.10
	356 T-6	30,000	28,800	3	0.96–1.05	1.00
	Dow H	32,000	27,700	3	1.03–1.08	1.06
Circular	195 T-6	32,000	31,200	3	0.90–1.07	0.96
	356 T-6	30,000	26,800	3	1.06–1.18	1.11
	Dow H	32,000	28,800	4	0.99–1.08	1.06
Tubular	195 T-6	32,000	40,000	3	0.80–0.93	0.88
	356 T-6	30,000	29,400	4	0.93–1.13	1.04
	Dow H	32,000	27,700	4	0.76–1.24	1.00
			Summary			
All Shapes	195 T-6			20	0.80–1.32	1.02
	356 T-6			22	0.93–1.33	1.09
	Dow H			20	0.76–1.52	1.16
All Beams				62	0.80–1.52	1.09

* Minimum specified values.

There were three to five beams of each type for each of the materials. Approximate dimensions were as follows:

Square—$^1/_2$ in. by $^1/_2$ in.
Rectangular—$^1/_2$ in. by 1 in.
I-beam—flanges 1 in. wide by $^1/_4$ in. thick; depth 2 in.; web $^1/_4$ in. thick
Circular—$^1/_2$ in. diameter
Tubular—2 in. diameter, $^5/_{32}$ in. thick

The results of this series of tests are shown in Table 2. The predicted ultimate moments were determined from the charts of Fig. 22, which are based on minimum specified values, and then corrected on the basis of the ultimate strength of coupons as compared with the specified values. Inspection of the data indicates that while general averages show reasonable correlation, the range of values is large. An examination of the distribution of results (not shown in the table) reveals that the ratio was less than 0.90 for only three tests and was greater than 1.20 for 15 beams, nine of Dowmetal and three of each aluminum alloy. Two-thirds of the ratios were greater than 1.00 and, therefore, were on the conservative side.

A part of the discrepancy may be attributed to the use of the correction factor and to the fact that the tension and compression stress-strain curves were not identical. The balance results from the difficulty in obtaining coupons that actually represent the material in a beam. Coupons from the same beam sometimes showed differences in the order of 30 per cent. Full stress-strain curves were obtained in a number of cases for coupons from the tested beams and from similar untested beams. If the curves were nearly alike, the theoretical result, based on the fundamental method, was within 10 per cent of the test value. (Supplementary tests described below also indicate this degree of accuracy is possible.) It was found also that standard $^1/_2$ in. diameter test specimens, cast with the beams and tested with the skin undisturbed, were not representative of the beam material. When the ratios of actual to predicted moment were computed on the basis of these specimens, the spread in values was still large and the results were on the unconservative side for all but nine tests.

Results obtained from a few tests of beams machined from 24 ST extruded bar stock were as follows:

Beam Shape	Specimen No.	Ratio: $\frac{M_u \text{ (Test)}}{M_u \text{ (Predicted)}}$
Rectangle	1	1.04
	2	1.03
I	1	0.93
	2	0.93
Tee	1	1.03

The correlation between predicted moments and test results for the complete plastic range are shown in Fig. 17 for an I-beam of Dowmetal H-HT. Points on the straight line representing test results were computed by simple statics. In order to obtain the predicted moment, strain measurements were made on top and bottom flanges during the test. Thus, for a given load the measured strain corresponded to a certain outer fiber stress, f_m, from which the moment could be calculated. The latter was based on a stress-strain curve for coupons from a similar untested beam but the variation in coupons made close correlation impossible.

The effect of shift of the neutral axis in the plastic range was investigated for one cast aluminum-alloy

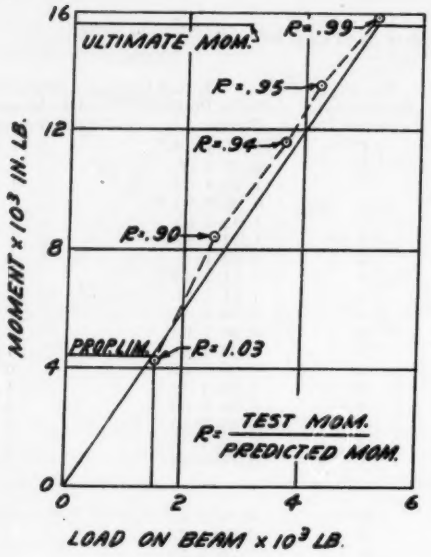

FIG. 17.

195-T6 T-beam and the results are shown in Fig. 18. Curve (a) represents the moment computed from the test load by simple statics. The neutral axis was located from electric strain gage readings at various stages of loading. Using measured outer fiber strains and the true neutral axis, the moment for a given load was then predicted. These values are shown by curve (b). In the same way moments were also computed, curve (c), assuming the neutral axis always remained through the centroid of the section. The ratios of test moment to predicted moment are shown in the figure. It will be noted that the discrepancy between curves (b) and (c) is not large even though the neutral axis shifted almost 10 per cent of the depth toward the compression flange. Strain remained nearly linear until the ultimate load was approached. Discrepancies at that time were probably due to nonlinear characteristics of the gages or to plastic flow during the recording period.

An analysis was made of a number of production castings that had failed in bending during inspection testing. The predicted ultimate moment, based on coupon results, was usually within 10 per cent of the test value. Various types of cross sections were investigated but all castings were of the cantilever type.

General Discussion

The method discussed above is based on the assumption that the relationship between stress and strain is the same for beam fibers as it is for simple tension and compression, and that this relationship holds for the full range of the stress-strain diagram. It appears to the author that the assumption is reasonable if the total strain is less than about 10 per cent. Maximum strains measured on the outer fibers of the cast beams agreed fairly well with tensile specimen strains. The measured strain at failure for a rectangular 24-ST duralumin beam, however, was found to be about 8 per cent, or less than half the tensile specimen elongation. This indicates that the beam fibers were not able to deform as if they were in simple tension. The computed outer fiber stress nevertheless was within 6 per cent of the ultimate strength of the tensile specimen. This correlation may be attributed to the fact that the stress-strain curve was almost flat beyond 10 per cent strain so that the area under the outer portion was practically a rectangle. The plastic bending factor, K_f, is changed a negligible amount by such an area.

The method uses no other approximations except those involved in the graphical solution. Most of the equations contain several terms, some of which must be evaluated by computing the strain at a certain distance from the neutral axis and then determining the plastic bending factor from the approximate curve. An approximate solution, which eliminates the latter step, may be made by assuming a ratio between the plastic bending factors involved. Suggested ratios are given in the Appendix.

Cross sections for which the neutral axis is not an axis of symmetry can be solved by the method. If the tension and compression stress-strain curves are reasonably alike, the available experimental evidence indicates that fair results can be obtained by assuming the neutral axis through the centroid. Actually it constantly shifts from this position after the proportional limit stress is exceeded in the outer fibers. The method can also be applied to the above problem when the stress-strain curves are not identical for tension and compression.

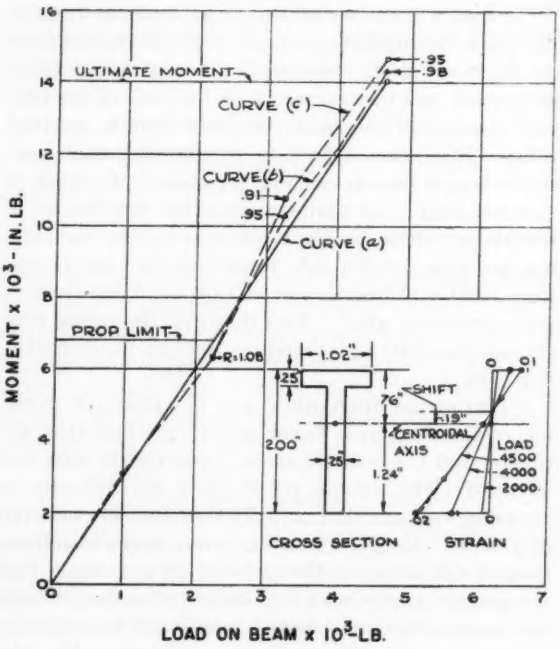

FIG. 18.

It sometimes happens that the ultimate strain in a coupon from an actual casting is considerably less than the specified value on which the plastic bending factor is based. The ultimate strength may agree reasonably well, however, with the specified ultimate strength. The plastic bending factor based on specified data still gives good results since it depends primarily on the ultimate strength and not on the ultimate strain.

It is difficult to apply Saint-Venant's approach to a cross section such as an I-beam with large fillets. If the fillets are neglected, the predicted result may be unduly conservative. One might compensate for the fillets by slightly increasing the actual flange and web thickness.

Those familiar with Cozzone's method[3] of solving problems in plastic bending will note that his stress intercept, f_0, when written in terms of the plastic bending factor, becomes

$$f_0 = 6K_f - 2f_m$$

where K_f is the factor corresponding to the stress f_m.

His moment equation may then be written

$$Mc/I = f_m(3 - 2K) + 6K_f(k - 1)$$

This equation may be used to construct curves for various values of k as Cozzone proposed. Cozzone's equation becomes identical with the author's when the cross section is a rectangle. The methods do not agree for other cross sections because of an approximation in Cozzone's approach to these problems. For example, an I-beam can be considered as made up of a rectangular web, extending the full depth of the beam, and the projecting flanges. The resisting moment of the web when computed separately from Cozzone's equation would be correct. However, that portion of the area under the stress-strain diagram which applies to the flanges should be replaced with a small trapezoidal area whose moment with respect to the origin is the same as that of the original area. The sloping line of this small trapezoid will not coincide with the corresponding line from f_m to f_0 in the larger trapezoid.

Another way of showing the approximation is to consider the total resisting moment of the I-beam as being equal to the resisting moment of the outer rectangle minus that of the inner rectangles. The trapezoid for the former will have ordinates f_0 and f_m, for the latter they will be f_0' and f_m', the latter being the true stress at the inner surface of the flange. A solution made in this way will give results identical with those obtained by the author. Following the same reasoning, Cozzone's method can be extended to shapes such as T-beams where the neutral axis is not an axis of symmetry.

In the preceding discussion, it is not intended to detract from Cozzone's method but rather to point out the reason why the two methods agree for rectangular beams but are not identical for other types of cross sections. The approximation that Cozzone makes is not large.

Appendix

Derivations and Numerical Examples

Bending moment expressions for various types of cross sections are derived below unless previously discussed. All numerical examples are for sand-cast aluminum-alloy 356-T6 beams. Data for this material will be found in Fig. 11. All solutions are based on identical stress-strain curves in tension and compression. Ultimate resisting moment may be computed from the derived expressions or from the data in Fig. 22.

Beam Shape No. 1—Rectangular Beam (Fig. 1b):

From Eq. (5): $M = 3(I/c)K_f$.

Example 1: $b = 1$ in., $h = 2$ in., $f_m = F_{tu} = 30{,}000$ lbs. per sq.in.

From Fig. 11, $K_f = 13{,}800$ lbs. per sq.in. for this value of f_m. $M_u = 3 \times 0.667 \times 13{,}800 = 27{,}600$ in.lbs.

Alternative solution: From Fig. 22, $R = 41{,}500$ lbs. per sq.in. $M_u = RI/c = 41{,}500 \times 0.667 = 27{,}700$ in.lbs.

Example 2: $b = 1$ in., $h = 2$ in., $M = 20{,}000$ in.lbs.

Then $K_f = 20{,}000/(3 \times 0.667) = 10{,}000$ lbs. per sq.in.

From Fig. 11, $f_m = 23{,}500$ lbs. per sq.in.

Beam Shape No. 2—Circular Beam (Fig. 6):

From Eq. (7), $M = {}^1/_2D^3J_f$.

Problems are solved in the same manner as for the rectangular beam, except that the J_f curve is used instead of the K_f curve in Fig. 11.

Beam Shape No. 3—Rectangular Cross Section with Central Hole (Fig. 22):

This case may be solved by subtracting the resisting moment of the inner rectangle from that of the outer rectangle.

Thus

$$M = 3\left(\frac{I}{c}K_f - \frac{I_1}{d/2}K_f'\right)$$

$$= \frac{bh^2}{2}\left[K_f - \left(\frac{d}{h}\right)^2 K_f'\right]$$

where

K_f = the plastic bending factor corresponding to stress f_m and strain e_m in the outer fibers

K_f' = the factor corresponding to stress f' and strain e' at the boundary of the hole. Since strain is linear, $e' = (d/h)e_m$.

Example 1: $b = 1$ in., $h = 2$ in., $d = 0.5$ in., $f_m = F_{tu} = 30{,}000$ lbs. per sq.in.

From Fig. 11, $K_f = K_{fu} = 13{,}800$ lbs. per sq.in. $e_m = e_u = 0.03$; $e' = (0.5/2.0) \times 0.03 = 0.0075$

From Fig. 11, $f' = 23{,}200$ lbs. per sq.in., $K_f' = 10{,}300$ lbs. per sq.in.

Substituting: $M_u = 26{,}300$ in.lbs.

Alternative solution: From Fig. 22, $R_b = 6{,}600$ lbs. per sq.in. for $d/h = 0.25$. $M_u = R_b bh^2 = 6{,}600 \times 1 \times 4 = 26{,}400$ in.lbs.

Example 2: Data are the same as above except that the bending moment, M, is known, and the outer fiber stress, f_m, is required. For an approximate solution assume a value for K_f'/K_f. Ranges of values are roughly as follows:

d/h	0.1	0.4	0.8
K_f'/K_f	0.3–0.6	0.7–0.9	0.9

For the assumed ratio, compute K_f from the formula and determine f_m from Fig. 11. The error can be determined by solving for the moment, M, corresponding to this stress as in Example 1. Further trials can be made if desired.

Beam Shape No. 4—Tubular Beam (Fig. 22):

The resisting moment of a tubular beam is equal to the moment for the outer cylinder minus the moment for the inner cylinder.

Hence

$$M = {}^1/_2 D^3 J_f - {}^1/_2 D_i^3 J_f'$$

where D and D_i are the outer and inner diameters, respectively. If t is the thickness of the tube, $D_i = D - 2t$ and

$$M = {}^1/_2 D^3 \left\{ J_f - [1 - (2t/D)]^3 J_f' \right\}$$

J_f = the plastic bending factor corresponding to stress f_m and strain e_m in the outer fibers

J_f' = the plastic bending factor corresponding to stress f' and strain e' at the inner surface

$$e' = \left(1 - \frac{2t}{D}\right) e_m$$

Example 1: $D = 2$ in., $t = 0.20$ in., $f_m = F_{tu} = 30{,}000$ lbs. per sq.in., $e_m = 0.03$, $e' = [1 - (0.4/2)]0.03 = 0.024$.

From the J_f curve (Fig. 11): $J_f = 9{,}000$ lbs. per sq.in., $J_f' = 8{,}700$ lbs. per sq.in.

Substituting: $M_u = 18{,}200$ in.lbs. assuming crippling is not a factor.

Alternative Solution (Fig. 22a): $D/t = 10$, $R_t = 2{,}300$ lbs. per sq.in., $M_u = R_t D^3 = 18{,}400$ in.lbs.

Example 2: If the moment is known and the stress is required, follow the procedure of Example 2, Beam Shape No. 3, assuming a value for the ratio J_f'/J_f. This ratio varies roughly from 0.7 to 0.95 for D/t ratios from 5 to 20.

Beam Shape No. 5—I-Beam (Fig. 5):

From Eq. (6):

$$M = \left(\frac{bh^2}{2}\right)\left[K_f - \left(1 - \frac{b'}{b}\right)\left(1 - \frac{2t}{h}\right)^2 K_f'\right]$$

Example 1: $b = 1$ in., $b' = 0.25$ in., $h = 2$ in., $t = 0.25$ in., $f_m = F_{tu} = 30{,}000$ lbs. per sq.in.

For an outer fiber stress, $f_m = F_{tu} = 30{,}000$ lbs. per sq.in., the corresponding strain, $e_m = 0.03$, and $K_f = 13{,}800$ lbs. per sq.in.

The strain at the inner surface of the flange (Fig. 5b) is $e' = [1 - (2t/h)]e_m = 0.0225$. Entering Fig. 11 with this value of strain, the stress-strain curve shows the corresponding stress to be 28,700 lbs. per sq.in. and $K_f' = 13{,}200$ lbs. per sq.in.

Substituting in the equation:

$$M_u = 2[13{,}800 - 0.75 \times (0.75)^2\, 13{,}200] = 14{,}500 \text{ in.lbs.}$$

Example 2: Data are the same as in Example 1 except that $M = 10{,}000$ in.lbs. is given and the outer fiber stress is required. An approximate solution may be obtained as follows:

The ratio, K_f'/K_f will vary from about 0.7 for thick flanges to 0.95 for thin flanges. Assuming a value of 0.90 and substituting in the equation: $K_f = 8{,}060$ lbs. per sq.in. and $f_m = 19{,}000$ lbs. per sq.in. Checking, the moment when computed for this stress as in Example 1 is 10,200 in.lbs.

Beam Shape No. 6—Channel with Neutral Axis Parallel to Web or Tee Beam with Neutral Axis Perpendicular to Web:

It is assumed in this case that the neutral axis is through the centroid of the area. Actually, it shifts from this position as plastic bending occurs. However, the resulting error in computing the ultimate moment appears to be small. The problem has two solutions depending on whether the neutral axis is in the web or in the flange.

Case 1. Neutral Axis in Web (Fig. 19):

The resisting moment of the area below the neutral axis is one-half of that for a rectangle of twice the depth or

$${}^1/_2 \frac{b_2(2c_2)^2}{2} K_{f2} = b_2 c_2^2 K_{f2}$$

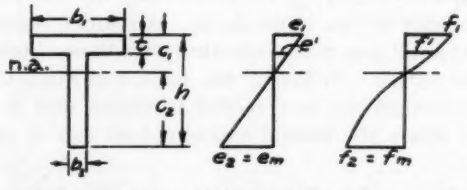

(a) T-SECTION (b) STRAIN (c) STRESS

FIG. 19.

The resisting moment of the area above the neutral axis is

$$b_1c_1^2K_{f1} - (b_1 - b_2)(c_1 - t)^2K_f'$$

Adding:

$$M = b_2c_2^2K_{f2} + b_1c_1^2K_{f1} - (b_1 - b_2)(c_1 - t)^2K_f'$$

$$= b_1c_1^2\left[\frac{b_2}{b_1}\left(\frac{c_2}{c_1}\right)^2K_{f2} + K_{f1} - \left(1 - \frac{b_2}{b_1}\right)\left(1 - \frac{t}{c_1}\right)^2K_f'\right]$$

where

K_{f2} = factor corresponding to stress f_2 and strain e_2
K_{f1} = factor corresponding to stress f_1 and strain e_1
K_f' = factor corresponding to stress f' and strain e'
e_1 = $(c_1/c_2)e_2$ = strain at top of flange
e_2 = e_m = maximum strain at bottom of web
e' = $[(c_1 - t)/c_2]e_2$ = strain at bottom of flange
f_1, f_2, and f' = stresses corresponding to strains e_1, e_2, and e', respectively, in stress-strain diagram

When the flange is in compression, obviously the tensile stress, f_2, in the web governs. However, it should be emphasized that when the flange is in tension and the load approaches the ultimate condition, the compressive stress, f_2, and the tensile stress, f_1, may have the same order of magnitude and the latter will reach a critical value when the compressive stress is below "block compression" ultimate.

For example, if the material is sand-cast aluminum alloy 356-T6 and $c_1/c_2 = {}^1/_2$, $f_2 = 30{,}000$ lbs. per sq.in. (compression), $e_2 = 0.03$, then $e_1 = {}^1/_2 \times 0.03 = 0.015$ and $f_1 = 26{,}700$ lbs. per sq.in. (tension).

Hence, the tensile stress in the flange is not far from its ultimate value even though the compressive stress is quite conservative if it is assumed that crippling is not a factor.

Example 1: $b = 1$ in., $h = 2$ in., $t = 0.25$ in., $b_2 = 0.25$ in., $f_m = F_{tu} = 30{,}000$ lbs. per sq.in., $e_m = e_u = 0.03$; flange in compression.

Assuming the neutral axis at the centroid: $c_1 = 0.76$ in., $c_2 = 1.24$ in., then

$e_2 = e_m = 0.03$
$e_1 = \frac{c_1}{c_2}e_2 = 0.018$
$e' = \frac{c_1 - t}{c_2} = 0.012$

$f_2 = f_m = 30{,}000$ lbs. per sq.in.
$f_1 = 27{,}600$ lbs. per sq.in.
$f' = 25{,}600$ lbs. per sq.in.
$K_{f2} = 13{,}800$ lbs. per sq.in.
$K_{f1} = 12{,}600$ lbs. per sq.in.
$K_f' = 11{,}500$ lbs. per sq.in.

Substituting: $M_u = 10{,}200$ in.lbs.

The problem may be solved more readily from the data in Fig. 22.

Example 2: When the moment is known and the stress, f_m, is desired, assume $K_f' = 0.9K_{f1}$, $K_{f1} = 0.9K_{f2}$, and solve for K_{f2}. Determine the corresponding f_m from Fig. 11.

Case 2. Neutral Axis in Flange (Fig. 20):

The resisting moment of the area above the neutral axis is $b_1c_1^2K_{f1}$.

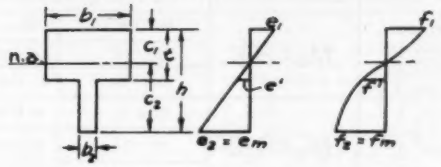

(a) T-SECTION (b) STRAIN (c) STRESS

FIG. 20.

The resisting moment of the area below the neutral axis is

$$b_2c_2^2K_{f2} + (b_1 - b_2)(t - c_1)^2K_f'$$

Adding:

$$M = b_1c_1^2K_{f1} + b_2c_2^2K_{f2} + (b_1 - b_2)(t - c_1)^2K_f'$$

$$= b_1c_1^2\left[\frac{b_2}{b_1}\left(\frac{c_2}{c_1}\right)^2K_{f2} + K_{f1} + \left(1 - \frac{b_2}{b_1}\right)\left(\frac{t}{c_1} - 1\right)^2K_f'\right]$$

$$e_1 = \frac{c_1}{c_2}e_2, \quad e' = \frac{t - c_1}{c_2}e_2$$

The nomenclature is the same as in the previous problem. Examples are solved as in Case 1.

Beam Shape No. 7—Cross or I-Beam Section with Neutral Axis Perpendicular to Flanges (Fig. 22):

This case may be solved by adding the resisting moments of the separate rectangles.

Thus

$$M = \frac{2tb^2}{2}K_f + \frac{(h - 2t)(b')^2}{2}K_f'$$

$$= tb^2\left[K_f + \left(\frac{h}{2t} - 1\right)\left(\frac{b'}{b}\right)^2K_f'\right]$$

where

K_f = factor corresponding to stress f_m and strain e_m
K_f' = factor corresponding to stress f' and strain e'
e' = $(b'/b)e_m$ = strain at face of web
f' = stress corresponding to strain e' in stress-strain diagram

Problems are solved as for Beam Shape No. 5. For approximate solution, the ratio K_f'/K_f varies from about 0.6 to 0.9 for b'/b ratios between ${}^1/_8$ and ${}^1/_2$.

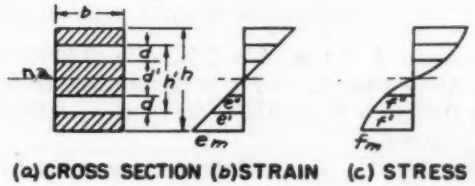

(a) CROSS SECTION (b) STRAIN (c) STRESS

FIG. 21.

BEAM SHAPE	ULTIMATE MOMENT
1. RECTANGLE	$M_u = R\frac{I}{c}$
2. CIRCULAR	$M_u = R_o D^3$

ULTIMATE MOMENT FACTORS		
MATERIAL	R	R_o
195-T6	44,500	4,820
356-T6	41,500	4,510
DOW H	39,800	4,220
14-ST	95,100	10,500

FIG. 22(a) - ULTIMATE MOMENTS VALUES
BASED ON MINIMUM SPECIFIED VALUES

MATERIAL	MIN. SPEC. VALUES F_{cu} (P.S.I.)	F_{tu} (P.S.I.)	ELONG. (%)
AN-QQ-A-390 S.C. AL. ALLOY 195-T6	32,000	18,000	3
AN-QQ-A-394 S.C. AL. ALLOY 356-T6	30,000	20,000	3
AN-QQ-M56 DOW METAL H-HT (COMP. A)	32,000	10,000	7
AN-QQ-A-367 AL. ALLOY FORGING 14-ST	65,000	50,000	10

3. RECTANGLE WITH CENTRAL HOLE — $M_u = R_h b h^2$

4. TUBE — $M_u = R_t D^3$

NOTE: VALUES GIVEN BELOW DO NOT PROVIDE FOR CRIPPLING FAILURE

BEAM SHAPE 5 — $M_u = R_i b h^2$

(a) I-BEAM (b) CHANNEL

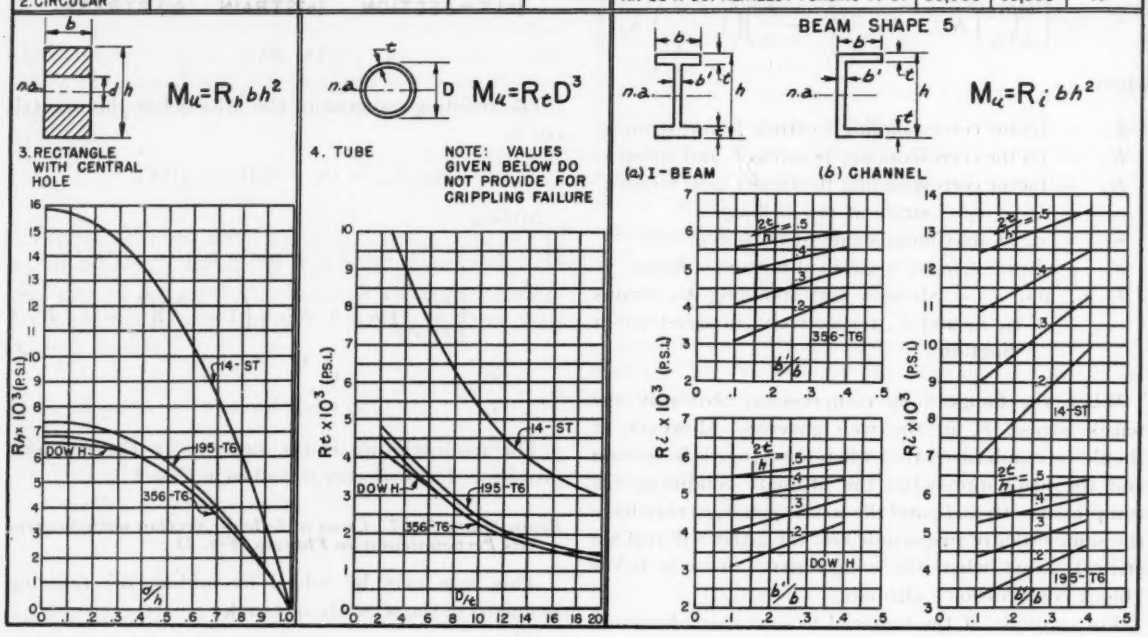

Beam Shape No. 8—Symmetrical Rectangular Cross Section with Two Holes (Fig. 21):

This case may be solved as a combination of a solid rectangular beam and Beam Shape No. 3 .

Thus

$$M = \frac{bh'}{2} K_f - \frac{b(h')^2}{2}\left[K_f' - \left(\frac{d'}{h'}\right)^2 K_f''\right]$$

where

K_f = factor corresponding to stress f_m and strain e_m
K_f' = factor corresponding to stress f' and strain e'
K_f'' = factor corresponding to stress f'' and strain e''
$e' = (h'/h)e_m$ = strain at outer boundary of a hole
$e'' = (d'/h)e_m$ = strain at inner boundary of a hole
f' and f'' = stresses corresponding to strain e' and e'', respectively, in stress-strain diagram

Example: $b = 1$ in., $h = 2$ in., $d' = 0.50$ in., $d = 0.25$, $h' = 1$ in., $f_m = F_{tu} = 30{,}000$ lbs. per sq.in., $e_m = 0.03$, $e' = {}^1/_2 \times 0.03 = 0.015$, $e'' = (0.50/2) \times 0.03 = 0.0075$.

From Fig. 11: $K_f = 13{,}800$ lbs. per sq.in., $K_f' = 12{,}200$ lbs. per sq.in., $K_f'' = 10{,}300$ lbs. per sq.in.

Substituting: $M_u = 22{,}800$ lbs. per sq.in.

Ultimate Moment Factors

The ultimate moment expression for various beam shapes can be reduced to the simple forms given in Fig. 22 and the results plotted as shown. The computation is somewhat laborious for some of the shapes and is scarcely worthwhile unless many beams are to be checked. However, the data of Fig. 22 may be used to good advantage for materials not shown by introducing the correction factor discussed previously. For example, the ultimate moment of the 24-ST extruded aluminum beams mentioned under "Test Results" may be computed from the data for 14-ST aluminum-alloy forging since the stress-strain curves of these two materials are of the same general shape. The average ultimate tensile strength of the 24-ST was 68,400 lbs. per sq.in. compared to 65,000 lbs. per sq.in., the minimum specified value for 14-ST. Hence, the correction factor is 1.05. When computed in this way, predicted moments have been found to be within 2 per cent of values determined from 24-ST diagrams.

It should be emphasized that the data in Fig. 22 are based on the assumptions that tension and compression stress-strain curves are identical and that crippling stress is not a factor.

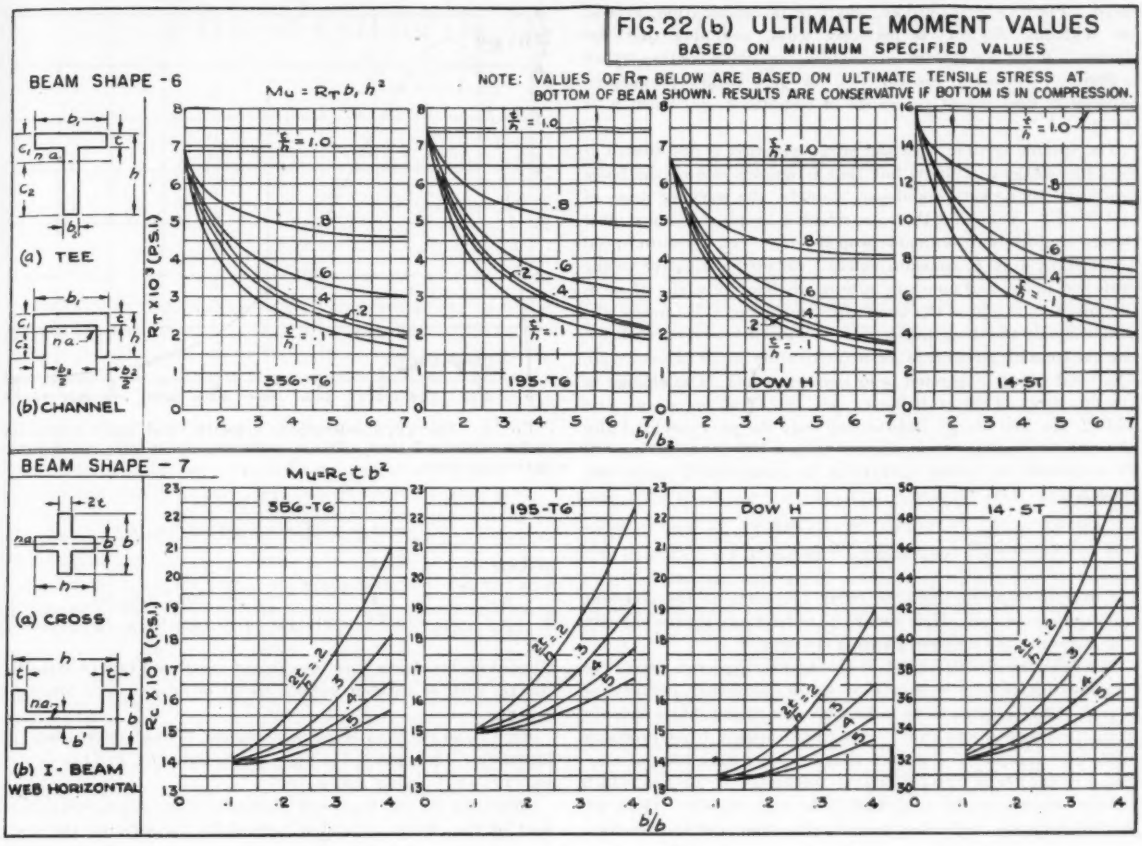

References

[1] Timoshenko, S., *Strength of Materials*, Part II, 2nd Ed., Chapt. VIII; D. Van Nostrand Company, Inc., New York, 1941.

[2] Timoshenko, S., and MacCullough, G. H., *Elements of Strength of Materials;* D. Van Nostrand Company, Inc., New York, 1940.

[3] Cozzone, Frank P., *Bending Strength in the Plastic Range*, Journal of the Aeronautical Sciences, Vol. 10, No. 5, p. 137, May, 1943.

[4] Beilschmidt, J. L., *The Stresses Developed in Sections Subjected to Bending Moment*, Journal of the Royal Aeronautical Society, Vol. XLVI, No. 379, pp. 161–182, July, 1942.

[5] Beilschmidt, J. L., *Strength of Light-Alloy Components*, Aircraft Engineering, Vol. XVI, No. 181, pp. 76–81, March, 1944.

[6] MacCullough, G. H., *An Experimental and Analytical Investigation of Creep in Bending*, Journal of Applied Mechanics, Vol. 1, No. 2, pp. 55–60, April-June, 1933.

[7] Hrennikoff, A., *Theory of Inelastic Bending, with Reference to Limit Design*, Proc. A.S.C.E., Vol. 73, No. 3, pp. 255–289, March, 1947.

Letter to the Editor

Dear Sir:

Consideration of an extreme or "theoretical" case is often the most practical means of clarifying thought and bringing out basic principles, such as Professor Williams has attempted in his Letter to the Editor in the JOURNAL OF THE AERONAUTICAL SCIENCES, page 236, April, 1947, but apparently without full use of the possibilities implied in his interesting approach.

Many writers have stressed the alleged inappropriateness of ordinary efficiency conceptions to rocket propulsion. But why set up arbitrary or conventional limitations in the use of such a broadly versatile parameter? In any use of efficiency as the ratio of useful to expended energy or power, each must, of course, be defined for the purpose at hand and the basic assumptions made clear; but, after all, energy remains the same kind of thing whether applied to pushing on an outside medium such as air or on mass initially carried in the craft itself. The differences in treatment are mainly concerned with the kind of energy ratios desired for comparative analysis and with the frame of reference chosen for the speed.

For simple momentum theory applied to propellers, this frame of reference is most naturally the medium through which the aircraft flies and on which the propeller acts to produce propulsive force. Here the useful power can certainly be defined, if desired, as the product of thrust and speed, regardless of whether such thrust is used for acceleration, for counteracting gravity, or exclusively for overcoming resistance to level flight at constant

speed. For *any* such purpose, singly or in combination, Professor Williams' Eq. (1) is perfectly valid, assuming that the change in mass, the slipstream rotation, and blade friction are all negligible. However, his Eq. (2), for pure rocket propulsion, apparently does not fit the range of conditions for which it is set up.

The specific trouble with the latter equation is not that it is used for accelerated flight but that it ignores one of the basic conditions of rocket propulsion—namely, the varying mass of unit itself.* Take first the case, which is simplest and also most closely analogous to ordinary propeller use—i.e., constant speed V, constant drag F, constant exhaust velocity v (relative to the propelled unit), and constant rate of discharge dm/dt. If m_0 is the initial mass and m the mass after traversing a distance s, the thrust equals the drag and is $F = -v(dm/dt) = v(m_0 - m)/t$, and the total drag energy is $Fs = (vs/t)(m_0 - m) = vV(m_0 - m)$. The total energy expended is in two terms: (1) The change in kinetic energy of the craft itself: $\Delta E_k = (V^2/2)(m_0 - m)$, and and (2) the fuel energy (considering only the part mechanically effective in creating momentum): $\Delta E_f = (v^2/2)(m_0 - m)$. If Fs is termed the useful energy, as in conventional usage, the efficiency is

$$\eta = \frac{Fs}{\Delta E_k + \Delta E_f} = \frac{2V/v}{V^2/(v^2 + 1)} \qquad (1)$$

the overall value in this case being the same as the constant instantaneous value. Here the frame of reference for the velocity V is naturally the medium creating the drag F.

It will be noted that Eq. (1),† as might be expected, gives zero efficiency for either $v = 0$ or $V = 0$, and a maximum of unity for $v = V$. As V increases to values greater than v, the efficiency again approaches zero (not ∞, as would appear from Professor Williams' equation). For no resistance other than inertia, a rational definition of "useful power" might be the rate at which kinetic energy of the propelled unit is increased. Thus, by similar methods, neglecting second order effects of the acceleration on the exhaust velocity, the instantaneous efficiency:

$$\eta_i = dE_k/dE_f = (V/v)[2 - (V/v)] \qquad (2)$$

the frame of reference for V being taken here as simply the state of rest (or "motion") when $m = m_0$. Such a reference in the general case is, of course, arbitrary and permits referring the result to any desired "initial" condition (ordinarily at rest relative to the earth). It is of interest that precisely the same result is obtained from the previous case by assuming that the reduction of mass imposes a negative increment on the useful energy instead of a positive increment on the total energy expended.

On the basis of Eq. (2), the efficiency still has a maximum value of unity when $V = v$ but drops to zero again when $V = 2v$. The negative efficiency values for still larger values of V can be explained by the fact that under such conditions the relative mass is decreasing faster than can be counterbalanced by the increase in V^2, thus actually reducing the kinetic energy (on the assumed basis of $V = 0$ when $m = m_0$).

For vertical rocket flight outside the atmosphere, a more practical concept of efficiency is based on the directly useful (because usable) kinetic energy attained by a residual mass m after discharge of its available fuel energy and its accompanying mass. On this basis, with constant acceleration a and allowance for an assumed constant g directly opposing the motion, the total effective fuel energy is the same as before: $E_f = (v^2/2)(m_0 - m_0)$ and the final kinetic energy for the mass m is of course $E_k = mV^2/2$. But for constant exhaust speed v, $F = -vdm/dt = a(m_0 - m) = m(a + g)$ which, integrated from the starting condition, gives $\log_e (m_0/m) = (t/v)(a + g)$. Then

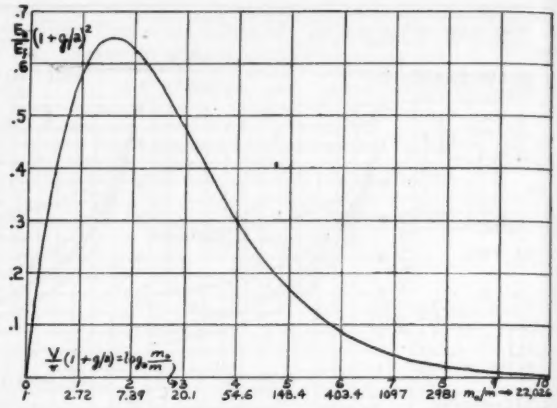

FIG. 1. Energy, acceleration, velocity, and mass ratios for rocket with constant exhaust velocity, constantly accelerated against gravity.

$$V = at = v/[1 + (g/a)] \log_2 (m_0/m)$$

making

$$\eta = \frac{E_k}{E_f} = \frac{V^2}{v^2(e^{(V/v)[1+(g/a)]} - 1)} = \frac{\log_e{}^2 (m_0/m)}{[1 + (g/a)]^2[(m_0/m) - 1]} \qquad (3)$$

Conditions involving variable exhaust speed and rate of mass discharge, with or without various forms of drag, can be similarly set up.

Eq. (3), so far from being meaningless, is most interesting and instructive. It is plotted in Fig. 1 in the form $(E_k/E_f)[1 + (g/a)]^2$ vs. $(V/v)[1 + (g/a)]$ and m_0/m.

Efficiency on this basis will obviously never reach unity, since part of the energy expended is used for accelerating the unexpended fuel mass in the wrong direction and a variable amount of energy in general remains in the expended mass. The well-known fact is further apparent that energy is economized by building up the kinetic energy of the rocket as rapidly as possible. Thus, the maximum efficiency (neglecting heat losses) is 0.647 for $a = \infty$ (or no gravity), which is further reduced to 0.450 for $a = 5g$ (apparent weight of 6 × gravity), probably the maximum desirable value for human beings.

From the same efficiency equation, the optimum dischargable mass, relative to the residual mass m, is $(m_0 - m)/m = 3.94$; in other words, optimum utilization of the available energy will be had by applying it to the discharge of material weighing nearly four times the total rocket weight with the rest of its useful load. It is of particular interest that this optimum dischargable mass is independent of other parameters such as acceleration, ultimate speed, and even the amount of fuel energy available; but, on the other hand, this makes the optimum proportion of energy to mass quite variable. Ordinary chemical energy is, of course, unavoidably saddled with an exhaust mass that, although inadequate for present airplane speeds, would be much more than optimum for many possible purposes. Nuclear energy, on the other hand, would apparently always require the addition of extra mass to be energized for propulsive use.

For example, a trip around the moon and return (still in the fantastic class to most aeronautical engineers, including the writer!) would require a speed of about 36,000 ft. per sec. at the end of the acceleration period (consuming not quite 4 min. at $a = 5g$). The corresponding kinetic energy, per pound of residual weight, would be $36{,}000^2/(2g) = 20.2 \times 10^6$ which, divided by the efficiency 0.45, gives a required mechanically effective fuel energy of 45×10^6 ft.lbs., or 57,800 B.t.u. per lb. The latter figure is about ten times the heat energy of the best known chem-

(*Continued on page 488*)

* A similar oversight is apparent in Mr. Krzywoblocki's Letter to the Editor, JOURNAL OF THE AERONAUTICAL SCIENCES, Vol. 14, No. 5, p. 310, May, 1947.

† Corresponds to Eq. (13), page 24, JOURNAL OF THE AERONAUTICAL SCIENCES, January, 1947, developed by Krzywoblocki and McCloy by a more circuitous method.

The Problem of Escape from the Earth by Rocket

FRANK J. MALINA* AND MARTIN SUMMERFIELD†

California Institute of Technology

ABSTRACT

The problem of imparting to a given pay load the necessary velocity to escape from the earth is re-examined in the light of recently released information on wartime rockets. The fundamental equations of motion of a rocket in outward radial flight are derived and the influence of each of the following design parameters is examined: c, the effective jet velocity; ζ, the ratio of propellant mass to initial mass; t_p, the time of powered flight; μ, the ratio of initial mass to maximum cross-sectional area; and C_d, the drag coefficient based on the same cross-sectional area.

The exhaust velocities attainable under standard conditions with rocket propellants range between 6,200 ft. per sec. for nitric acid-aniline and 10,200 ft. per sec. for oxygen-hydrogen, the former being representative of dense propellants and the latter of light propellants. On the basis of the design characteristics of the V-2 rocket, it is believed that the maximum practical value of ζ that may be realized is about 0.85. Therefore, it is concluded that single-step rockets utilizing propellants that develop their energy by chemical reaction cannot escape from the earth. Escape may be accomplished by single-step rockets, however, if nuclear sources of energy can be used to heat gases of low molecular weight in order to provide much higher exhaust velocities.

The analysis is extended to calculate the velocity achieved by a multiple-step rocket. The overall mass of the rocket and the maximum velocity of the last step are related to the number of steps and to the ratio of the masses of successive steps.

It is shown that the necessary velocity can be attained with any of the rocket propellants available by proper choice of the number of steps. Various examples of multiple-step rockets capable of projecting instrumental pay loads away from the earth are presented.

1. INTRODUCTION

MAN HAS LONG SPECULATED on the possibility of escaping from the earth, or at least of projecting bodies from the earth toward other bodies in space. Many papers have been written on various aspects of the subject, including the problems of navigation among the planets and questions of what may be discovered among the heavenly bodies.

Of all these questions the problem to be considered first is the means of escaping from the gravitational field of the earth. Calculations on various schemes have been previously presented by Ziolkowsky,[1] Goddard,[2] Lorenz,[3] Senftleben,[4] Oberth,[5] Rynin,[6] Campbell,[7] Ley,[8] Ackeret,[9] and others. Recent German and American achievements in the field of rocketry, as exemplified by the V-2 long-range rocket and the "WAC Corporal" high-altitude rocket,[10] justify the need for a re-evaluation of the feasibility of escape. It is on this problem that the present paper is concentrated.

In general, two methods of attaining the necessary high velocities have been considered: the gun and the rocket. Previous investigations have conclusively demonstrated, on theoretical grounds, that the maximum velocity that can be imparted to a projectile using a gun of unlimited length and propelled by the most energetic chemical propellants possible is insufficient to enable it to escape from the earth. The velocity attainable by a rocket, on the other hand, approaches that required for escape provided the mass ratio, i.e., the ratio of the contained propellant weight to the gross weight of the rocket, is made sufficiently high. Furthermore, by means of multiple-step rockets, the final velocity can be increased even more. On the basis of data on the exhaust velocity obtainable with different propellants, as presented below, the conditions required for escape have been calculated. It is concluded that it is now within engineering feasibility to propel a body with the required velocity.

NOTATION

a	= acceleration of rocket at any instant
A	= projected area of rocket
c	= effective exhaust velocity of rocket jet = F/m
c_a	= average value of c during powered flight
C_d	= drag coefficient based on area A
D	= drag due to air resistance = $C_d A(\frac{1}{2}\rho v^2)$
F	= thrust of rocket
g	= acceleration due to gravity at any point
g_0	= acceleration due to gravity at earth's surface
G	= overall mass ratio of step rocket = $M_0^{(1)}/M_l$
h	= altitude above surface of earth
K	= ratio of C_d of rocket to that assumed in Fig. 3
m	= mass ejected from rocket per unit time in exhaust jet
M	= mass of rocket at any instant
M_e	= mass of empty rocket (pay load and propellant excluded)
M_p	= mass of propellant in rocket
M_l	= mass of pay load carried by rocket
M_0	= initial gross mass of rocket = $M_e + M_p + M_l$
$M_e^{(n)}$	= empty mass of nth step of multiple-step rocket
$M_p^{(n)}$	= mass of propellant contained in nth step
$M_0^{(n)}$	= initial mass of nth step = $M_e^{(n)} + M_p^{(n)} + M_0^{(n+1)}$
n	= ratio of acceleration of rocket to g_0
N	= number of steps in multiple-step rocket; Nth step is last to fire
r	= distance from center of earth

Presented at the Sixth International Congress for Applied Mechanics (Section II) at Paris, France, September 22–29, 1946. Received February 24, 1947.

* On leave of absence with United Nations Educational Scientific and Cultural Organization (UNESCO), Paris, France.

† Chief, Rockets & Materials Division, Jet Propulsion Laboratory.

r_e = radius of earth
S = velocity ratio = $(v_N + g_0 t_p)/c_a$
t = time
t_p = duration of powered flight
v = velocity of rocket at any instant
v_e = escape velocity
v_n = velocity of rocket at end of firing of nth step
ϵ = structural factor = $M_e^{(n)}/(M_e^{(n)} + M_p^{(n)})$
λ = pay-load ratio = $M_1/M_0^{(N)}$
μ = gross mass per unit projected area of rocket = M_0/A
ρ_0 = atmospheric density at sea level
σ = ratio of atmospheric density to standard sea-level density
ζ = propellant loading ratio = $M_p/M_0 = (1 - \lambda)(1 - \epsilon)$

2. Requirements for Escape from the Earth

The familiar problem of the motion of a body in the earth's gravitational field can be analyzed to derive the value of the necessary velocity for escape. The acceleration of gravity at any distance from the earth's center is given by the following equation:

$$g = g_0(r_e^2/r^2) = g_0[r_e^2/(r_e + h)^2] \quad (1)$$

The minimum velocity of escape at any distance is calculable from the following equation, on the basis of conservation of energy:

$$^1/_2\, v^2 = \int_r^\infty g\,dr = \int_r^\infty g_0(r_e^2/r^2)dr = g_0(r_e^2/r) \quad (2)$$

$$v_e = r_e\sqrt{2g_0/(r_e + h)} \quad (3)$$

The radius of the earth at the equator is 21.0×10^6 ft., and the corresponding acceleration of gravity, corrected for the centrifugal effect of the earth's rotation, is 32.2 ft. per sec. per sec. Inserting these values in Eq. (3), the graph shown in Fig. 1 is obtained. The required velocity for escape at sea level is 36,700 ft. per sec.

The effect of air resistance is neglected in Eq. (3). The curve of Fig. 1 needs modification because of air resistance only within the height of the atmospheric layer, about 50 miles, if at all. However, for rockets of a size sufficiently large to accomplish the flight, the deceleration due to drag is so small that the velocity loss over the interval of traverse of the atmospheric layer can be neglected. That this size effect is favorable can be seen from the fact that, for similar bodies of various sizes, the air resistance is proportional to the square of any dimension whereas the mass varies as the cube of the same dimension. The deceleration, therefore, is inversely proportional to the linear size of the rocket. This question is treated quantitatively in Section 3.

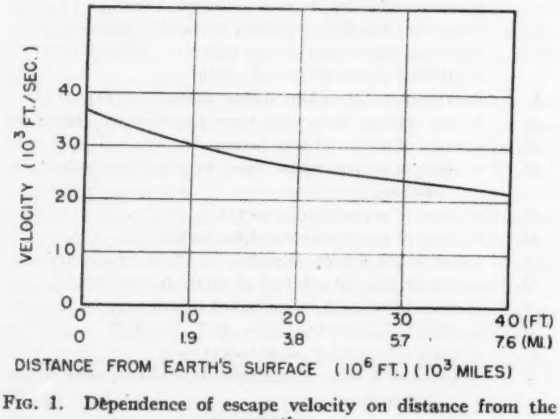

Fig. 1. Dependence of escape velocity on distance from the earth.

The peripheral speed of the earth's surface at the equator is 1,530 ft. per sec., less than 5 per cent of the escape velocity at the surface of the earth. It is considered permissible to neglect this quantity in the present analysis, although a more refined trajectory calculation would perhaps make use of some of this initial velocity.

The effect of the gravitational attraction of the moon on a rocket leaving the earth in a direction away from the moon can be neglected. The mass of the moon is $^1/_{81}$ that of the earth, and its distance is 60 times the radius of the earth; thus the initial potential energy of the rocket due to the moon's field is only 0.02 per cent that due to the earth. In the case of a rocket directed toward the moon, the proximity of the moon is sufficient to reduce the required initial kinetic energy by 2 per cent, or the required escape velocity, by 400 ft. per sec. The effects in both cases are considered negligible in the computations in this paper.

3. Performance Parameters of the Rocket

In this section the basic performance parameters of a rocket launched vertically from the earth's surface will be discussed. The parameters have been studied in connection with the sounding rocket.[11, 12] However, for purposes of the present investigation, a further consideration of their significance is desirable. An analysis of only the powered flight of the rocket is required. It will be assumed that the propulsion system delivers a constant thrust obtained from the ejection of mass carried wholly in the rocket. The energy of the ejected mass is acquired from either a molecular or a nuclear process.

During powered flight the mass of the rocket at any instant is given by the equation

$$M = M_0[1 - \zeta(t/t_p)] \quad (4)$$

and the fundamental equation of motion has the form

$$a = dv/dt = (F - D - Mg)/M \quad (5)$$

Substituting $F = mc = (M_p/t_p)c$, $D = C_d\rho_0\sigma A(v^2/2)$, and Eq. (4) in Eq. (5), the following relation is obtained:

$$\frac{dv}{dt} = \frac{\frac{\zeta c}{t_p} - C_d\rho_0\sigma\frac{v^2}{2}\frac{1}{\mu}}{1 - \zeta(t/t_p)} - g \quad (6)$$

and on integrating

$$v = \int_0^t \frac{\frac{\zeta c}{t_p} - C_d \rho_0 \sigma \frac{v^2}{2} \frac{1}{\mu}}{1 - \zeta(t/t_p)} dt - \int_0^t g\, dt + v_0 \quad (7)$$

For the case of flight in empty space, the drag term in Eq. (7) vanishes, and on integrating one obtains the well-known relation for the velocity of the rocket during powered flight if the variation of gravitational acceleration is neglected,

$$v = -c \ln [1 - \zeta(t/t_p)] - g_0 t + v_0 \quad (8)$$

At the end of powered flight when $t = t_p$

$$v_{max.} = -c \ln (1 - \zeta) - g_0 t_p + v_0 \quad (9)$$

It should be noted that Eq. (9) holds even if the thrust acting on the rocket is variable.

Returning to Eq. (7), it is seen that the performance of the rocket is determined by six design parameters—c, ζ, t_p, μ, C_d, and v_0, which can be varied by the designer, and by two parameters, g and $\rho_0\sigma$, which are independent of the rocket design.

The influence of the design parameters t_p, μ, and C_d on the maximum velocity that a rocket can achieve for the case $\zeta = 0.80$, $c_a = 7{,}700$ ft. per sec., $v_0 = 0$, and $g = g_0$ is shown in Fig. 2. The curves have been computed using the drag coefficient given in Fig. 3 and atmospheric density and temperature distributions given for the N.A.C.A. standard atmosphere.[13] The graph can be used equally well for rockets having a drag characteristic differing from that in Fig. 3 by a multiplicative constant. The drag factor K therefore has been introduced to permit the use of other drag coefficient curves that have a shape similar to the one shown in Fig. 3. In a like manner, by using a factor equal to the ratio of the density at sea level to that at the launching altitude, Fig. 2 can be made to apply approximately to the flight of rockets launched from high elevations where the atmosphere density is reduced.

In Fig. 4 the effects on the maximum rocket velocity of the propellant loading parameter ζ and of the effective exhaust velocity c are shown for the case $t_p = 30$ sec., $\mu/K = \infty$ (i.e., drag is neglected), $v_0 = 0$, $g = g_0$.

Several conclusions can be drawn from the curves in Figs. 2 and 4. First, the shorter the duration of firing, the larger will be the velocity of the rocket at the end of burning. This effect results from the decreased loss caused by the constant deceleration due to gravity. This principle cannot be applied to rocket design without considering the simultaneous effects of the increased mass of the propulsion system required for a short firing duration and the increased structural mass arising from high acceleration loads. Second, the greater the propellant mass loading ratio ζ, the higher will be the velocity at the end of burning, and, furthermore, as ζ approaches unity, the terminal velocity becomes infinite. Third, the loss in velocity due to atmospheric drag diminishes as the value of μ increases, the loss being inversely proportional to μ [cf. Eq. (7)]. For rockets of similar

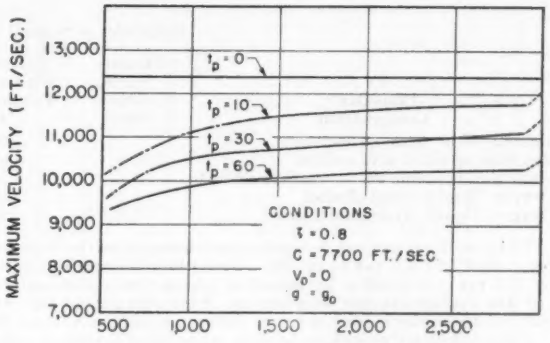

FIG. 2. Variation of maximum velocity with mass per unit cross-sectional area of rocket.

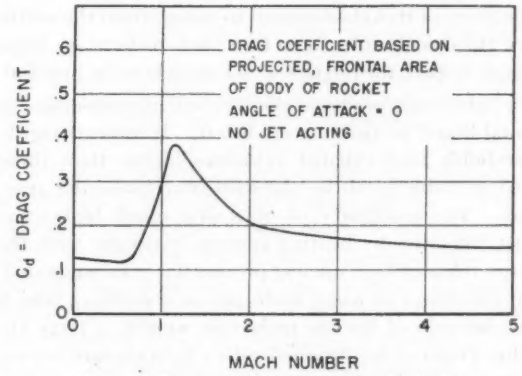

FIG. 3. Drag coefficient of typical rocket.

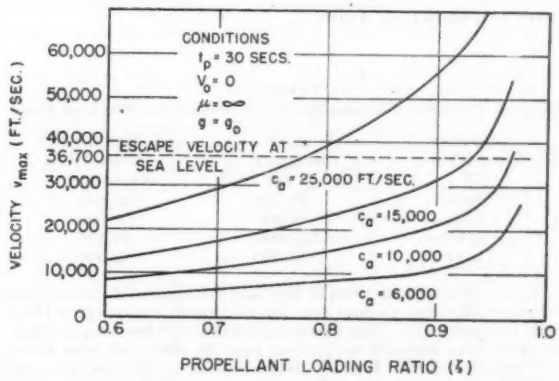

FIG. 4. Dependence of velocity at end of burning on propellant loading ratio.

geometrical shape propelled in the same trajectory, the parameter μ is proportional to the product of the average density and the length of the rocket. Consequently, the loss in velocity due to drag is inversely proportional to the length of the rocket. Fig. 2 shows that for $t_p = 30$ sec., $\zeta = 0.8$, and $c = 7{,}700$ ft. per sec., the loss is 10 per cent at $\mu = 650$ lbs. per sq.ft., and 3 per cent at $\mu = 2{,}000$. An acid-aniline rocket having an average den-

TABLE 1
Properties of Several Propellant Combinations

Propellant Combination	Mixture Ratio (Oxidizer/-Fuel)	Calculated Combustion Temperature (°F.)	Average Density (Lbs./Cu.Ft.)	Exhaust Velocity at Sea Level (Ft. per Sec.)	Average Exhaust Velocity (Ft. per Sec.)	Propellant Loading Ratio
Nitromethane (monopropellant)	...	3,950	71.0	6,150*	7,240†	0.995‡
Red fuming nitric acid-aniline	3.0	5,070	85.9	6,200	7,300	0.995
Hydrogen peroxide (87%)-methyl alcohol	4.0	4,160	75.5	6,300	7,420	0.995
Oxygen (liquid)-ethyl alcohol	1.5	5,260	60.4	6,870	8,090	0.991
Oxygen (liquid)-hydrogen (liquid)	3.0	4,390	14.8	10,150	12,000	0.960

* The sea-level exhaust velocities are calculated on the basis of a steady combustion pressure of 300 lbs. per sq.in. abs. and an exit pressure of 14.7 lbs. per sq.in. abs. An optimum nozzle area ratio is assumed (about 4.0). The theoretical values have been reduced by 12.5 per cent to allow for imperfect combustion and imperfect flow.

† The average exhaust velocities are 18 per cent greater than the sea-level values. This is the approximate average increase due to reduced atmospheric back pressure during an assumed vertical flight.

‡ The calculated propellant loading ratios listed in the last column are the minimum values required to enable a rocket to attain the escape velocity. A constant acceleration of $20g_0$ is assumed, and drag is neglected. (See Section 4.)

sity of 50 lbs. per cu.ft. will suffer a loss of only 3 per cent in terminal velocity due to drag if it is about 40 ft. long. This conclusion is significant in the later considerations of rockets designed to escape from the earth, since the calculations show that such rockets are large enough so that the neglect of the drag term is justified.

In Table 1 the practical effective exhaust velocities for several liquid propellants are listed. It appears highly improbable that exhaust velocities higher than those listed in Table 1 can be obtained from molecular reactions. The possibility of obtaining much higher exhaust velocities by heating gaseous hydrogen with the energy released by a nuclear process has been suggested. The advantage of using hydrogen as a working fluid is that, because of its low molecular weight, a large enthalpy drop can be obtained with a temperature not exceeding that already in use in rocket motors. Calculated exhaust velocities for various chamber temperatures are shown in Table 2.

TABLE 2
Exhaust Velocities Obtainable with Hydrogen as Working Fluid

Chamber Temperature (°F.)	Heat Required (B.t.u. per Lb.)	Exhaust Velocity (Ft. per Sec.)
5,000	20,700	23,400
7,000	49,000	29,100
9,000	113,000	36,400
11,000	152,000	42,300

NOTE: The calculations of the heat required and the exhaust velocity take into account the dissociation of hydrogen at these high temperatures. The theoretical values of the exhaust velocity have been lowered by 5.0 per cent to allow for heat losses and imperfect flow. The calculation assumes a chamber pressure of 300 lbs. per sq.in. abs. and an exit pressure of 14.7 lbs. per sq.in. abs. and flow with constant composition.

4. SINGLE-STEP ROCKETS DESIGNED TO ESCAPE FROM THE EARTH

The outward radial flight of a rocket starting at the earth's surface with zero initial velocity will now be considered with the aid of the data presented in the preceding section.

Several approximations will be used. First, the variation of the gravitational attraction with altitude will be neglected during the period of powered flight. A treatment in which the variation of gravitational acceleration is taken into account has been reported.[12] It can be shown that the corrections are negligible in the cases examined below. Second, the retardation due to drag will be considered negligible since the size of the contemplated rocket will be extremely large. Third, the initial velocity of the rocket due to the peripheral speed of the earth's surface will be neglected. Finally, the required velocity for escape will be taken as that at the earth's surface, namely, 36,700 ft. per sec., since it is consistent with the first assumption to assume that the altitude at which the propellant is exhausted is small compared with the earth's radius.

The equation of motion in this case can be integrated as above, regardless of the variation of thrust during the firing period.

$$v_{max.} = -c \ln (1 - \zeta) - g_0 t_p \qquad (10)$$

From Eq. (10) the necessary propellant loading ratio to achieve the escape velocity can be determined for each propellant listed in Table 1. First, a consideration of the optimum time of powered flight t_p is necessary. It is evident from Eq. (10) that the maximum velocity will be obtained when the $t_p = 0$; i.e., the propellant is consumed instantaneously. But the high thrust required would necessitate a heavy propulsion system, and the resulting high acceleration would require a heavy structure for the rocket, which would seriously decrease the value of ζ. A compromise burning time must therefore be chosen to obtain the best combination of ζ and t_p.

The optimum combination of ζ and t_p can be determined only by considering the many factors that enter into the design of a given type of rocket. The choice of t_p determines the rate of propellant consumption which, in turn, determines the mass of the rocket motor, the mass of the hydraulic lines and valves, the mass of the pumping plant or pressurization system, and the mass of the structure designed to support these components. Analytically, the relationship may be expressed as follows:

$$\zeta = f(t_p) \tag{11}$$

where the form of function f is dependent on the type of rocket being considered. In general, the function is such that ζ increases monotonically with t_p and asymptotically approaches a limiting value as t_p becomes infinite. By combining Eq. (11) with Eq. (10) for any specific function $f(t_p)$, a unique value of t_p can be obtained for which $v_{max.}$ will be greatest.

An alternate approach is usually dictated by the maximum acceleration allowable by the particular character of the pay load. In this event, two limiting cases are possible: (1) a rocket may be designed to deliver a constant thrust, in which case the maximum acceleration occurs at the end of burning when the mass of the rocket is least; or (2) the rocket may be designed to deliver a continually decreasing thrust so as to maintain a predetermined constant acceleration. In both cases, the burning time is determined by the acceleration selected.

For the case of the constant thrust rocket it can be shown that Eq. (10) takes the form:

$$v_{max.} = -c\left[\ln(1-\zeta) + \left(\frac{\zeta}{1-\zeta}\right)\left(\frac{1}{n+1}\right)\right] \tag{12}$$

where $n = a_{max.}/g_0$. The minimum value of t_p corresponding to a given maximum acceleration at the end of powered flight is:

$$t_{p\ min.} = [\zeta/(1-\zeta)][c/g_0(n+1)] \tag{13}$$

In Fig. 5 the ratio $v_{max.}/c$ is plotted as a function of ζ for various values of n according to the relationship given in Eq. (12).

It can be seen that the maximum value of the acceleration, denoted by n, limits the maximum velocity that can be obtained. For $n = 5$, the maximum velocity of the rocket is approximately equal to the exhaust velocity of the propellant; for $n = 20$, the maximum velocity is slightly more than twice as much. Furthermore, for each value of n there is a limiting value of ζ above which no improvement in rocket velocity can be expected, since in that case the thrust of the rocket does not exceed its initial weight. The limiting values of ζ lie on the dash-dot curve of Fig. 5.

In order to obtain the required high values of $v_{max.}/c$ it is necessary to tolerate accelerations in excess of 20g in rockets having propellant loading factors in excess of 0.9. It is believed impossible to meet these conditions.

The second alternative to be considered is the case of a rocket acted upon by a constant acceleration $a = ng_0$ during powered flight. For this case Eq. (10) becomes

$$v_{max.} = -c\left(\frac{n}{n+1}\right)\ln(1-\zeta) \tag{14}$$

The minimum value of t_p corresponding to the chosen value of the acceleration is

$$t_p = v_{max.}/ng_0 \tag{15}$$

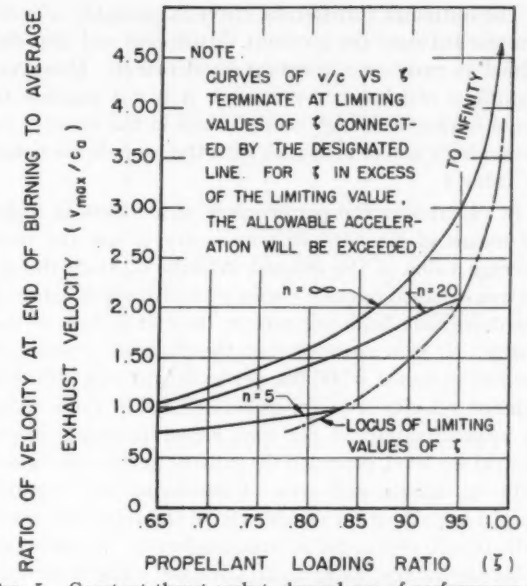
RATIO OF VELOCITY AT END OF BURNING TO AVERAGE EXHAUST VELOCITY (v_{max}/c_a)
4.50
4.00
3.50
3.00
2.50
2.00
1.50
1.00
.50
0
.65 .70 .75 .80 .85 .90 .95 1.00
PROPELLANT LOADING RATIO (ζ)
NOTE
CURVES OF v/c VS ζ TERMINATE AT LIMITING VALUES OF ζ CONNECTED BY THE DESIGNATED LINE. FOR ζ IN EXCESS OF THE LIMITING VALUE, THE ALLOWABLE ACCELERATION WILL BE EXCEEDED
TO INFINITY
n = ∞
n = 20
n = 5
LOCUS OF LIMITING VALUES OF ζ

FIG. 5. Constant thrust rocket, dependence of performance on maximum allowable acceleration.

In Fig. 6 the ratio $v_{max.}/c$ is plotted as a function of ζ for various values of n according to Eq. (14). For the constant acceleration rocket there is no limit to the value of v/c that can be attained regardless of the specified magnitude of n. Also, the constant acceleration rocket can attain the same value of v/c, with a lower value of ζ than is possible for the constant thrust rocket. It must be realized, of course, that the constant acceleration rocket requires a heavier and more complicated propulsion system, and that this increase in empty mass may actually overcome the advantage in ζ.

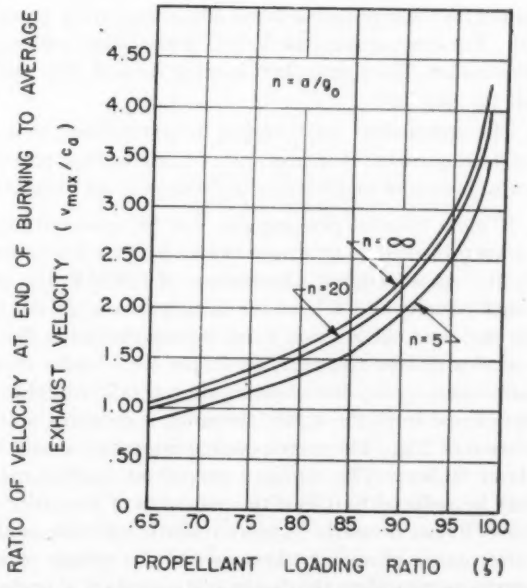

FIG. 6. Constant acceleration rocket, dependence of performance on allowable acceleration.

The optimum thrust-time curve is probably a compromise between the constant thrust case and that designed to produce a constant acceleration. However, regardless of what curve is used, it is not possible to avoid impractical, high accelerations in the attempt to obtain high rocket velocities with the propellants listed in Table 1.

In calculating the performance of a rocket in flight by means of Eq. (10) it is necessary to use the time average value of the exhaust velocity c_a, since the effective exhaust velocity varies with altitude because of the decreasing back pressure at the exit section of the nozzle. If it is assumed that the chamber pressure of the rocket motor is 300 lbs. per sq.in. abs., the effective exhaust velocity of the propellants listed in Table 1 can be approximately 50 per cent higher in empty space than at sea level, provided the exhaust nozzle is designed with an infinite exit area. Considering the required weight and size of the nozzle, a fixed and relatively small ratio of exit area to throat area is selected. In these calculations an area ratio of 25:1 is used. The maximum increase in exhaust velocity over the value at sea level is about 27 per cent. Although a correct evaluation of the average value c_a requires the computation of a trajectory for each case, an average increase of 18 per cent is assumed in this paper. Table 1 presents the average values computed in this manner.

Using these data, the minimum propellant loading ratio required to attain the escape velocity has been calculated for each of the propellants in Table 1. The maximum allowable acceleration was taken to be 20g, and Eq. (14) for flight with constant acceleration was used. The results are presented in the last column of Table 1.

It is apparent that the propellant loading ratios required for these propellants are all too high to be practical. For comparison, the V-2, a typical high-performance rocket, has a propellant loading ratio of 0.75 without the pay load.

The conclusion can therefore be established that a single-step rocket utilizing any of the chemical propellants heretofore suggested cannot escape from the earth.

A more hopeful performance can be expected of a rocket propelled by hydrogen heated by a nuclear power plant. At a chamber temperature of 5,000°F. the exhaust velocity at sea level is calculated to be 23,400 ft. per sec., and the average value during the entire firing period would be about 27,500 ft. per sec. Under these conditions, a propellant loading ratio of 0.73 would permit escape from the earth, assuming a constant acceleration of 20g. The corresponding firing time would be about 60 sec. The required propellant loading ratio may be reduced to 0.60 if temperatures of the order of 9,000°F. can be used. A more realistic estimate of the performance of such rockets awaits the release of information regarding the design and operation of nuclear power plants.

5. Multiple-Step Rockets Designed to Escape from the Earth

The velocity attainable with a single-step rocket is severely limited by the fact that propulsion energy must be utilized to accelerate the entire empty mass of the rocket continually even after the bulk of that empty mass is no longer useful. Earlier investigators have suggested the use of a rocket made up of a number of independent steps, each of which is equipped with a propulsion system and a portion of the total propellant load. As each step is exhausted, its empty mass is dropped from the rocket, the propulsion of the remainder being taken up by the next step. The pay load is carried in the last step of the rocket. In the following analysis the number of steps and their relative masses are considered from the point of view of the overall mass of the rocket required to project a given pay load away from the earth.

A multiple-step rocket is considered in which the number of steps is N, the pay load of mass M_l being located in the Nth step. A parameter called the pay-load ratio can be defined, for each step, as the ratio of the mass of the carried load or pay load to the mass of the rocket at the moment that step begins to fire. It is assumed in this analysis, and justified below, that the pay-load ratio is the same for each step, as expressed by the following equation:

$$\lambda = \frac{M_l}{M_0^{(N)}} = \frac{M_0^{(n+1)}}{M_0^{(n)}} = \frac{M_0^{(2)}}{M_0^{(1)}}, \quad 1 \leq n \leq N \tag{16}$$

This assumption simplifies the analysis since all the steps possess equal ballistic properties.

It is also assumed that all the steps can be designed with equal structural effectiveness. In accordance with the following equation, the ratio of the empty mass of a step to its mass when loaded with propellant (but with no pay load) is the same for all steps:

$$\epsilon = \frac{M_e^{(n)}}{M_0^{(n)} - M_0^{(n+1)}} = \frac{M_e^{(n)}}{M_e^{(n)} + M_p^{(n)}}, \quad 1 \leq n \leq N \tag{17}$$

From Eq. (16) it is readily seen that the mass of the entire N-step rocket is related to the mass of the pay load in the following manner:

$$M_l = \lambda^N M_0^{(1)} \tag{18}$$

Since ϵ and λ are the same for each step of the rocket, and if it is assumed that the average value of the exhaust velocity applies to each step, then each step contributes the same increase in the speed of the rocket, according to the following equation:

$$v_n - v_{n-1} = -c_a \ln\left(\frac{M_e^{(n)} + M_0^{(n+1)}}{M_0^{(n)}}\right) - g_0 \frac{t_p}{N} \tag{19}$$

It is assumed in this equation that the deceleration due to gravity is constant during powered flight, and

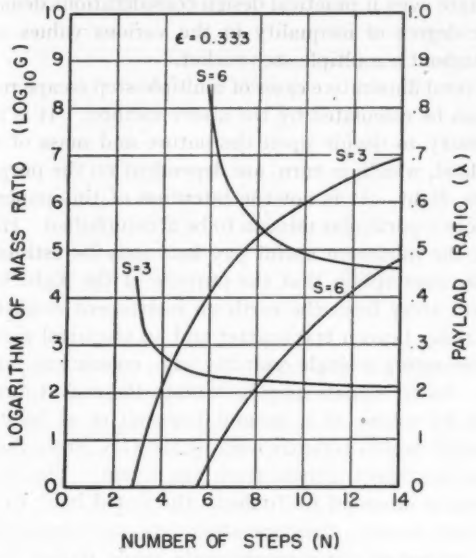

FIG. 7. Step rocket performance, $\epsilon = 0.333$.

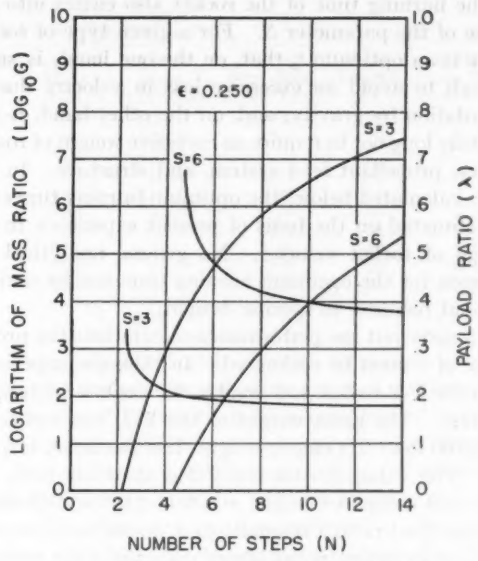

FIG. 8. Step rocket performance, $\epsilon = 0.250$.

equal to the sea-level value. The error introduced by this assumption is small, since the distance at which burning stops is small compared with the radius of the earth. This will be illustrated in the numerical examples presented below.

By means of Eqs. (16) and (17), and by means of the defining equation for $M_0^{(n)}$ given in the table of symbols, Eq. (19) can be reduced to the following equation:

$$v_n - v_{n-1} = -c_a \ln [\epsilon(1 - \lambda) + \lambda] - g_0 \frac{t_p}{N} \quad (20)$$

It is assumed that the firing of each step commences at the instant the preceding step ceases firing and the empty structure is cast away. The velocity of the rocket at the end of burning is merely N times the increase in velocity of each step.

$$v_N = -N c_a \ln [\epsilon(1 - \lambda) + \lambda] - g_0 t_p \quad (21)$$

The effect of atmospheric drag on the first one or two steps is neglected, since the value of μ for the rocket being considered is at least 1,000 lbs. per sq.ft. (Fig. 2).

Eqs. (18) and (21) can be put in dimensionless form by the introduction of two parameters:

$G = M_0^{(1)}/M_1$ = overall mass ratio
$S = (v_N + g_0 t_p)/c_a$ = velocity ratio

$$G = \lambda^{-N} \quad (22)$$

$$S = -N \ln [\epsilon(1 - \lambda) + \lambda] \quad (23)$$

In Figs. 7, 8, and 9, G and λ are plotted as functions of N and S for three values of ϵ.

The parameter S is computed from the average exhaust velocity of the propellant, the burning time of the rocket, and the desired final velocity of the rocket.

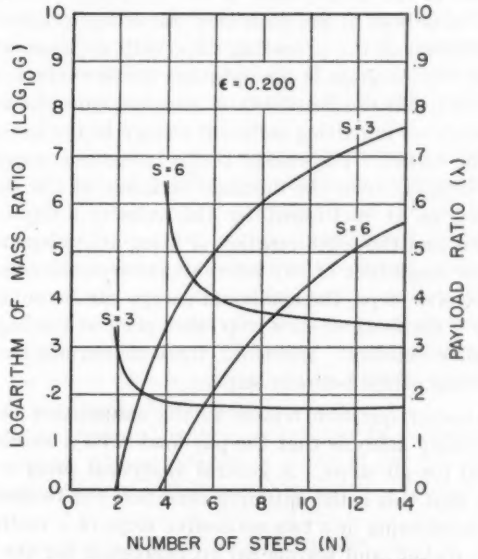

FIG. 9. Step rocket performance, $\epsilon = 0.200$.

It is generally considered that the propellant having the highest exhaust velocity is the most desirable. This advantage, however, is usually considerably reduced by the fact that such propellants have a low density and therefore necessitate the use of proportionally more tank and structural weight than in the case of the denser, low-performance propellants. The exhaust velocities and densities of several propellant combinations are presented in Table 1. The effect of the increased structural weight has been accounted for, in the examples below, by taking $\epsilon = 0.33$ for oxygen-hydrogen rockets and $\epsilon = 0.25$ for acid-aniline rockets.

The burning time of the rocket also enters into the value of the parameter S. For a given type of rocket there is an optimum t_p that, on the one hand, is small enough to avoid an excessive loss in velocity due to retardation by gravity, and, on the other hand, is sufficiently long not to require an excessive weight of rocket motor, propellant feed system, and structure. In the cases calculated below, the optimum burning times will be estimated on the basis of present experience in the design of rocket vehicles. No general analytical expression for the optimum burning time can be derived without recourse to specific designs.

To carry out the performance calculations the proper value of ϵ must be estimated. In this case experience with the V-2 rocket and similar devices can be used as a guide. The gross weight of the V-2, less war head, is 25,700 lbs. Its empty weight, less war head, is 6,400 lbs. The value of ϵ for the V-2 is therefore 0.25. In the cases computed below, ϵ is taken to be 0.25 where the pay-load ratio λ is small; and, to account for some increase in structure, at larger values of λ the value of ϵ is taken to be 0.33.

One of the assumptions in the foregoing analysis is that it is best to fire each step immediately after the exhaustion of the preceding step, with no time delay. That this program is the optimum one is evident from the fact that the possibility of escaping from the earth depends on imparting sufficient energy to the last step of the rocket. The energy of the last step is equal to the integral, over the duration of firing, of the thrust acting on it multiplied by the velocity. Since the thrust and the total duration of firing are independent of the magnitude of any intervals between the firing of successive steps, the maximum energy can be obtained only if the firing of each step takes place at the highest possible velocity. Therefore, there should not be any coasting period between steps.

Another question relates to the assumption in the preceding analysis that the pay-load ratio λ should be equal for all steps. A general analytical proof of the fact that this is the optimum condition can be derived by considering any two successive steps of a multiple-step rocket, and setting up an expression for the difference between the mass ratio G when the two values of λ are equal and G' for the case of unequal values of λ. To simplify the presentation in this paper, a numerical case can be examined. Let two such steps be designed to increase the velocity of the rocket by an amount such that $\Delta S = 2.0$. Then $\epsilon = 0.25$ and $\lambda = 0.157$ for each step. The overall mass ratio G is calculated to be 41.0. If two other steps were substituted for these to produce the same value of ΔS but with unequal values of λ, e.g., 0.200 and 0.118, the overall mass ratio would be 43.0. Thus, the minimum mass ratio is obtained with equal values of λ. It is of interest to note that the analytical derivation shows that G increases slowly as the values of λ deviate from equality. Therefore, the mass ratios computed from Eq. (22) are sufficiently accurate even if practical design considerations demand some degree of inequality in the various values of λ throughout a multiple-step rocket.

Several illustrative cases of multiple-step escape rockets can be calculated by the above method. It is first necessary to decide upon the nature and mass of the pay load, which, in turn, are dependent on the purpose of the flight. It is not the intention of this paper to propose a particular mission to be accomplished. However, the minimum useful pay load may be estimated on the assumption that the purpose of the flight is to project away from the earth an instrument consisting of a radar beacon transmitter and an electrical pickup for measuring a single quantity, e.g., cosmic ray intensity. Radar signals may be sent to the rocket during flight by means of a ground transmitter at least as powerful as that recently used by the U.S. Army Signal Corps to reflect signals from the moon. The radar beacon is intended to "reflect" the signal back to the receiver on earth, thus providing data on its trajectory. The values of the measurements made during flight could be incorporated in the return signal from the radar beacon. It has been boldly estimated that, if the utmost care is exerted in the design of the instrument, its weight may be kept to as low as 10 lbs. This figure will be arbitrarily used in the calculations to follow.

As a first example, a five-step acid-aniline escape rocket may be considered. As in the case of single-step rockets, the average value of the exhaust velocity c_a can be taken to be 7,300 ft. per sec. Allowing a burning time of 40 sec. for each step, the total burning time t_p is 200 sec. The required escape velocity varies with the distance from the earth at which the end of burning occurs (Fig. 1). In this case, propulsion ceases at about 600 miles from the earth's surface where the velocity of escape is 34,300 ft. per sec. The parameter S can be evaluated in the following manner:

$$S = \frac{v_e + g_0 t_p}{c_a} = \frac{34{,}300 + 32.2 \times 200}{7{,}300} = 5.57 \quad (24)$$

The use of 32.2 ft. per sec. per sec. instead of the time average value of g is conservative, and introduces an error of less than 2 per cent in the value of S.

Assuming a value of 0.25 for the structural factor ϵ, Eqs. (22) and (23) can be used to derive the pay-load ratio and the overall mass ratio: $\lambda = 0.104$, $G = 82{,}300$.

The gross mass of the rocket is then 823,000 lbs. The masses of the individual steps, each loaded with propellant, are: 739,000, 75,200, 7,880, 824, and 96 lbs., respectively. The mass of the last step includes the 10-lb. pay load. The thrust of the first step is of the order of 3,000,000 lbs. The thrust of each of the succeeding steps is in proportion to the mass of each step. Assuming that the average density of acid-aniline rockets is approximately 50 lbs. per cu.ft., the overall dimensions of the rocket can be estimated: length = 130 ft.;

TABLE 3
Characteristics of Multiple-Step Escape Rockets

Example No.	Propellant Combination	Number of Steps (N)	Structural Factor (ϵ)	Pay-load Ratio (λ)	Firing Time (Sec.)	Pay-load Mass (Lbs.)	Gross Mass (1,000 Lbs.)	Thrust First Step (1,000 Lbs.)	Estim. Length (Ft.)	Estim. Body Dia. (Ft.)
1	Acid-aniline	5	0.25	0.104	200	10	823.0	3,000	130	13.0
2	Acid-aniline	10	0.25	0.386	400	10	136.0	350	70	7.0
3	Acid-aniline	∞	0.25	1.000	400	10	37.0	...	...	...
4	Acid-aniline	10	0.20	0.425	400	10	52.0	136	51	5.1
5	Oxygen-ethanol	5	0.25	0.155	200	10	112.0	450	71	7.1
6	Oxygen-ethanol	10	0.25	0.432	400	10	44.0	118	52	5.2
7	Oxygen-ethanol	5	0.20	0.207	200	10	26.0	104	44	4.4
8	Oxygen-hydrogen	5	0.33	0.260	200	10	8.3	40	40	4.0
9	Oxygen-hydrogen	5	0.33	0.260	200	100	83.0	400	86	8.6
10	Oxygen-hydrogen	10	0.33	0.532	400	100	55.1	160	74	7.4

diameter of body = 13 ft. The characteristics of the rocket are summarized in Table 3.

Similar calculations may be carried out for a second example, a ten-step acid-aniline escape rocket carrying the same 10-lb. pay load. Although the pay-load ratio in this case must be somewhat larger than in the five-step example, the value of ϵ is still assumed to be 0.25.

The firing time of each step is assumed to be 40 sec., making a total period of firing of 400 sec. The results of the computation are that the overall mass of the required rocket is 136,000 lbs. and that the initial thrust is 350,000 lbs. These requirements are considerably less than those of the five-step rocket. The weighing of the advantages of a smaller rocket against the disadvantages of the greater complexity of an increased number of steps is a matter for the exercise of practical engineering judgment.

This simplified method of analysis becomes less satisfactory as the number of steps increases. The calculated mass ratio G is extremely sensitive to the assumed structural factor ϵ, a fact that can be verified by comparing Figs. 7, 8, and 9. Present experience indicates that ϵ is dependent on the scale of the rocket and on the burning time for which it is designed. It is considered unlikely that rockets having a mass of less than 500 lbs. or a firing time of less than 20 sec. can be constructed with ϵ as low as 0.25. As the chosen number of steps increases, the masses of the latter steps in the series become smaller and the individual burning times decrease. Therefore, although the simplified analysis indicates that the mass ratio continually decreases as the number of steps is increased, this principle may be expected to break down at some point. A more correct approach would be to establish, if possible, analytical relations expressing the dependence of ϵ on t_p, M_0, and λ, to be used in conjunction with Eqs. (22) and (23). The derivation of such relations is outside the scope of this paper.

It is nevertheless of interest to examine analytically the results of increasing the number of steps indefinitely while retaining the same values of S and ϵ. By eliminating λ between Eqs. (22) and (23) and letting N become infinite in the resulting expression for G, the limiting value of G is obtained:

$$G \longrightarrow e^{[S/(1-\epsilon)]} \text{ as } N \longrightarrow \infty \qquad (25)$$

By inserting $S = 6.15$ and $\epsilon = 0.25$, the values used in the ten-step rocket, the resulting value of 3,700 is obtained for G_∞. Therefore, in this hypothetical limiting case, the proposed 10-lb. pay load can be projected away from the earth by a 37,000-lb. acid-aniline rocket having an infinite number of steps. It can be seen that the greatest mass reduction was accomplished in going from five steps (823,000 lbs.) to ten steps (136,000 lbs.) and that a further increase in the number of steps would not be as beneficial.

The nitric acid-aniline combination is representative of the so-called standard propellants. It is interesting to consider multiple-step rockets that utilize a high-performance propellant, such as the liquid oxygen-liquid hydrogen combination.

Oxygen-hydrogen rockets possess the distinct advantage of requiring a much lower mass rate of propellant consumption for a given thrust than acid-aniline. On the other hand, the lower average density and the need for insulation compel the use of proportionally greater "dead" mass of structure, tanks, and propellant feed system, with the result that the advantage in propellant consumption is reduced. For the oxygen-hydrogen case, the value of ϵ is assumed to be 0.33 to account for this increase in dead mass.

As an example, a five-step rocket may be calculated. The average exhaust velocity is 12,000 ft. per sec., and a total firing time of 200 sec. is assumed. Then $S = 3.40$, $\lambda = 0.26$, and $G = 832$. If the same 10-lb. pay load described above is considered, the mass of the entire rocket becomes 8,320 lbs., and the initial thrust would be about 40,000 lbs. This reduction in mass as compared with the acid-aniline five-step rocket emphasizes the importance of developing practical high-performance rocket systems. The sharp reduction is a result of the exponential dependence of the mass on the reciprocal of the exhaust velocity, as expressed in Eq. (25).

Obviously the required mass of the rocket assembly would not be unreasonable even if the pay load were increased tenfold. A 100-lb. pay load could include a more powerful radar beacon to provide stronger and more accurate signals and a greater number of measuring instruments to provide more scientific data from the single flight. The required mass would be 83,200

lbs. and the initial thrust would be about 400,000 lbs. Possible dimensions for this rocket are given in Table 3, on the basis of an estimated average density for oxygen-hydrogen rockets of 17 lbs. per cu.ft.

Other cases of multiple-step escape rockets are summarized in Table 3 for comparison with the cases that have been discussed in the preceding paragraphs. Additional examples of rockets capable of escaping from the earth, as well as examples of orbital rockets and rockets capable of escaping from the solar system, are presented in reference 14.

6. Conclusion

It can be concluded that it is possible from the engineering point of view to construct rockets that are capable of escaping from the earth's gravitational field.

One of several systems can be selected for the purpose. A multiple-step acid-aniline rocket can be used, but the size of rocket required to carry even a 10-lb. pay load is larger than any rocket heretofore constructed or designed. A more reasonable multiple-step rocket can be designed utilizing oxygen and hydrogen, and in this case a pay load of the order of 100 lbs. may be conveniently carried. Larger pay loads can be carried with proportionally larger rockets.

In the case of single-step rockets, it is only by the introduction of power plants operating on nuclear energy that the velocity of escape may be achieved. Single-step rockets operating on the most energetic chemical propellants known would fall far short of the required velocity.

Thus, although many problems of navigation, flight control, instrumentation, etc., remain to be investigated, the basic technique is available by which a body can be propelled with the necessary velocity to escape from the earth.

References

[1] Ziolkowsky, K. E., *Rockets in Cosmic Space*, published in 1903 and reprinted in 1924 (in Russian).

[2] Goddard, R. H., *A Method of Reaching Extreme Altitudes*, Smithsonian Miscellaneous Collections, Vol. 71, No. 2, 1919.

[3] Lorenz, H., *The Possibility of Space Travel*, V. D. I. Zeitschrift, Vol. 71, pp. 651–654, 1927.

[4] Senftleben, H. A., *On the Mechanics of Space Rockets*, Z.F.M., Vol. 19, pp. 319–323, 1928.

[5] Oberth, H., *Methods of Space Travel*, 3rd Ed.; R. Oldenbourg, Munich, 1929.

[6] Rynin, N. A., *Astro-Navigation*, Vol. 9; Leningrad, 1932.

[7] Campbell, J. W., *Rocket Flight to the Moon*, Phil. Mag., Vol. 31, p. 24, 1941.

[8] Ley, W., *Rockets*, Viking Press, New York, 1944.

[9] Ackeret, J., *On the Theory of Rockets*, Helvetica Physica Acta, Vol. 19, p. 103, 1946.

[10] Malina, F. J., *Is the Sky the Limit?* Army Ordnance, Vol. 31, No. 157, p. 45, July-August, 1946.

[11] Malina, F. J., and Smith, A. M. O., *Flight Analysis of the Sounding Rocket*, Journal of the Aeronautical Sciences, Vol. 5, No. 5, pp. 199–202, March, 1938.

[12] Tsien, H. S., and Malina, F. J., *Flight Analysis of a Sounding Rocket with Special Reference to Propulsion by Successive Impulses*, Journal of the Aeronautical Sciences, Vol. 6, No. 2, pp. 50–58, December, 1938.

[13] Brombacher, W. G., *Altitude Pressure Table Based on the U.S. Standard Atmosphere*, N.A.C.A. Report No. 538, 1935.

[14] Seifert, H. S., Mills, M. M., and Summerfield, M., *The Physics of Rockets*, American Jour. Physics, January-February, March-April, May-June, 1947.

Errata

Several errors appeared in "Systematic Analysis of Thermal Turbojet Propulsion," by Hans Reissner (Journal of the Aeronautical Sciences, Vol. 14, No. 4, p. 197, April, 1947). They are corrected below:

(1) Page 198, right column. Line 7: $D_h \equiv$ twice area/circumference . . . . . Line 9: $\zeta\varphi^2/2D_h$ . . . . .

(2) Page 201, right column. Eq. (5c): . . . . . $\frac{\zeta h}{2D_h}$ . . . . . Eq. (5d): . . . . $+ \zeta l/2D_h$ . . . . .

(3) Page 203, right column, 1st line of text following Eq. (17b): From Eq. (15b) . . . . .

(4) Page 206, right column, 3rd line of text under main head and subhead: . . . . . of head $(\zeta\varphi^2/2D_h)$ per unit . . .

(5) Page 207, left column. Text following Eq. (7e): . . . . . $z = \zeta l/2D_h$.

Equations between Eqs. (5f) and (5g): $C_\mu \equiv \mu/(\mu - \lambda)$, $C_\lambda = \lambda/(\mu - \lambda)$

In Eqs. (5g), (26), and (27) note that the mu should be inferior to c (c_μ) and that i and s in Eq. (5g) denote limits of the integral. In Eq. (28), 1 and 0 denote limits of the integral, and μi are inferior to the c ($c_{\mu i}$).

Numerical Procedures for Calculation of Stress Distribution in Sheet-Stringer-Frame Combinations

MARVIN STERN*

Republic Aviation Corporation

SUMMARY

Stress distribution problems encountered in the homogeneous isotropic material that comprises the pure monocoque structure can usually be resolved by straightforward applications of the mathematical theory of elasticity. However, when these same problems arise in the sheet-stringer and frame combinations of the semimonocoque aircraft structure, their solutions become much more difficult.[1,2]

Standard rational methods for performing such shear lag calculations have been found to be too involved and time-consuming for practical design purposes. The method described in this paper combines theory of elasticity with a technique of successive approximations. The method can be employed by calculators with little previous training, and converges rapidly to an exact solution.

The same differential equations are developed here as appear in available literature on this problem. These equations are then solved by use of the method of finite differences. As a result, the sheet-stringer problem is conveniently reduced to an analogous homogeneous or thick sheet problem.

This method proves to be convenient when the problem involves sheet doublers, varying stringer thicknesses, and tapered panels.

In this paper the simple case of "one-directional shear lag" is illustrated. Although the more involved shear lag problems are handled in a similar manner, they are not treated here.

INTRODUCTION

IN STRESS ANALYSIS three basic conditions need be satisfied: (1) static equilibrium, (2) Hooke's law, and (3) compatibility (of strains).

For the homogeneous isotropic material, and for the case where there are no body forces present, the three conditions are combined mathematically into the following form:

$$\left(\frac{\partial^2}{\partial x^2}+\frac{\partial^2}{\partial y^2}\right)(\sigma_x+\sigma_y)=0$$

An arbitrary function $\varphi(x, y)$ can be introduced such that $\nabla^4\varphi = 0$ where

$$\sigma_x = \partial^2\varphi/\partial y^2, \quad \sigma_y = \partial^2\varphi/\partial x^2, \quad \tau_{xy} = -(\partial^2\varphi/\partial x\,\partial y)$$

Many of the problems of stress distribution in the homogeneous material are solved by searching for a value of this function φ which satisfies the existing boundary conditions. Further, mathematical theorems can be derived which show the uniqueness of such a solution. Such stress distribution problems as that of a concentrated load applied at the edge of the infinite half-plane, or that of the concentration around a hole are solved in this manner.

It is to be noted that when these same problems arise in the sheet-stringer and frame structure, they are referred to as "shear lag" problems. The fundamental difference between the sheet-stringer combination and the thick sheet, or pure monocoque, is that in the semimonocoque structure there is more material available for taking axial load than there is for taking shear; e.g., condition (1) must be written as

$$t'\frac{\partial\sigma_x}{\partial x}+t\frac{\partial\tau_{xy}}{\partial y}=0$$

If this is taken into account, the subsequent mathematical manipulations become much more involved. Only in special simple applications can an exact analytical answer be arrived at.

Before developing an approximate method of analysis, it would be well to examine the potential function, by the method of finite differences. In doing so, a well-known theorem in potential theory can be proved; i.e., the value of $(\sigma_x + \sigma_y)$, which will be referred to as ψ, at any point within the region must be the mean of its four nearest neighboring values. This can be shown in the following manner.

Let the lattice shown in Fig. 1 represent a region wherein $\nabla^2\psi = 0$.

By the definition of the derivative,

$$\frac{\partial^2 x}{\partial x^2}=\frac{(\psi_{n,\,m+1}-\psi_{n,\,m})-(\psi_{n,\,m}-\psi_{n,\,m-1})}{(\Delta x)^2}$$

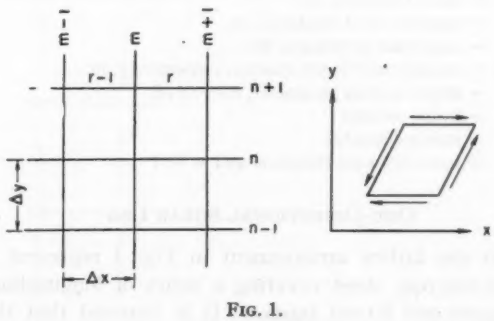

FIG. 1.

Received January 2, 1947.

* Senior Stress Analyst.

$$\frac{\partial^2\psi}{\partial y^2} = \frac{(\psi_{n+1,\,m} - \psi_{n,\,m}) - (\psi_{n,\,m} - \psi_{n-1,\,m})}{(\Delta y)^2}$$

Therefore, letting $\Delta x = \Delta y$, and setting $[(\partial^2/\partial x^2) + (\partial^2/\partial y^2)]\psi = 0$, it is found that

$$-4\psi_{n,\,m} + \psi_{n,\,m+1} + \psi_{n,\,m-1} + \psi_{n+1,\,m} + \psi_{n-1,\,m} = 0$$

This leads to a numerical method for solution of the Laplace equation. Any numerical method of handling a differential equation necessarily involves the replacement of the continuum of points on the boundary and in the interior of the region by a discrete set of points. The values of the function are considered only at these points, rather than at every point in the region.

One method of handling Laplace's equation is an iterative procedure. This consists of covering the region with a square net; approximate values are assigned to the function at the interior points—known values at the boundary points. One then traverses the net repeatedly, replacing the value at each interior point by the mean of the values at the four neighboring points, using the new values immediately in the improvement of succeeding points. The function will then converge to a solution of the Laplace difference equation which will be an approximation to the solution of the Laplace differential equation. The smaller the interval Δx, the better will be the approximation.

In the following material it will be shown that by satisfying the conditions of static equilibrium, Hooke's law, and compatibility, and by properly taking into account the comparative sheet and stringer stiffnesses, an approximation of the same general form as that above can be arrived at. This relationship can then be used in a rapidly converging iteration process to obtain a solution.

Notation

- u = displacement along x, in.
- ϵ_x = strain along x, in. per in.
- γ_{xy} = shear strain, in. per in.
- E = modulus of elasticity, lbs. per sq.in.
- G = shear modulus, lbs. per sq.in.
- σ = normal stress, lbs. per sq.in.
- τ = shear stress, lbs. per sq.in.
- A_z = effective area of stringer, sq.in.
- A_0 = nominal effective area, sq.in.
- t = sheet thickness, in.
- t_0 = nominal sheet thickness, in.
- P = axial load in stringer, lbs.
- λ, l = stringer and frame spacing, respectively, in.
- β^2 = dimensionless parameter, $tGl^2/\lambda A_z E$
- m = frame number
- n = stringer number
- r = panel between frames m and $m + 1$

One-Directional Shear Lag

Let the lattice arrangement in Fig. 1 represent a shear-carrying sheet covering a series of longitudinal stringers and lateral frames. It is assumed that the capacity of the sheet for carrying axial load can be predetermined. This can then be concentrated at the panel boundaries, thus giving effective areas for stringer and frame. It is then permissible to assume in the ensuing calculations that the sheet carries shear alone. Further, the stringers and frames are considered to offer no resistance to bending. For one-directional shear lag, the stringers are assumed to be elastic under the action of axial load while the frame is not. Finally, one-directional shear lag is characterized by the action of axial loads on the stringers of a plane sheet-stringer combination with infinitely rigid transverse ribs, producing deformations in the stringer directions only.

Let u represent the point displacement in the x direction, such that $\epsilon_x = \partial u/\partial x$. The restrictions imposed in a one-directional shear lag problem leave only one component to express the shear strain; i.e., $\gamma_{xy} = \partial u/\partial y$. By differentiating the expression for shear strain with respect to both x and y, and then substituting the expression for normal strain, the following compatibility condition can be obtained:

$$\frac{\partial^2\gamma_{xy}}{\partial x\,\partial y} = \frac{\partial^2\epsilon_x}{\partial y^2}$$

Hooke's law for this problem is simply

$$E\epsilon_x = \sigma_x, \qquad G\gamma_{xy} = \tau_{xy}$$

Combining Hooke's law with the compatibility condition gives

$$\left(\frac{E}{G}\right)\left(\frac{\partial^2\tau_{xy}}{\partial x\,\partial y}\right) = \frac{\partial^2\sigma_x}{\partial y^2} \tag{1}$$

For this case assume that the effective areas of stringers, the stringer and frame spacing, and the sheet thickness remain constant throughout. Then, referring to Fig. 2, it is seen that the static equilibrium condition can be written as

$$A_z\frac{\partial\sigma_x}{\partial x}\,\delta x + t\delta x\,\frac{\partial\tau_{xy}}{\partial y}\,\delta y = 0$$

Differentiating this with respect to x and combining with Eq. (1) yields

$$\left(\frac{E}{G}\,\frac{A_z}{t\cdot\delta y}\,\frac{\partial^2}{\partial x^2} + \frac{\partial^2}{\partial y^2}\right)\sigma_x = 0 \tag{2}$$

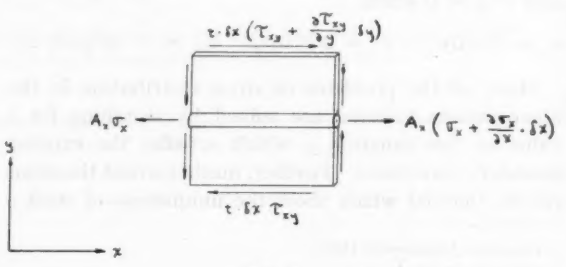

Fig. 2.

This is the equation to be used in an iterative procedure to obtain solutions to the one-directional shear lag problems.

Let $\Delta x = l$ and $\Delta y = \lambda$. Then multiplying by A_x, and using finite differences as before, an expression for the axial load at the junction point (n, m) is obtained:

$$P_{n,m}2(1+\beta^2) = P_{n,m+1} + P_{n,m-1} + \beta^2 P_{n+1,m} + \beta^2 P_{n-1,m} \quad (3)$$

If (n) were a free edge stringer, the expression would be:

$$P_{n,m}(2+\beta^2) = P_{n,m+1} + P_{n,m-1} + \beta^2 P_{n-1,m} \quad (4)$$

Application

For any application one can usually choose a hypothetical frame spacing, l, such that the dimensionless parameter, β^2, becomes equal to unity. Then in the case of one-directional shear lag, the axial load $P_{n,m}$, becomes the mean of its nearest neighboring values. This length, l, shall be referred to as the "characteristic length." Its physical significance is of importance. For a particular sheet-stringer combination the characteristic length is that length which takes into account the comparative sheet and stringer stiffnesses in such manner as to reduce the sheet-stringer problem to an analogous thick sheet one.

In a problem where the frame spacing is specified, the actual value of β^2 may be calculated and used as such. It can be shown, however, that the stress distribution is practically independent of the frame spacing. Therefore, by assuming a hypothetical frame spacing—that of the characteristic length—the resulting stress distribution would not be much different from the original. In most calculations, therefore, it would seem advisable to assume a hypothetical spacing equal to that of the characteristic length, thus reducing the numerical work required. One method for solving problems under these circumstances is the iterative procedure explained before.

Take the problem shown in Fig. 3 as the first example of one-directional shear lag. For convenience the frame spacing was chosen to be the characteristic length. As in all problems of this sort, the symmetry is such as to permit no shear to exist in the panel between stringers b and b'. This panel can then be assumed to be nonexistent and the calculations need be performed for only half the structure.

Working with the left half of the structure, the four boundary conditions are known. The first approximation is that 50 lbs. tension exists at each junction (Fig. 4a). By cutting the panel, both (a) and (b) have been made edge stringers. The condition to be satisfied for all junction points in this case, therefore, is that expressed in Eq. (4). For this illustration, point 2b will be chosen as the starting point. Isolating this point with its nearest neighboring values (Fig. 4b), it can be

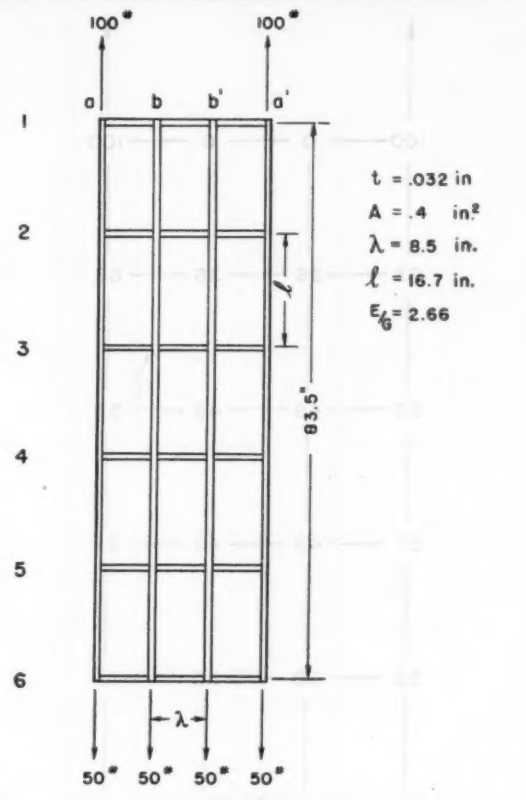

Fig. 3.

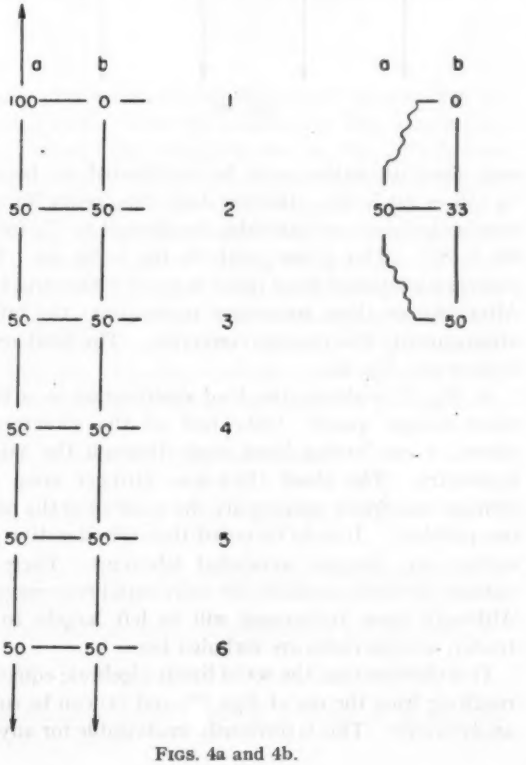

Figs. 4a and 4b.

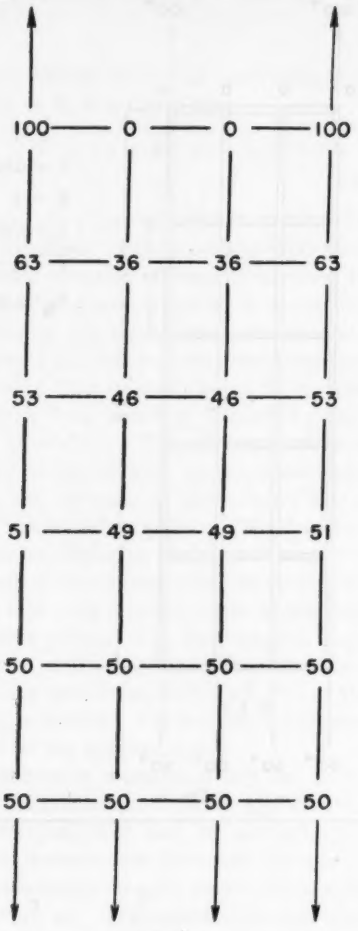

FIG. 4c.

seen that its value must be readjusted to become $^1/_3$ (50 + 50 + 0). Having done this, point 3b may now be isolated and its value readjusted to $^1/_3$ (50 + 50 + 33). This gives point 3b the value 44. This process is continued from point to point in the structure. After two or three successive passes over the lattice arrangement, this process converges. The final result is shown in Fig. 4c.

In Fig. 5 is shown the load distribution in a large sheet-stringer panel. Only half of the structure is shown, a cut having been made through the axis of symmetry. The sheet thickness, stringer area, and stringer and frame spacing are the same as in the previous problem. It is to be noted that this iterative procedure may become somewhat laborious. There are various methods available for more rapid convergence.[3] Although these techniques will be left largely to the reader, several notes are included here.

It is obvious that the set of linear algebraic equations resulting from the use of Eqs. (3) and (4) can be solved analytically. This is obviously inadvisable for any but

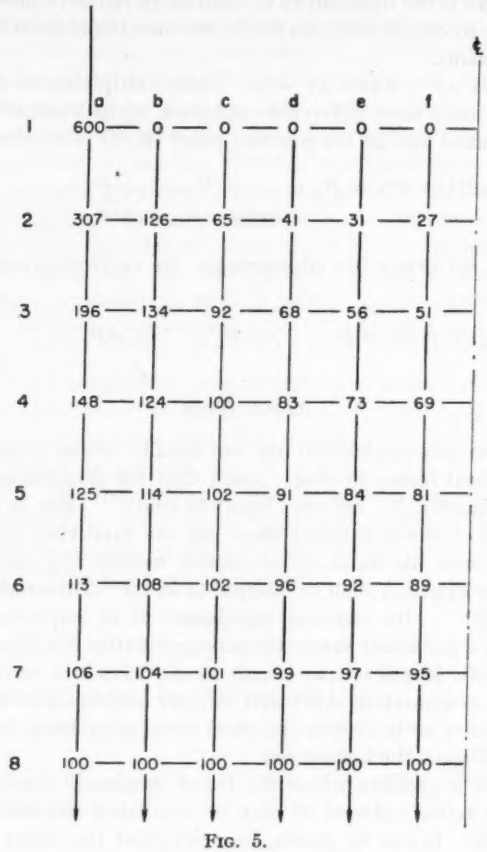

FIG. 5.

the smallest and simplest of nets. This can be used to advantage, however, for a number of blocks of points within the net.

Considering the invariance of $\nabla^2\psi = 0$, a simple transformation would allow ψ_0 to be expressed in terms of its eight surrounding points (Fig. 6):

$$20\psi_0 = 4(\psi_1 + \psi_2 + \psi_3 + \psi_4) + \psi_5 + \psi_6 + \psi_7 + \psi_8$$

This expedient obviously cuts down the work considerably. Care should be taken, however, when working near the boundary points. The boundary values need not satisfy the potential equation. Therefore, the invariance property and the equations resulting from it cannot be used in the neighborhood of these points.

A further saving in labor is achieved by carrying out the successive approximations on the difference function. This is done by first making an initial approximation. This approximation is then improved upon by one traverse over the net. The initial net values are then subtracted at each point from this set of improved values. These differences may now be treated with the same improvement formulas as the original set of values. The boundary values for the difference function all become zero. The number of significant figures in the ensuing calculations are reduced. Besides these

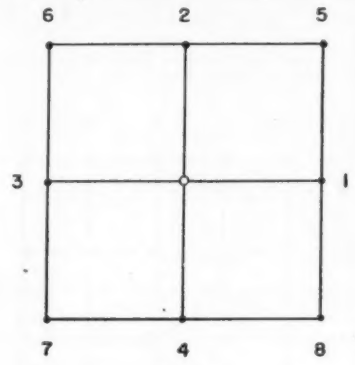

FIG. 6.

advantages, the use of the difference function allows for an accurate extrapolation to the solution by the use of the eigenvalues.

After several traverses over the net, it will be found that the ratio of the difference function between the new and the last improved values will become fairly constant for all points of the net. ($\delta^{[k]}/\delta^{[k-1]} = L$.) The sum of the succeeding difference functions (δ) can now be extrapolated $\{[1/(1-L)]\delta^{[k]}\}$.[3]

One of the advantages of an iterative procedure for the practical stress analyst is that he may choose the initial approximation to the solution. The more nearly the arbitrarily assigned values of the initial approximation approach the correct ones, the more rapid will be the convergence of the iterative procedure. However, any finite assigned values whatever will lead to the correct result.

VARIATIONS IN STRINGER AREA, SHEET THICKNESS, AND PANEL TAPER

In the original derivation, let: (1) the stringer area vary from point to point; (2) both λ and t vary with x and remain constant with y; (3) the frame spacing l, remain constant.

Under these circumstances, Eqs. (3) and (4) become

$$P_{n,m}\left(2\beta^2\frac{A_0}{A_{n,m}}+\frac{t_0}{t_r}\frac{\lambda_r}{\lambda_0}+\frac{t_0}{t_{r-1}}\frac{\lambda_{r-1}}{\lambda_0}\right)=$$

$$P_{n,m+1}\frac{t_0}{t_r}\frac{\lambda_r}{\lambda_0}+P_{n,m-1}\frac{t_0}{t_{r-1}}\frac{\lambda_{r-1}}{\lambda_0}+$$

$$P_{n+1,m}\beta^2\frac{A_0}{A_{n+1,m}}+P_{n-1,m}\beta^2\frac{A_0}{A_{n-1,m}} \quad (3a)$$

$$P_{n,m}\left(\beta^2\frac{A_0}{A_{n,m}}+\frac{t_0}{t_r}\frac{\lambda_r}{\lambda_0}+\frac{t_0}{t_{r-1}}\frac{\lambda_{r-1}}{\lambda_0}\right)=$$

$$P_{n,m+1}\frac{t_0}{t_r}\frac{\lambda_r}{\lambda_0}+P_{n,m-1}\frac{t_0}{t_{r-1}}\frac{\lambda_{r-1}}{\lambda_0}+$$

$$P_{n\pm1,m}\beta^2\frac{A_0}{A_{n\pm1,m}} \quad (4a)$$

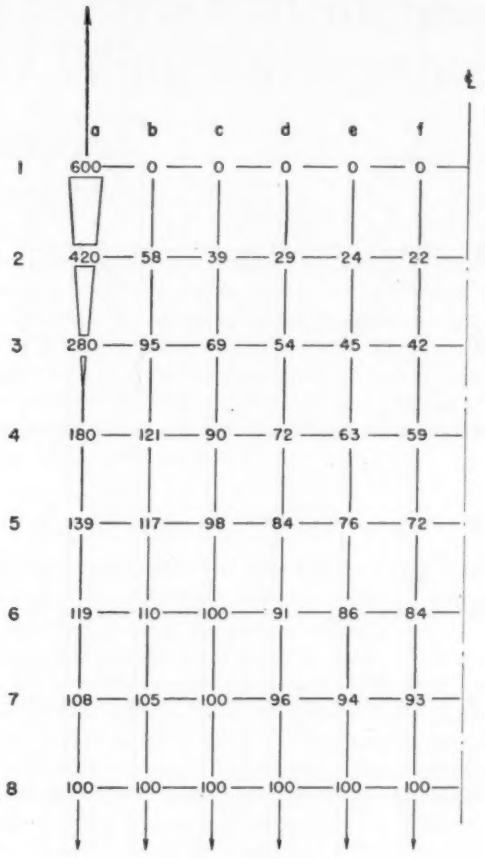

FIG. 7.

These expressions merely show that the averages are now weighted. Take the problem in Fig. 7 as an example. From the results shown in Fig. 5 it is seen that in order to bring about a more desirable axial stress distribution, the edge stringer must have a greater area at the point of load application, and then taper in some manner till it reaches the nominal stringer area once again. In the problem shown in Fig. 7, the edge stringer area was assumed to start at 2.6 sq.in. ($6^1/_2A_0$) and taper uniformly to the nominal area, 0.4 sq.in., at a point midway between frames 3 and 4. The rest of the structure was assumed to remain the same.

The expression for point 2a is now:

$$P_{2a}\left(\frac{A_0}{A_{2a}}+2\right)=P_{1a}+P_{3a}+P_{2b}$$

This would make P_{2a} larger than the average of its surrounding values.

In a similar manner, the expression for point 2b, is:

$$4P_{2b}=P_{1b}+P_{3b}+P_{2c}+P_{2a}\,(A_0/A_{2a})$$

This makes P_{2b} less than the average of its nearest neighboring values.

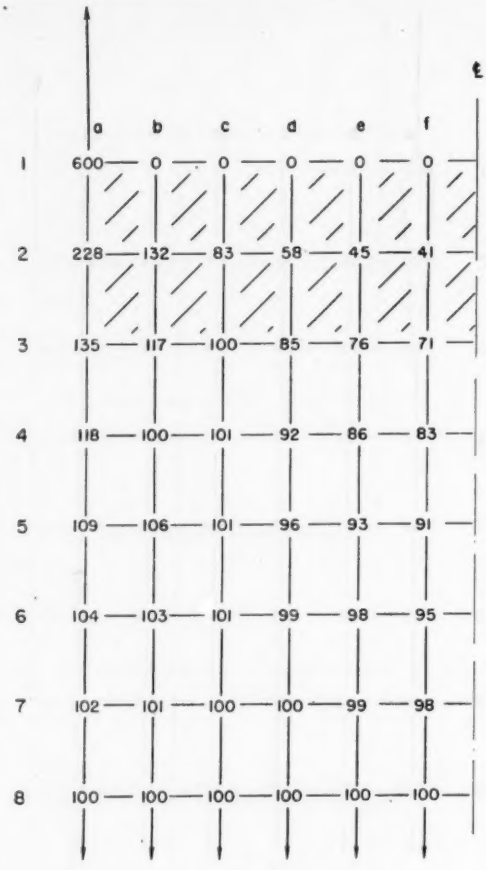

FIG. 8.

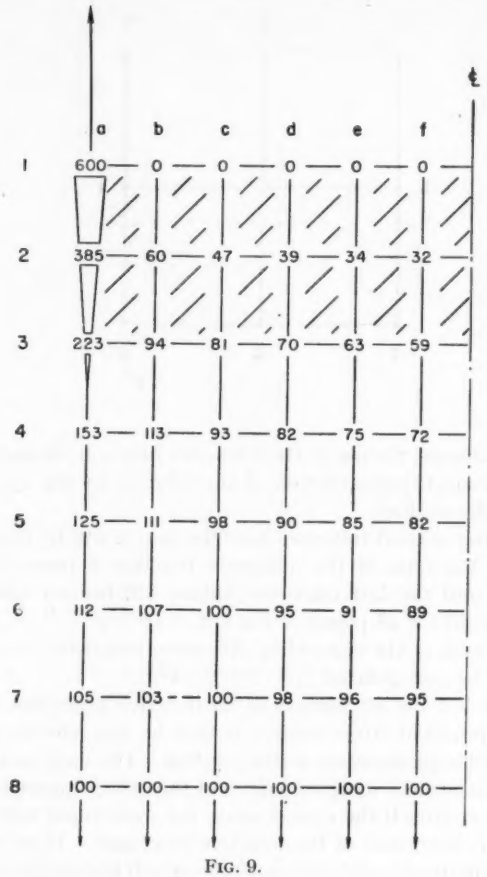

FIG. 9.

Similar expressions hold for points 3a and 3b. The remaining points satisfy the direct averaging equation. From the results shown in Fig. 7, it is seen that the effect of increasing the area of the edge stringer is to permit this member to increase the load it carries and to hinder the distribution of load through the panel.

The effect of increasing the sheet thickness in the first two bays is to cause a more even distribution of load through the panel. The effect of using a sheet of $3t_0$ thickness in the first two bays is shown in Fig. 8. A typical equation for a point within the region of increased sheet thickness is:

$$P_{2b}(2 + {}^1/_3 + {}^1/_3) = {}^1/_3P_{1b} + {}^1/_3P_{3b} + P_{2a} + P_{2c}$$

This shows that P_{2b} is more dependent upon P_{2a} and P_{2c} than it is upon P_{1b} and P_{3b}. The tendency, therefore, is for more stringer-to-stringer distribution.

Finally, in order to make the intermediate stringers more effective, and simultaneously to limit the load per unit area in the edge stringer, the combined effect of doubler and longeron area variation is introduced, as shown in Fig. 9. The same longeron area variation is used as that in Fig. 7. The sheet thickness over the first two bays, however, is only $2t_0$.

This general approach has been carried out in much greater detail and has been used successfully in design calculations. Its greatest asset lies in its simplicity and ease of application. The method has been extended to include problems in two-directional shear lag; i.e., where $\gamma_{xy} = \partial u/\partial y + \partial v/\partial x$. This is the case that occurs in bending and torsion problems.

REFERENCES

[1] Goodey, W. J., *Stress Diffusion Problems*, Aircraft Engineering, p. 195, June, 1946.

[2] Hoff, N. J., Levy, R. S., and Kempner, J., *Numerical Procedures for the Calculation of the Stresses in Monocoques, Part I; Diffusion of Tensile Stringer Loads in Reinforced Panels*, N.A.C.A. Technical Note No. 934, 1944.

[3] Shortley, G. H., Weller, R., and Fried, B., *Numerical Solution of Laplace's and Poisson's Equations*, Ohio State University Studies, Engineering Series, Bulletin No. 107, September, 1940.

A Tabulation Method for the Calculation of the Critical Speed of Wing Divergence

WALTER P. TARGOFF*
The Glenn L. Martin Company

ABSTRACT

The similarity between torsional aerodynamic moment and an inertia torque is noted. Holzer's method is then modified by the substitution of aerodynamic for inertia moments and a sample divergence calculation is given.

SYMBOLS

M = torsional aerodynamic moment about wing elastic axis, lb. in.
b = wing semichord, in.
a = distance of wing elastic axis from the mid-chord location, positive when aft, as a fraction of the wing semichord
α = relative angle of wing torsional deformation
ρ = density of air, lbs.-mass per cu.in.
V_d = critical speed of wing divergence, in. per sec.
X = variable dimension in wing spanwise direction, in.
L = wing semispan, in.
C = torsional stiffness of wing between stations, lb. in. per rad.
ΔX = distance between stations, in.

DISCUSSION

THE CRITICAL SPEED of wing divergence is the speed at which a balance of aerodynamic moments and resisting elastic moments may be maintained regardless of the absolute value of the angle of torsional deformation. The aerodynamic moment per unit of wing length is given in reference (1) as

$$M = K_d b^2(1/2 + a)\alpha \qquad (1)$$

where $K_d = 2\pi\rho V_d^2$.

Essentially the solution resolves itself into the boundary value problem of finding the value of K_d which will give a deflection curve satisfying the end conditions that: $\alpha = 0$ when $X = 0$ and $\alpha = 1$ when $X = L$. Considering this and the form of 1, it becomes immediately apparent that the critical speed can be easily obtained by a calculation analogous to Holzer's method for the determination of the natural frequencies of torsional vibrations. If for K_d, $b^2(1/2 + a)$, and α we write ω^2, J, and θ, then

$$M = \omega^2 J\theta \qquad (2)$$

which is the equation for inertia torque of a torsional vibration of amplitude $\theta(= \alpha)$, circular frequency $\omega(= \sqrt{2\pi\rho V_d^2})$, and inertia $J[= b^2(1/2 + a)]$.

A typical calculation is given in Table 1. The wing has been broken up into ten stations of discrete length. Column headings are given in terms of Eq. (2), as well as Eq. (1), in order to make the comparison with Holzer's method obvious. In practice, a tabulation is performed for various trial values of K_d and the amplitude at the fuselage station plotted against K_d. Where this curve passes through zero determines the critical value of K_d.

This method has several advantages. It is simple and quick. It is possible to check with but one trial tabulation if a particular wing stiffness curve is satisfactory, as far as divergence is concerned. This same trial shows where added stiffness is required or where excess stiffness may be removed. That is, knowing the design speed requirements, K_d is determined and a tabulation is performed with this value. If α remains positive at all stations the critical speed is above the design. Conversely, if there are negative values for α, the critical speed is too low. A glance at column 8 of the tabulation, which shows the deflections between stations, will

Received February 6, 1947.
* Senior Vibration Engineer, Structures Section.

TABLE 1

$K_d = 2\pi\rho V_d^2 = 130.52$ $\qquad$ $V_d = 841$ m.p.h.

1 Station No.	2 Station Location	3 $b^2\Delta X(1/2 + a)$ $[J]$ $\times 10^{-6}$	4 $K_d \times$ Three $[\omega^2 \times J]$ $\times 10^{-6}$	5 α $[\theta]$	6 $\Sigma K_d\alpha \times$ Three $[\Sigma\omega^2 J\theta)$ $\times 10^{-6}$	7 C $[C]$ $\times 10^{-6}$	8 $\Sigma K_d\alpha \times$Three$/C$ $[\Sigma\omega^2 J\theta/C]$
1	635	0.01706	2.2260	1.00000	2.2260	70.20	0.03171
2	600	0.03691	4.8179	0.96829	6.8911	42.53	0.16203
3	525	0.05092	6.6466	0.80626	12.2500	88.61	0.13825
4	475	0.05413	7.0644	0.66801	16.9691	112.50	0.15084
5	410	0.06997	9.1327	0.51718	21.6923	165.00	0.13147
6	350	0.10382	13.5508	0.38571	26.9190	137.20	0.19620
7	250	0.13807	18.0204	0.18951	30.3340	320.10	0.09476
8	177	0.14613	19.0731	0.09474	32.1410	507.40	0.06335
9	100	0.14967	19.5344	0.03140	32.7543	1058.00	0.03096
10	0			0.00044			

indicate where the wing is weakest and, accordingly, where stiffening should be added.

Applications to wing-aileron divergence and aileron reversal are obvious.

REFERENCES

[1] AAF MR ENG-M-51/VF 18, ADD. 1, *The Computation of the Critical Speeds of Aileron Reversal, Wing Torsional Divergence and Wing-Aileron Divergence*, dated December 19, 1942.

Letter to the Editor

(*Continued from page 470*)

ical fuel (liquid hydrogen and oxygen) but is far less than apparently obtainable from nuclear fission. A practical working efficiency for this purpose is thus apparently unattainable with chemical fuel but could be obtained with nuclear energy under proper control by means of additional mass.

If such trips ever become feasible, not to mention the much shorter trajectories between widely separated terrestrial points, it seems a safe guess that "efficiency," expressed as the commonly understood ratio of useful energy realized to total energy expended will continue to be an important criterion of design and performance.

RALPH H. UPSON
Professor in Aeronautical Engineering
University of Minnesota

Library Facilities of the Institute of the Aeronautical Sciences

To serve Institute members and others in the aeronautical industry, the Institute of the Aeronautical Sciences offers the facilities of:

The W. A. M. Burden Library
2 East 64th Street
New York 21, N.Y.

The facilities of this library are available for reference study at the Institute.

The Paul Kollsman Lending Library
2 East 64th Street
New York 21, N.Y.

This library loans books without charge to members and others in the United States over eighteen years of age. Full information will be sent on request.

The Pacific Aeronautical Library
6715 Hollywood Boulevard
Los Angeles 28, Calif.

This is a service and reference library for West Coast members and organizations. Full information as to its facilities will be sent on request.

utation of
Divergence

the com-
al energy
esign and

UPSON
ngineering
Minnesota

cal

een

as